

Dissertation

submitted to the

Combined Faculties for the Natural Sciences and for Mathematics

of the Ruperto-Carola University of Heidelberg, Germany

for the degree of

Doctor of Natural Sciences

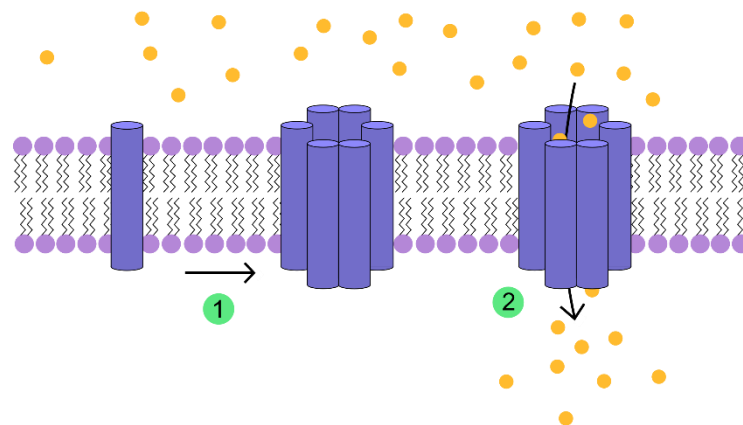
presented by

M.Sc., **Clemens Bretscher**

born in: Tübingen, Germany

Oral examination: 01.10.2018

The SAT Protein of the Minute Virus of Mice Induces the
Lysis of the Cell through the Formation of
Viroporin-like Structures.



Referees: Prof. Dr. Ralf Bartenschlager

Dr. Steeve Boulant

Statement of authorship

I hereby declare that the following work was written by myself without any illegitimate help of others. I did not use any other materials and sources than the ones stated. Citations of other sources are indicated. This work or a similar form has not been used as a dissertation for any other faculty.

Ich erkläre hiermit, dass ich die vorliegende Arbeit selbstständig und ohne unzulässige Hilfe Dritter verfasst habe. Ich habe keine anderen als die angegebenen Hilfsmittel und Quellen verwendet. Zitate aus anderen Werken habe ich als solche kenntlich gemacht. Diese Arbeit oder eine ähnliche Form wurde nicht als Dissertation bei einer anderen Fakultät eingereicht.

Clemens Bretscher, Heidelberg 12.07.2018

Summary

The prototype minute virus of mice (MVMp) and the H-1 virus belong to the family of *Parvoviridae* and can be used as oncolytic agents that infect, replicate in and kill human cancer cells. In preclinical trials the viruses were shown to be very successful to eradicate tumors in mice and rats. A phase I/IIa clinical trial with patients suffering from recurrent glioblastoma multiforme showed that parvovirus is safe to use in humans and that the therapy induces an infiltration of immune cells into the tumor tissue.

Many aspects of the parvoviral life cycle have been studied over the last decades. The entry, replication, transcription and packaging mechanisms of the virus are well understood. However, the process of the virally-induced lysis of the cell is still unknown. The viral non-structural protein 1 (NS1) was suggested to have cytotoxic features but a direct lytic mechanism could not be shown. Recently, the porcine parvovirus (PPV) was found to express the short transmembrane protein SAT. Mészáros and coworkers showed that a knockout of SAT led to a reduced lytic capacity of the virus (Mészáros et al., 2017). In the current study we show that the SAT protein of MVMp is also important for the lysis of the cell. A knockout of SAT in the genome of MVMp reduced the lytic capacity of the virus and SAT-ko viruses were also found to be less infectious than the wild type virus. The sole expression of SAT induced lysis and it exceeded the lytic capacity of NS1 by multiple times. Mészáros and coworkers suspected SAT to induce an irreversible stress in the endoplasmic reticulum which eventually led to the death of the cell. However, a direct mechanism of this process could not be shown. We suspect SAT to function as a viroporin - a class of virally-encoded transmembrane proteins that oligomerise to form pores through membranes. We could show that SAT is transported to the plasma membrane where it oligomerises in multimers and makes the plasma membrane permeable to the small molecule Hygromycin B. A computer simulation of the protein confirmed that SAT oligomerises in symmetrical complexes. However, pore-like structures were not observed. Furthermore, an increase in the permeability of ions such as calcium and sodium, which is often seen for other viroporins, was not found.

In an attempt to increase the lytic capacity of MVMp we created the SUPER virus. The position of SAT was altered in the genome of SUPER in order to increase its translation. We could show that the translation of SAT was indeed increased for the SUPER virus which led to an accelerated lysis of the cells. However, the production of the SUPER virus

was not very efficient. In order to increase the production of SUPER, we constructed shRNA constructs to knockdown *SAT*. Although the production of SAT was decreased, this approach did not increase the production of the virus. Nevertheless, the SUPER virus could be a promising candidate for the therapy with oncolytic parvoviruses. We suspect its increased lytic potential to release tumor antigens more efficiently compared to the lytic potential of the wild type virus. The released tumor antigens are suspected to stimulate cells of the immune system such as dendritic cells and cytotoxic T-cells in order to recognise and attack non-infected tumor cells.

Zusammenfassung

Das prototypische Minute virus of mice (MVMp) und das H-1 virus gehören der Familie der *Parvoviridae* an und können als onkolytische Agenzien eingesetzt werden, die humane Krebszellen infizieren, in ihnen replizieren und sie zerstören. In präklinischen Versuchen wurde gezeigt, dass das Virus mit großem Erfolg Tumore in der Maus und der Ratte zerstören kann. Eine klinische Phase I/IIa Studie, in der Patienten behandelt wurden, die an wiederkehrendem Glioblastoma multiforme litten, hat gezeigt, dass das Parvovirus sicher für den Einsatz am Menschen ist und dass die Therapie zu einem Influx von Immunzellen in das Tumorgewebe führt.

Viele Aspekte des parvoviralen Lebenszyklus wurden in den letzten Jahrzehnten erforscht. Die Prozesse der Aufnahme, der Replikation, der Transkription und des Verpackens von Nachkommenviren sind gut verstanden. Allerdings ist der Prozess der virus-induzierten Zelllyse noch nicht gut erforscht. Es wurde vermutet, dass das virale Nicht-Strukturprotein 1 (NS1) zytotoxische Eigenschaften hat. Allerdings konnte ein direkter lytischer Mechanismus nicht gezeigt werden. Vor kurzem wurde entdeckt, dass das porcine Parvovirus (PPV) das kurze Transmembranprotein SAT exprimiert. Mészáros und seine Mitarbeiter zeigten, dass ein Knockout von SAT eine geringe lytische Kapazität des Virus zur Folge hatte (Mészáros et al., 2017). In der hier vorliegenden Studie haben wir gezeigt, dass auch im MVMp das SAT Protein wichtig für die Lyse ist. Ein knockout von SAT im Genom von MVMp reduzierte die lytische Kapazität des Virus und SAT-ko Viren waren weniger infektiös als wildtypische Viren. Die alleinige Expression von SAT induzierte die Lyse und die lytische Kapazität von SAT war um ein Vielfaches größer als die von NS1. Mészáros und seine Mitarbeiter vermuteten, dass SAT einen irreversiblen Stress im endoplasmatischen Reticulum induzieren würde, was letztendlich zum Tod der Zelle führen würde. Allerdings konnte ein direkter Mechanismus dieses Prozesses nicht gezeigt werden. Wir vermuten, dass SAT als ein Viroporin funktioniert - eine Klasse von viralen Transmembranproteinen, die oligomerisieren und Poren in Membranen bilden. Wir konnten zeigen, dass SAT an die Plasmamembran transportiert wird, dort in Multimeren oligomerisiert und die Plasmamembran durchlässig für das kleine Molekül Hygromycin B macht. Eine Computersimulation bestätigte die Oligomerisierung von SAT in symmetrische Komplexe. Allerdings wurden keine poren-ähnlichen Strukturen beobachtet. Eine erhöhte Permeabilität für Calcium- und Natriumionen, wie sie bei anderen Viroporinen oft beobachtet wurde, wurde ebenfalls nicht gefunden.

Um die lytische Kapazität von MVMp zu erhöhen, entwickelten wir das SUPER Virus. Die Position von SAT wurde im Genom von SUPER verändert, um die Translation von SAT zu erhöhen. Wir konnten zeigen, dass die Translation von SAT im SUPER Virus erhöht war, was zu einer beschleunigten Lyse der Zellen führte. Allerdings war die Produktion des Virus nicht sehr effizient. Um die Produktion von SUPER zu verbessern, wurden shRNA-Konstrukte angefertigt, um einen knockdown von *SAT* hervorzurufen. Obwohl die Produktion von SAT dadurch verringert wurde, konnte dieser Ansatz die Produktion des Virus nicht verbessern. Nichtsdestotrotz könnte das SUPER Virus ein vielversprechender Kandidat für die Therapie mit onkolytischen Parvoviren sein. Wir vermuten, dass das gesteigerte lytische Potential eine effizientere Freisetzung von Tumorantigenen zur Folge hat, verglichen mit dem lytischen Potential des wildtypischen Virus. Die freigesetzten Tumorantigene könnten Zellen des Immunsystems, wie dendritische Zellen und zytotoxische T-Zellen, aktivieren, um nicht-infizierte Tumorzellen zu erkennen und anzugreifen.

Acknowledgments

First of all, I want to thank Dr. Jürg Nüesch for his supervision and his permission to work freely and independently in his lab. My work in his lab was very formative for my development as a scientist and as a person. Second of all, I want to thank Prof. Dr. Jean Rommelaere for harboring me in his department and for the input he gave me on my project. I also want to thank our technicians Claudia Plotzky and Alexandra Stroh-Dege for their practical help in the lab. I want to say a big thank you to Dr. Kashif Sadiq, Dr. Ghulam Mustafa and Prof. Dr. Rebecca Wade of the HITS institute in Heidelberg, who conducted the *in silico* simulations of SAT for me, which was a great support for my project. I could not have done it without them. I also want to acknowledge the work of Dr. Stefan Titz who conducted the calcium measurements for me. I am very thankful for the scientific input that I received from Dr. Steeve Boulant and Prof. Dr. Ralf Bartenschlager, who helped me a lot during our TAC meetings, and I also appreciated the input of Dr. Christiane Dinsart and Dr. Antonio Marchini. I also want to acknowledge the support by the core facility for light microscopy, especially Manuela Brohm and Dr. Damir Krunic for their kind introduction into the fluorescent microscopes, and I also want to acknowledge the support by the core facility for flow cytometry, especially Tobias Rubner for his detailed introduction into the FACS machine. I want to thank the DKFZ for the organisation of many interesting courses that I attended throughout my PhD. I want to thank my girlfriend Eleonora Nushi, my WG in the Hegenichstrasse 49 and my band Apes in Suits for keeping me from spending even more time in the lab. Finally, I want to thank my parents who made my studies possible and supported me throughout the years.

Table of contents

1 Introduction	13
1.1 Features of oncolytic viruses	13
1.2 What makes Parvovirus an oncolytic virus?	15
1.3 Basic features of parvovirus	17
1.4 The parvoviral capsid	21
1.5 The genome of parvovirus	23
1.6 Stages of the parvoviral life cycle	24
1.6.1 Cell entry	24
1.6.2 The replication process	26
1.6.3 Packaging of genomes and release of progeny viruses	29
1.7 The parvoviral proteins	31
1.7.1 NS1	31
1.7.2 NS2	33
1.7.3 The capsid proteins	33
1.7.4 SAT	34
1.8 Viroporins	35
1.9 Aim of this work	38
2 Material and Methods	39
2.1 Material	39
2.1.1 Cell lines	39
2.1.2 Bacterial strain	39
2.1.3 Viral strands	39
2.1.4 Reagents	40
2.1.5 Antibiotics	40
2.1.6 Antibodies	41
2.1.7 Enzymes	41
2.1.8 Kits	41
2.1.9 Solutions	42
2.1.10 Plasmids	43
2.1.11 Primer	44
2.1.12 Technical equipment	47
2.2 Methods	48
2.2.1 Construction and production of plasmids	48

2.2.2 Handling of and experimenting with eukaryotic cells.....	53
2.2.3 Production and titration of parvovirus	54
2.2.4 Protein analytics	58
2.2.5 Preparation and implementation of coarse-grained molecular dynamics simulation....	64
3 Results.....	66
3.1 Sequence comparison of SAT between MVMp - PPV	66
3.2 The SAT-knockout virus produces smaller plaques than the wild type virus	68
3.3 The SAT-ko virus is not inhibited in its replication	70
3.4 The spreading capacity of the SAT-ko virus is restrained.....	72
3.5 A knockout of SAT decreases the lytic activity of MVMp and inhibits the release of HMGB1	74
3.6 The SAT protein has a higher lytic potential than NS1.....	76
3.7 The SAT protein of MVMp is transported to the plasma membrane and its lytic potential depends on this transport	78
3.8 Monomers of SAT form stable interactions with each other.....	83
3.9 Mutations in its transmembrane domain abolish the killing potential of SAT but do not inhibit its homo-oligomerisation	87
3.10 SAT makes the plasma membrane permeable to Hygromycin B	92
3.11 The SAT oligomer is not permeable to calcium or sodium ions	95
3.12 A coarse-grained computer simulation of SAT reveals oligomerisation but does not show pore-formation	98
3.13 Morphological changes of cell-death induced by SAT	104
3.14 pSUPER kills cells more efficiently than pMVM-wt.....	106
4 Discussion.....	116
4.1 A Knockout of SAT is followed by a reduced cell lysis	116
4.2 The transport of SAT is crucial for its lytic function.....	117
4.3 SAT shows properties of a viroporin	118
4.4 Cell-death in MVM-wt or SAT-ko-infected cells and the function of SAT	125
4.5 Potential therapeutic applications of SAT	128
5 Supplement	135
6 Abbreviations	136
7 Figures	138
8 Bibliography	140

1 Introduction

1.1 Features of oncolytic viruses

Early in the 20th century observations were made that tumors of patients shrank in size when the patients were coincidentally infected with measles virus at the same time. This oncolytic effect was also seen for many other viruses such as vaccinia virus or Newcastle disease virus. Many experiments and clinical trials followed in which viruses were tested for their potential to eradicate tumors. Such efforts often led to success in treated patients, but remissions were still common (Kuruppu and Tanabe, 2005). Today, oncolytic virology is still a dynamic field of research. About ten different viruses are currently investigated in clinical trials regarding their oncolytic activities. These include Reovirus, Vaccinia virus and also parvovirus H1 (Kuruppu and Tanabe, 2005; Marchini et al., 2015). An attenuated herpesvirus expressing the granulocyte-macrophage stimulating factor (GM-CSF), under the name Talimogene Laherparepvec (T-VEC), was recently approved by the Food and Drug Administration (FDA). In clinical trials with patients suffering from melanoma T-VEC proved to be safe and the treatment provoked a minor increase in the median overall survival (Andtbacka et al., 2015).

The mechanisms by which oncolytic viruses are able to lyse cancer cells are different. Some oncolytic viruses express toxic proteins, others are harmful to the cell due to their excessive viral replication which drains energy supplies and metabolic resources from the cell. Additionally, tumor cells often have defects in their innate immune system which includes deficiencies in antiviral defense mechanisms. This feature makes them perfect targets for oncolytic virotherapy. While healthy cells fight against viruses, transformed cells have partly lost this ability. Type I interferon (IFN), e.g., is a key regulator in defense mechanisms against viruses. In healthy cells type I IFN can induce apoptosis upon infection in order to inhibit the further spreading of the virus. Cancer cells, however, frequently express reduced amounts of type I IFN, which makes them susceptible to viral infections. This circumstance is an example how successful infections with oncolytic viruses are restricted to cancer cells sparing out healthy cell.

Oncolytic viruses can also be modified to specifically target cancer cells. For example, an oncolytic Adenoviruses was engineered to include a motif of arginine–glycine–aspartic acid

(RGD) in its capsid. The RGD motif can bind to $\alpha v\beta 3$ and $\alpha v\beta 5$ receptors that are overexpressed on the cell surface of ovarian cancer cells (Jhavar et al., 2017). Another example of an engineered oncolytic virus is the herpes simplex virus rQNestin34.5. Here, the expression of a viral gene which is crucial for the viral life cycle was put under the control of a tumor-specific promoter in order to restrict a successful infection to cancer cells. This viral gene, called $\gamma 1\ 34.5$, is important to inhibit an innate immune response of the infected cell which would otherwise induce the total shutoff of all protein synthesis leading to an abortive infection (Chou and Roizman, 1994). $\gamma 1\ 34.5$ was put under the control of the nestin-specific promoter. Nestin is an intermediate filament and its promoter is especially active in malignant gliomas. This approach increases the selectivity for cancer cells (Kambara et al., 2005).

Lysis of cancer cells by viruses often leads to the release of tumor-associated antigens that can be taken up and processed by cells of the adaptive immune system which leads to an activation of immune cells and an immunising effect against cancer cells (figure 1). This feature can be combined with antibodies against CTLA4 and PD1. CTLA4 and PD1 are membrane proteins that are involved in the downregulation of immune cells. Cancer cells are able to influence these proteins and to induce the downregulation of immune cells which would otherwise attack the cancer cells. Antibodies against CTLA4 and PD1 have the capability to block this mechanism of downregulation. A combination of T-VEC with these agents is already under investigation and countless other combinations with oncolytic viruses are imaginable (Lawler et al., 2017).

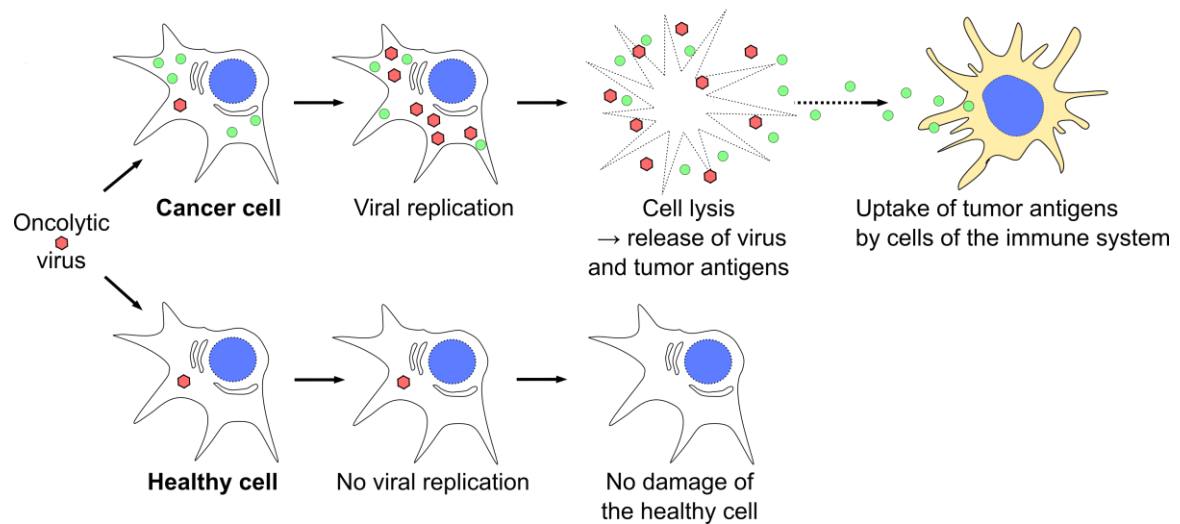


Figure 1: Infection of a cancerous cell or a healthy cell with an oncolytic virus has two different outcomes. Healthy cells defend themselves against the virus or do not provide a beneficial environment for the viral replication. The cell usually survives an infection and the virus eventually disappears. Cancer cells often lack antiviral mechanisms and support the replication of an oncolytic viruses which leads to their lysis. Tumor antigens (green spheres) are released and taken up by cells of the immune system which leads to their activation. The acquired tumor-immunity helps to fight the cancer.

Another important feature of oncolytic viruses is their ability to replicate in cancer cells and spread within a tumor. This feature is thought to allow oncolytic viruses to reach every single cancer cell within a patient even when the primarily injected viral dose only infected only a few cancer cells. Thereby, the progeny viruses are believed to reach distant metastases. However, it has to be considered that the adaptive immune system will recognise viral capsids during this process and produce antibodies against them which inhibits their spreading through the tissue (Kuruppu and Tanabe, 2005).

1.2 What makes Parvovirus an oncolytic virus?

The prototype minute virus of mice (MVMp) and H1 parvovirus can infect mice and rats, respectively. An infection of healthy human cells is usually abrogated since the replication of the virus is restricted. However, many human cancerous cell lines, which are originally derived from glioma, pancreatic cancer or colon cancer, are susceptible to an infection with parvovirus (Di Piazza et al., 2007; Josupeit et al., 2016; Marchini et al., 2015; Moehler et al., 2001; Mousset et al., 1994). This is most likely due to their increased proliferative nature which is crucial for the life cycle of parvovirus. Parvovirus requires cellular factors of the S-

phase for its replicative cycle, but it is unable to drive the cell into S-phase. (Marchini et al., 2015). A multitude of other factors that are overexpressed or activated in cancer cells also plays an important role when rodent parvoviruses infect human cancer cells. These factors include Ets and ATF transcription factors, Raf-1, and the proteins involved in the PDK1 pathway (Angelova et al., 2015). Especially the PDK1 pathway was found to be an important regulator of the permissiveness for parvovirus. This pathway is usually stimulated by growth factor-receptors but was found to be constitutively activate in several cancer cell lines. Non-permissive healthy cell lines were shown to become permissive for parvoviral infection when they expressed constitutively active PDK1. The PDK1 pathway was found to be important for the phosphorylation and regulation of the parvoviral non-structural protein 1 (NS1) which is one of the most important key players in the viral life cycle (Bär et al., 2015).

The role of the innate immune system in a parvoviral infection is unclear. In mouse cells an infection with parvovirus led to the induction of a type I IFN response (Grekova et al., 2010a). In healthy and cancerous human cells, however, this defense mechanism did not play a role in the antiviral defense against parvovirus (Paglino et al., 2014). Various hints were found that the activation of the adaptive immune system plays one of the most important roles in the oncolytic therapy with parvovirus. Tumor-bearing mice, that survived a treatment with parvovirus MVMP, developed an immunity against a second implantation of the tumor (Grekova et al., 2012). Such an immunity could also be observed when splenocytes of tumor-bearing and H1-treated rats were transferred to tumor-bearing, mock-treated mice. The recipient rats showed an increased survival compared to rats that received splenocytes of mock-treated tumor-bearing rats (Grekova et al., 2010b). Furthermore, Grekova and coworkers observed an improvement of the parvoviral oncolytic activity in tumor-bearing rats when interferon γ , an activator of T-cells, was additionally applied (Grekova et al., 2011). These results point to a strong involvement of the adaptive immune system in the oncolytic therapy. The release of tumor-antigens from parvovirus-infected cancer cells seems to activate immune cells and targets their killing activity against non-infected tumor cells. Moehler and coworkers could show that tumor cell lysates of H1-infected cancer cells induced the maturation of dendritic cells. The activated dendritic cells cross-presented tumor antigens to cytotoxic T-cells and released proinflammatory cytokines (Moehler et al., 2005). Additionally, parvovirus can be genetically modified to express immune-regulatory proteins such as IP-10 which was shown to improve the survival of

tumor-bearing mice. Here, activated lymphocytes, expressing IFN γ were found within tumors that were previously infected with IP-10-expressing parvovirus. However, such modifications of the viral genomes often require the deletion of capsid genes since the genome of parvovirus does not allow any incorporation of additional genes. Therefore, these recombinant viruses are unable to produce progeny particles by their own. For their production they depend on a helper construct that expressed the required capsid protein (Giese et al., 2002).

Rommelaere and coworkers started a phase I/IIa clinical trial with parvovirus H1 on patients with recurrent glioblastoma. The outcome of the trial confirmed that the treatment with parvovirus is safe for the patients and the treatment had a beneficial effect on the progression-free survival and overall survival of patients. Furthermore, it was shown that immune cells were activated and recruited to the tumor. The largest populations of immune cells were CD4- and CD8-positive T-cells. The tumor-infiltrating T-cells expressed granzyme B and perforin - two markers for the cytotoxic potential of the T-cells. Additionally, the immunostimulatory cytokines interferon- γ (IFN- γ) and interleukin (IL)-2 were detected. These findings underscore the importance of the involvement of the immune system in the outcome of the therapy. Furthermore, during the clinical study a seroconversion was observed, which is suspected to have negative effects on the spreading of the virus within the tumor and within the body which might inhibit the virus to reach distant metastases (Geletneky et al., 2017). However, this limitation might be overcome by pseudotyping of the capsid.

1.3 Basic features of parvovirus

The minute virus of mice belongs to the family of autonomous parvoviruses. These non-enveloped, small viruses have a capsid diameter of about 25 nm and a single-stranded DNA genome with a length of about 5100 bps (Astell et al., 1983; Cotmore and Tattersall, 2007). The prototype strain of MVM (MVMp) infects mouse fibroblasts and the immunosuppressive strain (MVMi) replicates in mouse T-lymphocytes and hematopoietic precursors which can cause severe combined immunodeficiency syndrome (SCID) in mice (Brownstein et al., 1991; Brownstein et al., 1992; Tattersall and Bratton, 1983). Other members of the family of autonomous parvoviruses comprise canine parvovirus (CPV), feline parvovirus (FPV), porcine parvovirus (PPV), the rat parvovirus H1 and human

Cutavirus. Autonomous parvoviruses are related to adeno-associated viruses (AAV). However, AAVs are dependent on the co-infection with a helper virus such as adenovirus, whereas autonomous parvoviruses replicate independently (Cotmore and Tattersall, 2007). Another group of parvoviruses, the Densovirinae, infect insect cells. Figure 2 shows a phylogenetic tree of the family of *Parvoviridae* based on the amino acids of the non-structural protein 1 (NS1), one of the viral proteins.

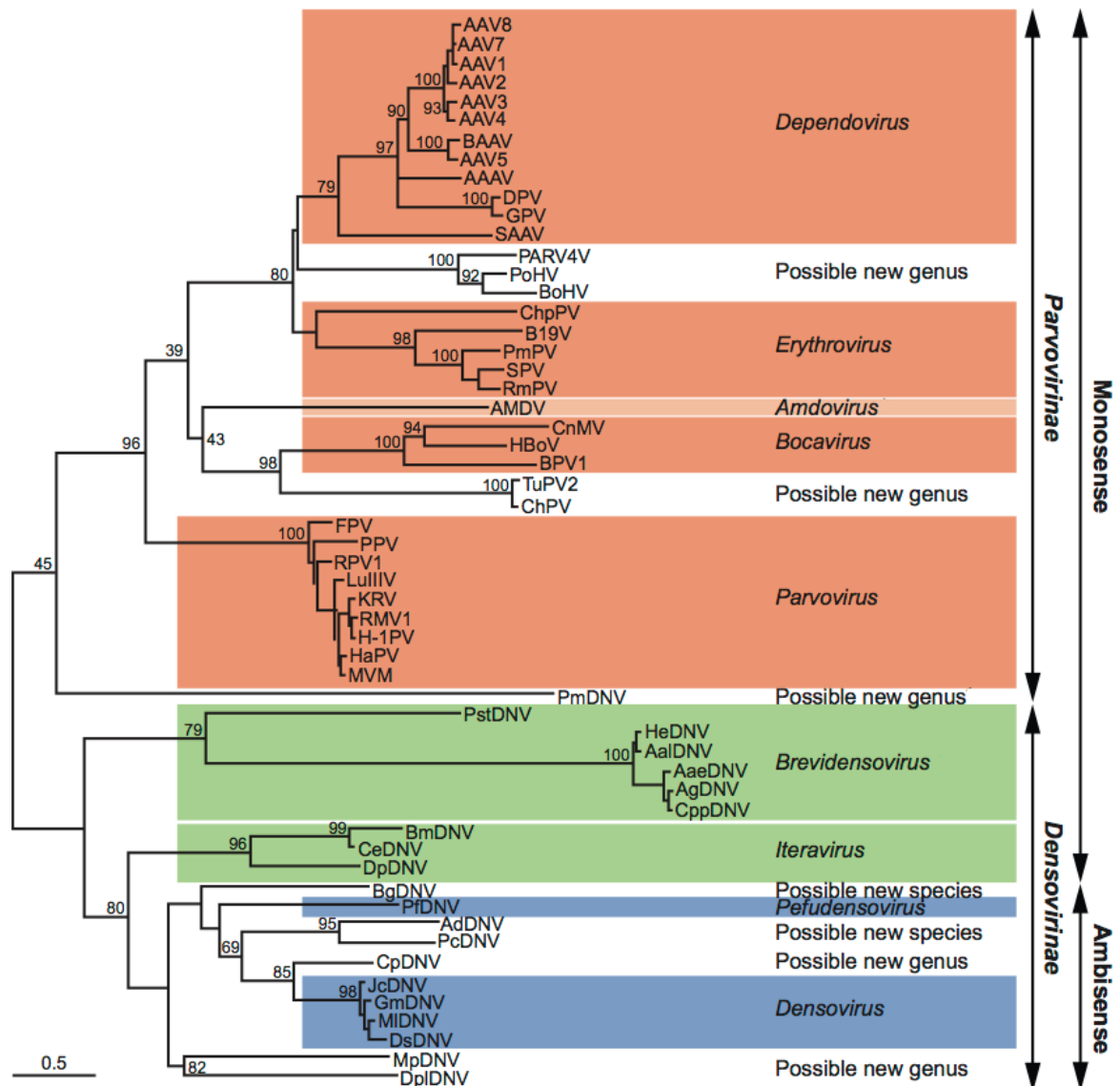


Figure 2: Phylogenetic tree of the family *Parvoviridae* based on their NS1 protein. The tree was constructed with the programs included in the Phylip package at the <http://mobyle.pasteur.fr/cgi-bin/portal.py> website (ClustalW-multialign, Phylip distance matrix, PROTDIST, Neighbor-Joining method, and phylogenetic tree drawing). The percentage of replicate trees in which the associated taxa clustered together in the bootstrap test (1000 replicates) are shown next to the branches. The scale bar represents the rate of amino acid substitutions. (https://talk.ictvonline.org/ictv-reports/ictv_9th_report/ssdna-viruses-2011/w/ssdna_viruses/152/parvoviridae-figures)

Infections with most autonomous parvoviruses cause gastrointestinal problems such as gastroenteritis or anorexia. But also reproductive failure and embryonic death was documented after infection with porcine parvovirus (Johnson and Dudleenamjil, 2011). Since parvovirus depends on proliferating cells, constantly growing tissues such as the gut or embryonic tissue represent the ideal environment for the virus. Organisms that are infected with parvovirus usually shed progeny virions in their feces and urine. The

subsequent infection of healthy organisms occurs via the oronasal route (Cotmore and Tattersall, 2007).

The three human protoparvoviruses bufavirus (BuV), tusavirus (TuV) and cutavirus (CuV) were discovered in the last six years in fecal samples of children and are suspected to cause gastrointestinal problems such as diarrhea. CuV was also found in one sample of skin melanoma and in skin samples of patients with cutaneous T-cell lymphoma. It is currently under investigation whether there is a causative relationship between the CuV infection and the formation of cancer (Väisänen et al., 2017).

The basic life cycle of parvovirus is depicted in figure 3 and discussed in more detail in chapter 1.6 “Stages of the parvoviral life cycle”. As a first step the non-enveloped virus binds to a cell surface receptor and is taken up in intracellular vesicles which are transported to the endosome. With the help of an enzymatic activity the virus escapes the endosome and is subsequently transported to the nucleus. The genome is released, converted to a double stranded DNA molecule and replicated. The newly synthesised single-stranded genomes are packaged within the nucleus into assembled empty capsids. The full capsids are transported to the cytoplasm and released from the cell after cell-lysis takes place.

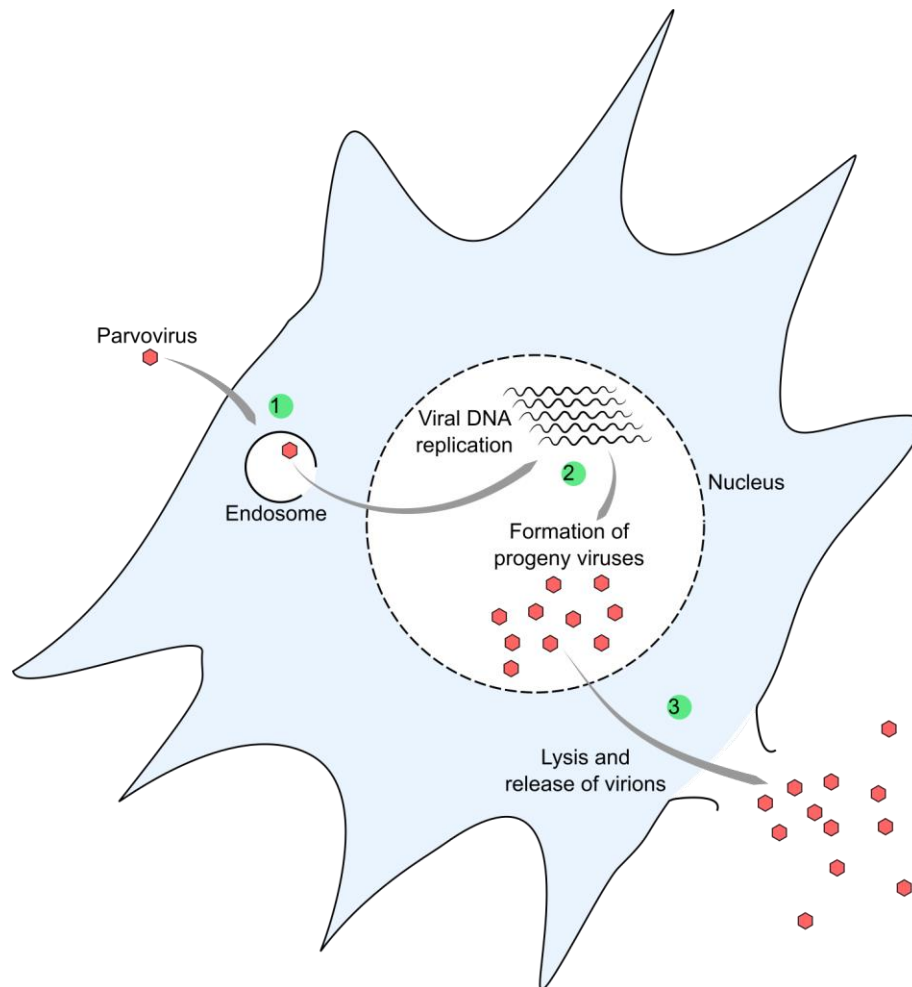


Figure 3: Basic infectious cycle of parvovirus. The virus binds at a cell surface receptor and enters the cell via receptor-mediated endocytosis. It is transported to the endosome, from which it escapes and is transported to the nucleus. The genome is released in the nucleus, converted to its active form and is replicated. Newly-synthesised genomes are packaged into empty capsids and the full progeny viruses are transported to the cytoplasm. As soon as the plasma membrane is broken down the progeny viruses are released from the cell.

1.4 The parvoviral capsid

The capsid of parvovirus is a non-enveloped icosahedric particle with a diameter of about 25 nm. 60 copies of the capsid proteins VP1 and VP2 interlock with each other to make up one capsid with a T-number of 1 (Cotmore and Tattersall, 2014). The molar ratio of VP1 and VP2 for one particle is about 1:10, respectively. It has a three-fold, two-fold, and five-fold symmetry axis (figure 4). With its small and rugged nature, the parvoviral capsid is very persistent to environmental stresses and can retain its infectivity for up to five months outside the host's body (Gordon and Angrick, 1986). Three-dimensional capsid structures were visualised for various different parvoviruses such as canine parvovirus (CPV) (Xie and

Chapman, 1996; Tsao et al., 1991), feline parvovirus (FPV) (Agbandje et al., 1993), H1 (Halder et al., 2013) and MVM (Llamas-Saiz et al., 1997). These structures share three main characteristics that are involved in the binding and tropism of the virus to its receptor: (i) a spike-like elevation at the three-fold axis, (ii) a depression at the two-fold axis, (iii) a cylindrical projection at the five-fold axis. The projections at the five-fold axis form a pore that is used to transfer the viral DNA inside and outside the capsid (Cotmore and Tattersall, 2014). During the binding of the capsid to its cell surface receptor sialic acid which is frequently attached to various membrane proteins, was found to interact with residues near the two-fold axis of symmetry. Small changes in this area have been shown to change the tropism of the virus. For example, Marchini and coworkers altered residues in this area of the capsid of the H1 parvovirus which made it more affine to certain cancer cells (Allaume et al., 2012). Furthermore, in an experiment, in which H1 was allowed to freely adapt itself to a glioma cell line, changes in residues around the two-fold axis were observed which underscore the importance of this surface-area on the capsid. At the inner surface of a full particle various sites were found to make unspecific contacts to the viral DNA (Halder et al., 2013). These interactions are likely to be required for the viral capsid to adapt its final conformational shape.

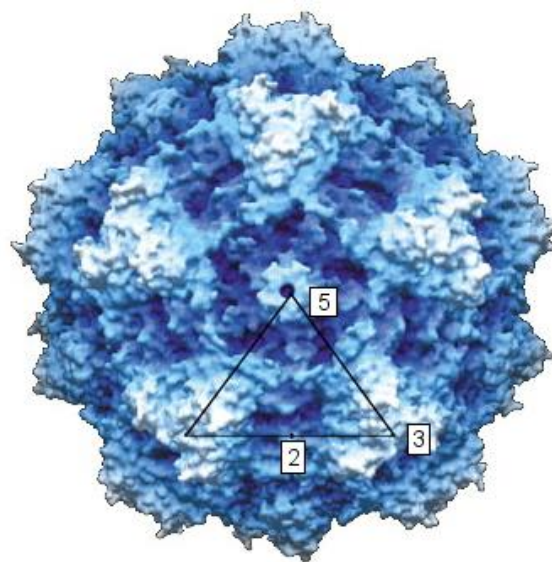


Figure 4: Molecular structure of the capsid of MVMi (Agbandje-McKenna et al., 1998). The colouring of the capsid is based on the distance of the respective point to the center of the capsid. The lighter the depicted colour, the greater the distance to the capsid's center. The five-fold, three-fold and two-fold axis of symmetry are marked with the numbers 5, 3 and 2, respectively.

1.5 The genome of parvovirus

When packaged into capsid particles the parvoviral genome is a negative sense, single-stranded DNA molecule with a length of 5.1 kb (Crawford et al., 1969). The genome ends at both sides with double-stranded, palindromic sequences which form a rabbit-ear-like shape at the 3'-end ("left end") and a t-shape on the 5'-end ("right end"). These sequences are important sites for the replication and the encapsidation of the genome (Bourguignon et al., 1976; Astell et al., 1983). When the virus enters the cell, the single-stranded genome is released from the capsid and subsequently converted to its active double-stranded form which allows transcription of viral genes (Cotmore and Tattersall, 1987). For a better navigation, the viral genome can be subdivided in 100 equal segments. At segment 4 and 38 promoter regions were found on the (+)strand. These promoters were termed P4 and P38 promoter, respectively. The two promoters give rise to eight spliced transcripts: three forms of R1, three forms of R2, R3 and R3'. They are translated into the viral proteins non-structural protein 1 (NS1), three isoforms of non-structural protein 2 (NS2-P, -L, and -Y), the capsid proteins VP2 and the non-structural protein SAT, and the capsid protein VP1, respectively. Polyadenylation signals are only found on the right-end side of the genome (Astell et al., 1983) (figure 5). The P4 promoter is stimulated early during infection by host factors such as E2F and ATF/CREB while the P38 promoter is activated late during infection by NS1. The replication of the viral genome is carried out in a mechanism that resembles the rolling-circle mechanism found in bacteriophages. For further details see chapter 1.6.2 "The replication process".

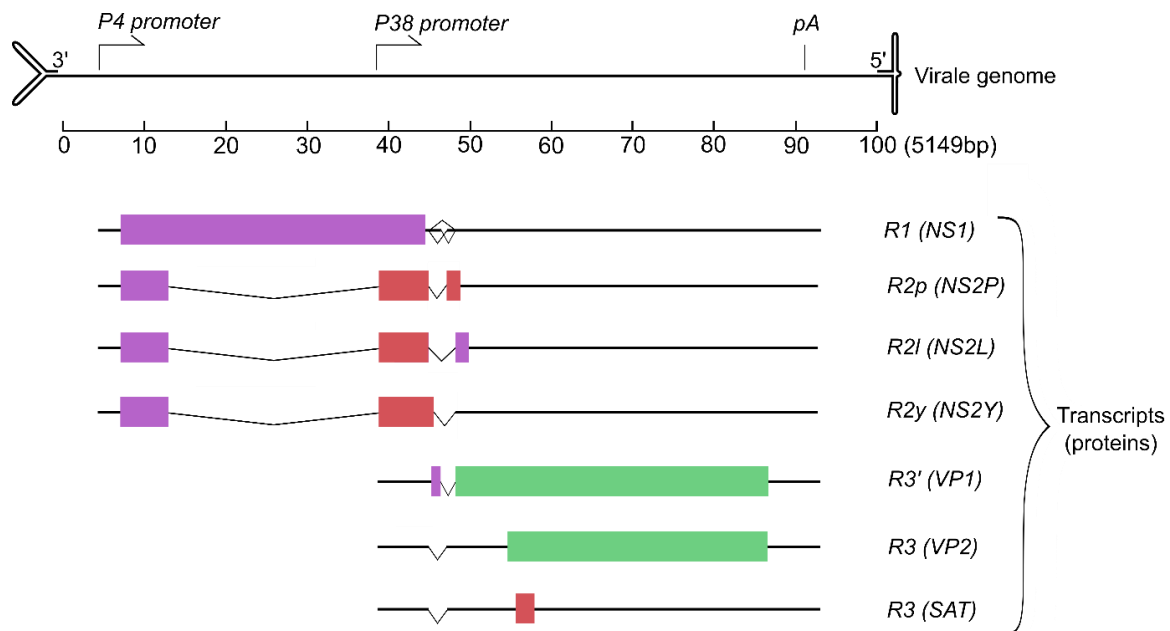


Figure 5: The genome of parvovirus and the transcribed mRNAs. The viral genome is depicted at the top of the figure as a single-stranded molecule which is divided in 100 regions. The two promoters are in region 4 and 38 and are termed P4 and P38, respectively. The four different transcripts, termed R1, R2, R3, R3', are coloured according to their open reading frame (green: ORF 1, red: ORF 2, purple: ORF 3). All sequences end at the polyadenylation site at the right-end side of the genome (pA). The names of the translated proteins are given in brackets.

1.6 Stages of the parvoviral life cycle

1.6.1 Cell entry

Summarised, the parvoviral particle enters the cell by the following pathway: The non-enveloped capsid enters the cell through receptor-mediated endocytosis and is subsequently transported to the endosome. Through conformational changes and an enzymatic activity, the virus escapes the endosome in order to avoid lysosomal digestion. The capsid is then transported to the nucleus where the viral genome is released (figure 6). The detailed process is outlined in the following paragraphs.

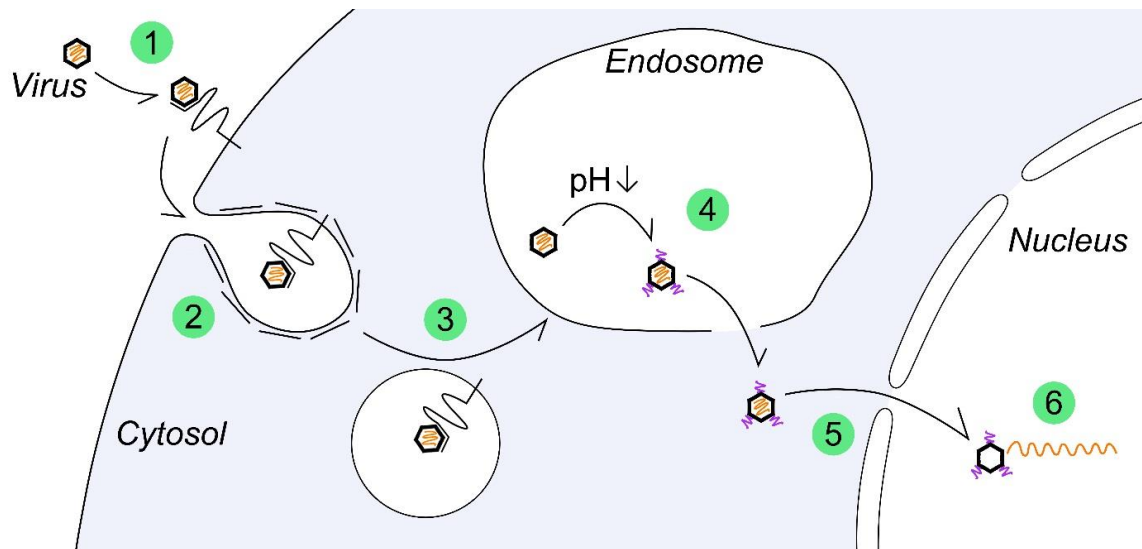


Figure 6: Entry mechanism of parvovirus. 1.) The virus binds to an unknown cell surface receptor. 2.) The virus-receptor complex is taken up in a clathrin-coated vesicle via receptor-mediated endocytosis. 3.) The vesicle loses the clathrin coat (black sticks) and is transported to the endosome. 4.) The acidic environment of the endosome induces a conformational change in the capsid that leads to the externalisation of the N-terminal domain (purple) of the capsid protein VP1. This domain harbours an enzymatic domain that cleaves the endosomal membrane. 5.) The virus escapes the endosome and is transported to the nucleus. 6.) The viral genome (orange) is released from the capsid.

The capsids of CPV and FPV were found to bind to the cell surface receptor transferrin (Parker et al., 2001) which is only expressed on proliferating cells such as cells of the intestinal wall or of the hematopoietic system (Trowbridge and Omary, 1981). Since parvoviruses can only replicate in proliferating cells, the binding of the capsid to the cell-receptor represents a first selective step for parvovirus in order to enter susceptible cells only. For MVMp and H1 the cell surface receptor is not known. However, sialic acid was shown to play an important role for the cell-attachment of many parvoviruses including MVMp and H1. Sialic acid is a sugar moiety, which is frequently found on cell surface proteins, and it was shown to interact with the parvoviral capsid at the capsid's depression at the two-fold axis of symmetry. Removing sialic acid from the cell surface by neuraminidase inhibits the uptake of parvoviral particles (López-Bueno et al., 2006).

Following binding to its receptor, the virus/receptor-complex is internalised in clathrin-coated pits (Linser et al., 1979; Parker and Parrish, 2000) which are transported on microtubules to eventually reach the late endosome (Vihinen-Ranta et al., 1998). The low pH of the endosome triggers conformational changes that allow the N-terminal domain of the capsid protein VP1 to be externalised from the inside of the capsid. The externalisation

occurs through the pore at the five-fold axis of symmetry. The VP1 N-terminal domain harbours a phospholipase A2 (PLA2) motif that is similar to cellular phospholipases and has the ability to attack the endosomal membrane from the inside to induce the formation of small holes. The virus escapes the endosome through these holes and is released into the cytoplasm (Cotmore et al., 1999; Dennis, 1997; Mani et al., 2006; Suikkanen et al., 2003b; Zádori et al., 2001). In addition to the PLA2 motif, the externalised N-terminal domain of VP1 carries a nuclear localisation signal (NLS). Together with a structural nuclear localisation motif that can be found on the surface of the capsid both signals promote the nuclear transport of the capsid along microtubules with the help of the motor protein dynein (Lombardo et al., 2000; Lombardo et al., 2002; Suikkanen et al., 2003a; Vihinen-Ranta et al., 2000).

Whether the full capsid or only the viral genome translocates through the nuclear pore is not known. Porwal and coworkers suggested that parvovirus induces a nuclear envelope breakdown in order to enter the nucleus. However, in this study extremely large amounts of parvoviral particles of up to 1000 particles per cell were used which makes it questionable if these findings reflect the natural processes when a single virus infects a cell (Porwal et al., 2013). When the genome is finally supposed to be decapsidated, the viral DNA is thought to leave the capsid through the pore at the five-fold axis of symmetry (see chapter 1.4 “The parvoviral capsid”) (Cotmore and Tattersall, 2012).

1.6.2 The replication process

The parvoviral replication takes place in the nucleus and the whole replication process strongly depends on cellular factors that are only present during S-phase of the cell cycle (Siegl, 1984; Spalholz and Tattersall, 1983; Tattersall 1978). However, parvovirus is not able to induce the onset of the S-phase. In fact, the viral genome is suggested to stay inside its capsid until the cell progresses into S-phase. Once decapsidated the single-stranded DNA genome is converted by the host cell replication machinery into the replicative double-stranded DNA form. The free 3'-end of the double-stranded left hairpin serves as a primer for this process (Cotmore and Tattersall, 2014). The conversion was shown to depend on the presence of the cell cycle complex cyclin A/CDK2 that is only present during the S-phase (Bashir et al., 2000). After conversion of the genome to the double-stranded active form, the P4 promoter is stimulated by E2F, ATF/CREB, ETS and NF-Y – cellular factors that are overexpressed during S-phase (Deleu et al., 1999; Nüesch et al., 2012). The

subsequent production of NS1 is crucial since it acts as an orchestrator for the parvoviral replication process.

The replication is carried out in a rolling hairpin replication that is similar to the rolling circle replication. In a first step NS1 binds to the [ACCA]₂ motif in the 3'-origin of replication (3'ori) of the genome (Cotmore et al., 1995; Rhode and Richard, 1987). Here, it induces a single-stranded nick in the DNA, which simultaneously binds NS1 covalently to the 5'-end of the DNA via its amino acid residue Y210 (Cotmore and Tattersall, 1994; Cotmore and Tattersall, 2014). The free 3'-end of the DNA is used as a primer to start replication by DNA-polymerase δ in a unidirectional fork. The (-) strand is used as a template and the (+) strand is displaced (Cotmore and Tattersall, 2014). In order to conduct the replication process, NS1 binds to proteins of the replication machinery such as replication protein A (RPA) 1-3 and these interactions are thought to sequester whole replication complexes to the parvoviral genome (Christensen and Tattersall, 2002). During the viral replication NS1 acts as a helicase by forming a homo-oligomer, which is believed to form a ring-like structure resembling a helicase that wraps around the DNA. A similar homo-oligomer is the large T antigen of SV40 (Li and Rhode, 1990; Pujol et al., 1997; Wilson et al., 1991).

When the polymerase reaches the right-end hairpin, NS1 melts down the hairpin and the polymerase replicates the stretched-out sequence till the end of the genome. Next, NS1 reassembles the double-stranded hairpin and the polymerase uses the newly synthesised (+)strand to continue the replication while displacing the (-)strand (Willwand et al., 2002). The hairpin serves as a hinge to send the polymerase back on the newly synthesised strand. Once the left end is reached the hairpin is stretched out and the polymerase continues till the end. This process then continues for multiple rounds leading to concatemeric DNA species. Later the complexes are resolved in smaller units at the left-end hairpin. NS1 and parvoviral initiation factor (PIF) are involved in this process by inducing a nick at this site (Christensen et al., 2001; Cotmore and Tattersall, 2003) (figure 7). The different concatemeric DNA species can be experimentally visualised by a Southern blot using a radioactive probe against a short sequence taken from the *NS1* gene. In the Southern blot the viral genome is visualised in a monomeric, dimeric and tetrameric form as well as oligomers of higher order. Additionally, the single-stranded form of the genome can be seen in the blot which is a sign that new progeny viruses have been produced since only progeny

viruses contain the single-stranded form of the genome (see chapter 1.6.3 “Packaging of genomes and release of progeny viruses”).

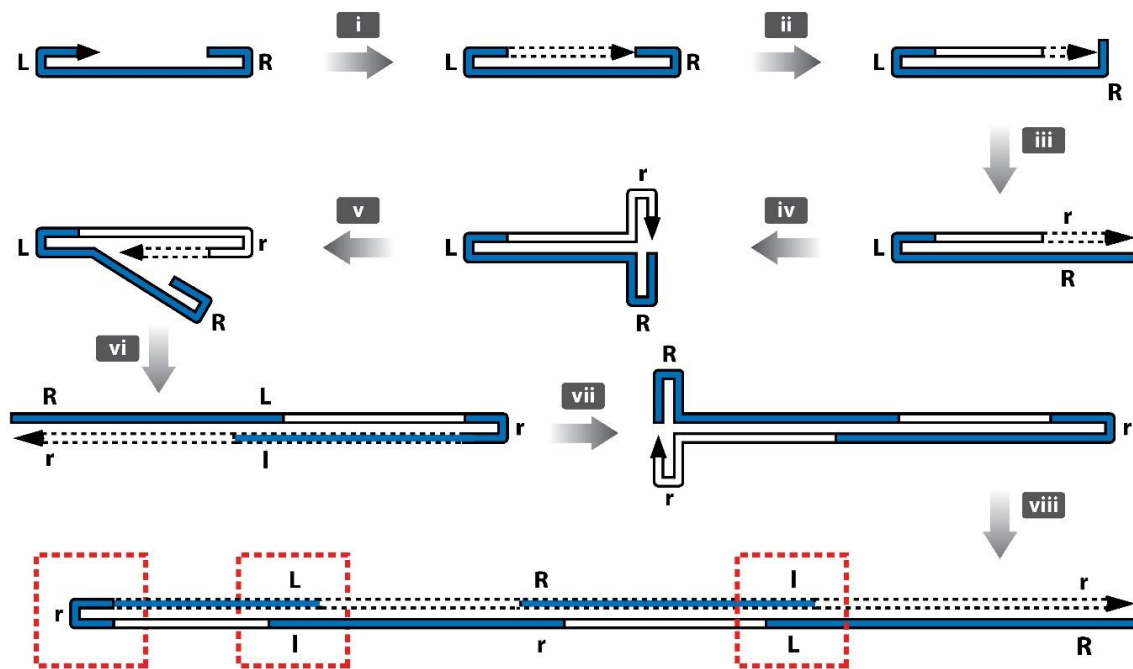


Figure 7: Conversion and replication of parvovirus (Cotmore, and Tattersall, 2014). The left-end and right-end sides are marked with L/l or an R/r. i.) The single-stranded genome is converted into a double-stranded form. ii and iii.) The replication starts at the right-end side of the genome. The (+)strand (white strand) is displaced while the (-)strand (blue strand) is used as a template. The full sequence is replicated until the end of the genome. iv and v.) The right hairpin is formed and directs the replication back on the newly-synthesised strand thereby displacing the (-)strand. vi.) The replication machinery replicates the left-end side of the genome and continues until the right-end side is reached. Here, steps iii to vi can be repeated. viii.) The replication process leads to the development of concatemeric DNA species.

The parvoviral replication takes place in so-called autonomous parvovirus-associated replication (APAR) bodies. These nuclear aggregations of protein and viral DNA include viral proteins such as NS1, and proteins of the cellular replication machinery such as RPA, PCNA, DNA polymerase α and δ , and cyclin A (Bashir et al., 2000; Christensen and Tattersall, 2002). Over time these centers grow in size and incorporate viral capsid proteins for the production of progeny viruses. It was also found that factors of the DNA damage response (DDR) such as γ H2AX, Nbs, Ataxia Telangiectasia Mutated (ATM), accumulate in the APAR bodies. The DDR is a molecular protection system that is able to repair lesions of the DNA which were introduced by a faulty DNA replication or damaging factors such as reactive oxygen species. In the context of a parvoviral infection, this DDR is likely to be

induced by the terminal hairpins of the parvoviral genome and has a stimulating and accelerating effect on the parvoviral replication. Other reports believe that NS1 introduces unspecific nicks in the host genome which trigger the DDR. The precise role of the DDR, however, is not fully understood. The ATM pathway was found activated in infected cells and its inhibition had severe negative effects on the viral replication. However, the exact mechanism, how these responses help the virus to replicate, is largely unclear (Adeyemi et al., 2010; Cotmore and Tattersall, 2013). The DDR and NS1 were found to induce a cell cycle arrest that is crucial for the replication of the viral genome (Adeyemi and Pintel, 2012; Op De Beeck et al., 1995). In this context it was also found that p53 - an important regulator of the cell cycle - was activated during infection, but its downstream target p21 was surprisingly degraded by the proteasome (Adeyemi and Pintel, 2012). p21 is usually involved in the processes of cell cycle arrest. However, the observed cell cycle arrest is suggested to be rather the result of a two-step process: First, the serine/threonine kinase Chk2 is activated during an infection with MVMP which is accompanied by a proteasomal degradation of the cell cycle protein CDC25A. Second, cyclin B1 is depleted and in consequence cyclin B1-CDK1 complexes cannot form which inhibits the entry of the cell cycle into mitosis. These processes induce a pre-mitotic, pseudo-S-phase state which represents an ideal environment for the parvoviral replication since all the factors, that are required for replication, are present (Adeyemi and Pintel, 2014).

1.6.3 Packaging of genomes and release of progeny viruses

At the end of the infectious cycle empty capsid shells are assembled and the viral DNA is packaged into them. This process is orchestrated by NS1 which transfers a (-)single-stranded copy of the viral genome into the capsid. The exact mechanism of this transfer is not known and a direct interaction between NS1 with the capsid has not been reported. During the transfer NS1 is attached to the 5'-end of the genome but does not enter the capsid. It rather stays attached to the genome outside of the capsid and is cleaved off later by a protease or a DNase which cuts the DNA to which NS1 is attached to. Its presence at the fully assembled particle is not necessary regarding the infectivity of the virus (Cotmore and Tattersall, 1989).

Once the viral genomes are loaded into the capsids the full particles exit the nucleus whereas empty particles remain inside the nucleus. This selection is achieved via the short

N-terminal part of VP2 which adopts a different conformation in the full capsids compared to the empty capsids. This conformational change allows for the interaction between full capsids with the nuclear export machinery (Maroto et al., 2004). The full particles stay in the cytoplasm as long as the plasma membrane stays intact. Once the plasma membrane is broken down the progeny viruses are released to the outside.

Baer and coworkers suggested that progeny virions are transferred into the endoplasmic reticulum (ER) after their translocation from the nucleus to the cytoplasm. However, a direct transport mechanism of the virions into the lumen of the ER was not shown and it is questionable if a whole capsid is able to cross the ER membrane. It was suggested that the virions were further transported in vesicles from the ER to the Golgi and finally released at the plasma membrane which was assumed to induce the lysis of the infected cell. It was shown that interfering with important regulators of this vesicular transportation pathway such as Sar1, Sec24, Rab11 or Rab1 strongly reduced the lysis of infected cells and the release of progeny viruses. Furthermore, this interference had a negative effect on the infectivity of the produced progeny viruses (Bär et al., 2013). However, a direct mechanism of the disintegration of the plasma membrane remained elusive. In our current study we focused on this process of lysis and the release of progeny viruses from the cell. The SAT (short alternatively translated) protein is strongly involved in this process (see chapter 1.7.4 “SAT”).

1.7 The parvoviral proteins

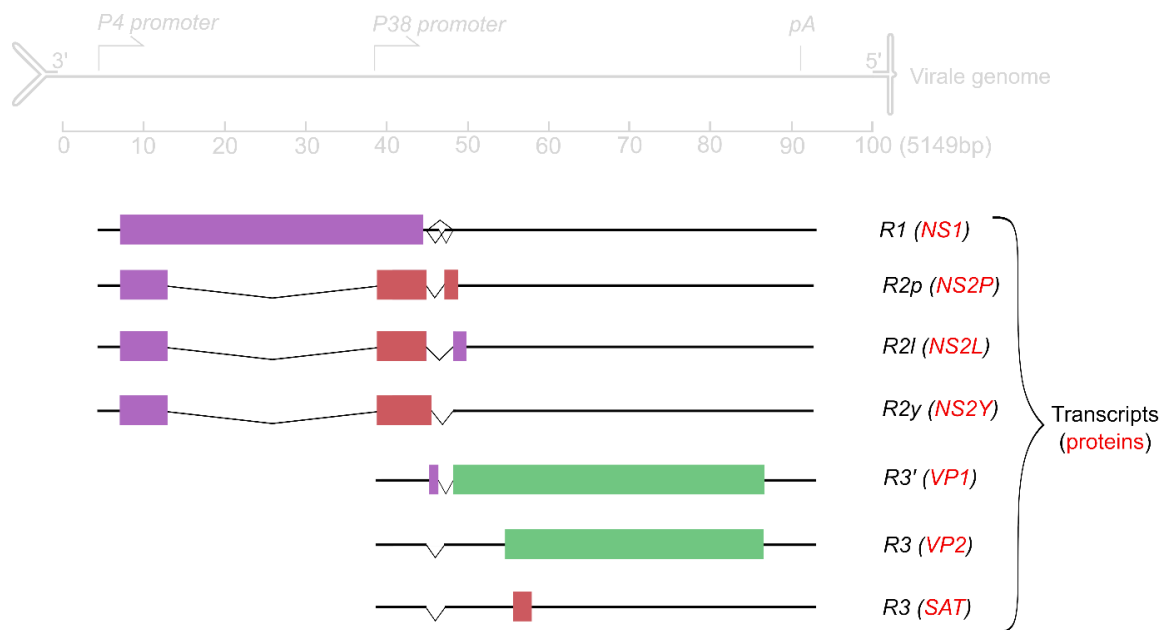


Figure 8: The mRNAs of the parvoviral proteins: NS1, three isoforms of NS2 (NS2P, NS2L, NS2Y), VP1, VP2 and SAT.

1.7.1 NS1

A huge amount of research has been conducted on NS1 which makes it the most studied parvoviral factor. In this report I am listing the most important features of NS1. Its functions during replication were already outlined in the chapter 1.6.2 “The replication process”. For a detailed insight into NS1 I refer to the review “Tumor Suppressing Properties of Rodent Parvovirus NS1 Proteins and Their Derivatives” (Nüesch and Rommelaere, 2014) and to the book “Parvoviruses” (Kerr et. al, 2006).

The 83-kDa multifunctional NS1 protein is expressed under the control of the P4 promoter and is mainly localised in the nucleus due to a nuclear localisation sequence (NLS) (Cotmore and Tattersall, 1986a; Legendre and Rommelaere, 1994; Nüesch and Tattersall, 1993). Its main functions are the replication of the viral genome and the transactivation of the P38 promoter (Doerig et al., 1988; Rhode, 1985). To fulfill these tasks NS1 interacts with cellular factors such as CKII α (Nüesch and Rommelaere, 2007) and exerts helicase, ATPase and DNA-nicking activity. Its multiple functions are regulated via phosphorylation by members

of the PKC family (Nüesch et al., 2003; Nüesch et al., 2012) and via acetylation (Li et al., 2013). A schematic overview of NS1 and its domain structure is shown in figure 9.

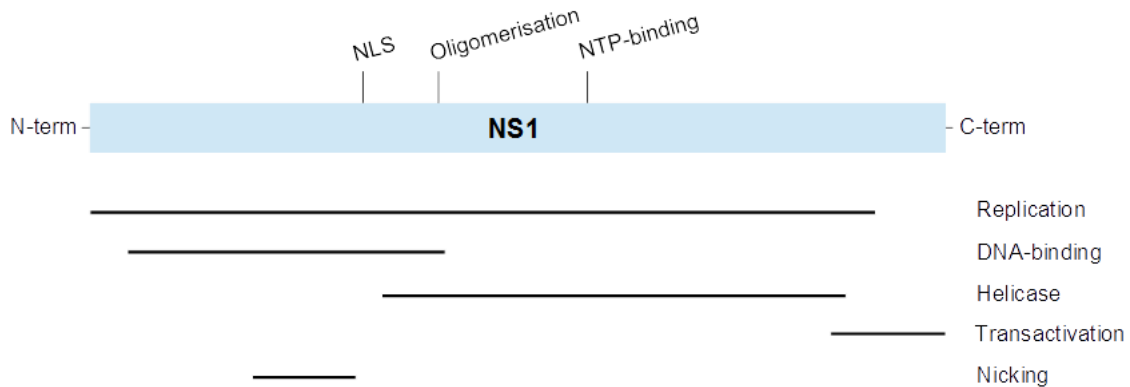


Figure 9: Domain structure of NS1. The NS1 protein contains different domains that fulfill various functions. The vertical bars indicate the region of the respective function.

1.7.1.1 NS1 regulates the transcription of P38

NS1 was found to drastically induce the activity of the P38 promoter which has usually a low basal activity (Ahn et al., 1992). NS1 binds to the P38 promoter at an NS1-interactive element ($[ACCA]_2$), called *tar*-element which is similar to the element found in the parvoviral 3'ori. ATP is required for this binding process (Christensen et al., 1995). In close proximity to the *tar*-element an Sp1-binding site was found at which the transcription factor Sp1 binds to and interacts with NS1. Additionally, NS1 was found to directly interact with two further members of the general transcription machinery, TFIIA ($\alpha\beta$) and TBP. The assembled complex then initiates the transcription of the R3 and R3' transcripts (Kradý and Ward, 1995; Lorson et al., 1998).

1.7.1.2 Cytotoxic functions of NS1

Besides its functions in replication and transcription various reports observed cytotoxic properties of NS1.

The expression of NS1 was shown to induce a cell cycle arrest at the G2 phase (Op De Beeck et al., 1995). Such an effect might be caused by the nicking activity of NS1. Nicks in the host genome were found after the expression of NS1 which eventually inhibited the

replication of the host genome (Op De Beeck and Caillet-Fauquet, 1997). In this context the interaction of NS1 with RPA 1-3 was suggested to sequester a significant amount of replication complexes from the host genome. This rearrangement was thought to disturb the replication of the host genome (Christensen and Tattersall, 2002). The long-term expression of NS1 also led to an increase in the intracellular concentration of reactive oxygen species (ROS) and subsequent cell death (Hristov et al., 2010). However, a direct mechanism of how NS1 induces the increase of ROS could not be shown. NS1 was also shown to be involved in the disassembly of actin and tropomyosin fibers (Nüesch and Rommelaere, 2007; Nüesch et al., 2005). The expression of NS1 was associated with apoptosis, lysosomal cell death and necrosis depending on the cellular system used. Direct mechanisms of how NS1 induces cell death are still elusive (Nüesch and Rommelaere, 2014).

1.7.2 NS2

The NS2 protein shares the same N-terminal domain with NS1 (Cotmore and Tattersall, 1986b). However, its function is still elusive.

Three different isoforms of NS2 were found, termed NS2L, NS2Y, NS2P which are produced by alternative splicing and differ in their C-terminal ending. All three isoforms mainly reside in the cytoplasm but can also be found in the nucleus. NS2 interacts with the nuclear export factor Crm1 and this interaction was suggested to be involved in the export of progeny viruses from the nucleus to the cytoplasm (Eichwald et al., 2002; Ohshima et al., 1999). NS2 was also thought to be involved in viral replication and assembly of capsids (Li and Rhode, 1991; Naeger et al., 1990). However, in some transformed cell lines NS2 was not required for the viral life cycle (Naeger et al., 1990). Despite its elusive function it should be mentioned that NS2 accumulates three times faster than NS1 but also has a higher turnover-rate than NS1 (Cotmore and Tattersall, 1990).

1.7.3 The capsid proteins

The expression of capsid proteins is regulated by the P38 promoter that is activated by NS1 late during infection (Cotmore and Tattersall, 1990). There are three types of capsid proteins VP1, VP2, and VP3 that share a large common C-terminal part. VP1 and VP2 are products of alternative splicing (Jongeneel et al., 1986; Morgan and Ward, 1986). Preceding

the nuclear transport of VP1 and VP2, the proteins assemble into trimers (Lombardo et al., 2000). Nuclear localisation signals then coordinate their translocation to the nucleus (Lombardo et al., 2002; Vihinen-Ranta et al., 1997). The capsid-trimers are then assembled into empty particles consisting of about ten copies of VP1 and 50 copies of VP2 (Tattersall et al., 1977). Later NS1 transfers the viral genome into the capsid through the particle's pore at the five-fold axis of symmetry (Plevka et al., 2011). Post assembly a small part of the N-terminus of VP2 is cleaved off which can happen inside the host cell, outside in the medium or in the cell that is infected next. The remaining C-terminal part is termed VP3 (Tattersall et al., 1976; Tattersall et al., 1977).

1.7.4 SAT

The SAT protein was unknown for a long period of parvoviral research. 2009 Zádori and coworkers discovered the short *SAT* gene which is expressed under control of the late P38 promoter (Zádori et al., 2005). The *SAT* gene is located in the coding region of *VP2* but in an alternative reading frame. Both proteins VP2 and SAT are translated from the same mRNA. This is possible through leaky scanning of the ribosome. Leaky scanning is a mechanism in which a single mRNA molecule contains two start codons of AUG that are separated only by a few bases. If the first AUG is located in a suboptimal Kozak sequence (PNNAUGG, where P is a purine and N is any nucleotide) it is sometimes skipped during mRNA-scanning of the ribosome and the following nearby AUG is used as the initiation of translation (Kozak, 2002; Kozak, 1995). The initiation site of VP2 is embedded in a suboptimal Kozak sequence which makes it possible for the ribosome to start translation at the nearby AUG of the SAT gene. Hence, the protein sequence of SAT completely differs from VP2. It should be mentioned that leaky scanning is not a sloppy mechanism as the name might suggest. It is rather a well-calculated strategy to regulate gene expression when the amount of coding material is restricted which is the case for many viral genomes.

The SAT protein of MVMp is 58 amino acids long and harbours a single pass α -helical transmembrane domain. In PPV the protein was found in the ER. Mészáros and coworkers discovered that a knockout of *SAT* in the genome of PPV strongly inhibited the lysis of infected cells. They suggested that SAT induced an ER-stress which finally led to the lysis of PPV-infected cells. They could show that the ER-stress marker CCAAT/-enhancer-binding protein homologous protein (CHOP) translocated into the nucleus in wt-infected cells but not in cells that were infected with a virus that carried a knockout of SAT (SAT-ko).

Nuclear translocation of CHOP is associated with the induction of apoptosis. However, a direct mechanism of these processes has not yet been found for the SAT protein. Therefore, it is not clear in which way SAT directly induced the ER-stress response (Mészáros et al., 2017).

1.8 Viroporins

This work concentrates on the parvoviral protein SAT and we hypothesise that it has viroporin-like features. In this chapter features of viroporins are described.

In 1978 researchers observed that cells infected with EMC virus, Semliki Forest virus or Mengo virus became permeable at their plasma membrane to the small molecule GppCH₂p. It was not known which viral factor increased the permeability of the plasma membrane (Carrasco, 1978). Today we know that viroporins are the cause for this observation. Viroporins are expressed by many different viruses such as HCV, Ebola virus, HIV, or JC polyomavirus. These proteins are typically short and have one or two transmembrane domains. Upon expression they localise to various membranes such as the plasma membrane (Madan et al., 2007; Suzuki et al., 2010), the endosome (Zebedee and Lamb, 1988), the endoplasmic reticulum (Hussain et al., 2007) or the viral envelope (Zebedee and Lamb, 1988) and fulfill various functions. Viroporins homo-oligomerise within these membranes and form pores that are permeable to small molecules such as ions (figure 10).

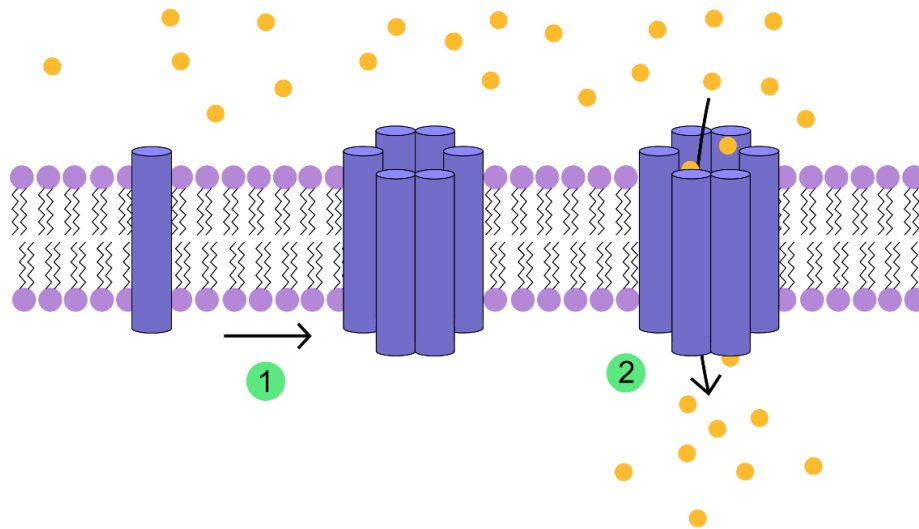


Figure 10: Formation of viroporins. 1.) The transmembrane helix of a monomeric viroporin protein homo-oligomerises to parallel bundles to form a pore. 2.) The pore allows the passage of small molecules that are otherwise impermeable to the membrane.

The function of viroporins cannot be generalised for all viruses since viroporins of different viruses take influence in many different steps of the viral life cycle (Nieva et al., 2012). The following paragraphs illustrate a few examples.

p7 is the viroporin protein of HCV. It has two transmembrane domains that are linked with a short loop. p7 was found to equilibrate the H^+ gradients of intracellular vesicles which was found to be an important step for the maturation of progeny viruses (Wozniak et al., 2010). It is also involved in the processing of the HCV polyprotein in the E2-p7-NS2 region and in the release of progeny virions (Steinmann et al., 2007). A computer simulation suggested that the pore is formed by six or seven monomers of p7 and that the diameter of the pore is about 6 Å (Chandler et al., 2012). Furthermore, p7 was shown to induce caspase-dependent apoptosis. This process was surprisingly independent of its ion channel activity. The exact mechanism still remains unclear.

Rotavirus expresses the viroporin protein NSP4. This protein localises to the endoplasmic reticulum and disrupts the calcium gradient by its pore-forming activity. The influx of Ca^{2+} into the cytoplasm was found to be important for the replication of rotavirus as it is involved in the development of the viroplasm - the site of rotavirus replication (Sen et al., 2007). NSP4 was found to oligomerise into a tetramer (Bowman et al., 2000).

Matrixprotein 2 (M2) of influenza A virus is also a viroporin that is permeable to protons (Pinto et al., 1992). M2 oligomerises to a tetramer (Georgieva et al., 2015) and can be found in the envelope of the virions. When the virion enters the cell, it is transported to the endosome. Here, M2 is activated by the acidic milieu and allows protons to pass through the viral envelope inside the virion. This process leads to the dissociation of the viral genome from matrix proteins and to the fusion of the viral envelope with the endosomal membrane which releases the viral genome to the cytoplasm (Cady et al., 2009). However, Watanabe and coworkers state that M2 is not necessary for viral entry since a mutant influenza virus lacking a functional M2 was still able to replicate in cell culture (Watanabe et al., 2001). M2 was also found to be involved in the scission of newly formed virions from the plasma membrane where it localises to the necks of budding viral vesicles and induces the curving of the membrane (Rossman et al., 2010).

The proteins of some viroporins are also able to interact with cellular factors. For example, Vpu, the viroporin protein of HIV, interacts with CD4 and tetherin. Both factors usually inhibit the release of progeny viruses from the cell surface. However, the interaction between Vpu and CD4 leads to the proteasomal degradation of newly formed CD4 (Binette et al., 2007; Magadán et al., 2010) and the interaction between Vpu and tetherin inactivates tetherin which would otherwise cause retention of progeny viruses at the cell surface to inhibit their release (McNatt et al., 2013; Neil et al., 2008).

There are also inhibitors of viroporins. The small molecule amantadine can be used prophylactically against infections with influenza A. Amantadine binds inside the viral pore formed by M2. It inhibits the infection and the assembly of new progeny virions (Hay et al., 1985). However, evolutionary mutations of specific residues in M2 help the virus to escape the inhibiting effects of the drug (Hay et al., 1986). Amantadine was also found to block the viral pore of p7 of HCV (Griffin et al., 2003).

Some researchers analysed the structures of assembled viroporins by computer simulations (Chandler et al., 2012; Fischer, 2003; Shukla et al., 2015). Chandler and coworkers analysed the stability of various oligomers of p7 in different orientations over time within an artificial membrane (Chandler et al., 2012). These studies are often based on already existing NMR structures of monomers or on assembled viroporins taken from electron microscopy

analyses. In this thesis we conducted a computer simulation of SAT. Crystal structures of SAT were not known, so the structure of the protein was predicted de novo.

1.9 Aim of this work

This thesis concentrates on the mechanism of cell lysis by the small virally-encoded protein SAT. The lytic, parvoviral mechanisms are still elusive and the investigation of these processes might help to improve and shape future strategies for oncolytic cancer treatment. We found SAT to be transported from the endoplasmic reticulum to the plasma membrane where it oligomerises to make the membrane permeable to the small molecule Hygromycin B. We suggest that SAT acts in a viroporin-like way to kill the cell. Furthermore, we could show that a recombinant viral genome that produces an increased amount of SAT is more potent in lysing cells compared to the wild type parvoviral genome. Such a “SUPER” virus might be used in the future for an improved oncolytic therapy with parvovirus.

2 Material and Methods

2.1 Material

2.1.1 Cell lines

- A9 cells, mouse fibroblasts (Tattersall and Bratton, 1983)
- Human embryonic kidney cells 293 (HEK293T) (Pear et al., 1993)

2.1.2 Bacterial strain

E. coli “SURE” e14(McrA), Δ (mcrCB-hsdSMR-mrr) 171, endA1, supE44, thi-1, gyrA96, rel A1, lac, recB, recJ, sbsC, umuC:Tn5(Kanr), uvrC [F⁺proAB, laqI^qZ Δ M15, Tn10(Tetr)]^c (Stratagen, USA)

2.1.3 Viral strands

- MVMp wt
- SAT-ko: MVMp with a knockout of SAT which carries two mutations in its genome (figure 11).

		Start VP2		Start SAT			
MVM-wt:	2787	TCAAACC	ATG	AAGTGA	ATG	GCACCAGCCAACCTGACAG	2823
SAT-Ko:	2787	TCAAACC	ATG	AAGTGA	C	GGCACCAGCCAACCTGACAG	2823
					No start of SAT		
MVM-wt:	2824	CGGAAACGCTGTCCACTCAGCTGCAAGAGTTGAAC					2857
SAT-Ko:	2824	CGGAAACGCTGTCCACTCAGCTGCAAGAG	TAG	AAC			2857
					Stop (ORF of SAT)		

Figure 11: The genome of SAT-ko carries two mutations. The genome area around the start site of VP2 and SAT is depicted. The translational start sites of VP2 and SAT are coloured in orange or blue, respectively. Mutations are depicted in red. The SAT-ko genome carries one mutation that eliminates the start codon of SAT and one additional mutation that induces a translation stop of SAT.

2.1.4 Reagents

● Acrylamide mix	Roth
● Alkaline phosphatase	Roche
● Bacto Agar	BD
● Digitonin	Merck
● Dimethylsulfoxid (DMSO)	SIGMA
● Disuccinimidyl suberate (DSS)	Thermo Scientific
● Dynabeads	Thermo Scientific
● Hoechst 33342 (nuclear stain)	Thermo Scientific
● Midori Green	Nippon Genetics
● Nitrocellulose Blotting membrane 0.45 µm	Amersham
● Perm/Wash buffer	BD
● Photo-leucine	Thermo Scientific
● Pluronic F-127	Thermo Scientific
● Propidium iodide	Thermo Scientific
● Proteinase Inhibitors	Roche
● Proteinase inhibitors (complete Mini)	Roche
● Radioactive methionine	PerkinElmer
● Skim milk powder	Gerbu
● Sodium Green Tetraacetate, cell permeant	Thermo Scientific
● TaqMan Universal PCR Master Mix 2x	Applied Biosystem
● TEMED	Sigma
● Triton X-100	AppliChem
● Tween 20	AppliChem
● Western Lightning Plus-ECL	Perkin Elmer

2.1.5 Antibiotics

● Ampicillin	Agilent Technologies
● Hygromycin B	Thermo Scientific
● Puromycin	Sigma

2.1.6 Antibodies

- | | |
|------------------------------------|--------------------|
| ● Alexa Fluor secondary antibodies | Thermo Scientific |
| ● GAPDH (365062) | Santa Cruz |
| ● GFP (NB600-308) | Novus Biological |
| ● HMGB1 (ab18256) | abcam |
| ● HRP coupled secondary antibodies | Promega |
| ● Myc mouse (9B11) | Cell Signaling |
| ● NS1-c | Self-made antibody |
| ● V5 (2F11F7) | Invitrogen |

2.1.7 Enzymes

- | | |
|------------------------|-------|
| ● EcoRI-HF | NEB |
| ● EcoRV | NEB |
| ● Neuraminidase | Sigma |
| ● NotI | NEB |
| ● Proteinase K | Roche |
| ● Q5 2x Master PCR mix | NEB |
| ● SalI | NEB |
| ● T4 ligase | NEB |
| ● XhoI | NEB |

2.1.8 Kits

- | | |
|----------------------------------|-------------------|
| ● BCA kit | Thermo Scientific |
| ● Duolink | Sigma |
| ● Lipofectamine 3000 | Thermo Scientific |
| ● Megaprime kit | Amersham |
| ● Plasmid Maxi Prep | Qiagen |
| ● Qiamp MiniElute Virus Spin Kit | Qiagen |
| ● QIAprep Spin Miniprep Kit | Qiagen |
| ● QIAquick Gel Extraction Kit | Qiagen |

2.1.9 Solutions

2.1.9.1 Solutions for cell culture

- 2X MEM Gibco
- DMEM Gibco
- DMEM without Methionine/leucine Gibco
- FCS Gibco
- L-Glutamine Gibco
- PBS (137 mM NaCl, 2.7 mM KCl, 8.1mM Na₂HPO₄, 1.15 mM KH₂PO₄, pH 7.3)
- Penicillin-Streptomycin Gibco
- Trypsin-EDTA Gibco

2.1.9.2 Other solutions

- 2X PBS
 - Solution 1: 16 g NaCl, 0.4 g KCl, 800 ml H₂O; Solution 2: 1.33 g KH₂PO₄, 0.62 g K₂HPO₄ x 3H₂O, 200 ml H₂O; mix solution 1 and solution 2
- Digitonin buffer
 - 50 mM Tris-HCl, pH 8.0, 150 mM NaCl, and 5 mM EDTA, 1 % Digitonin, Proteinase inhibitors
- HBSS
 - 50 mM Hepes, 1.5 mM Na₂HPO₄ x 2 H₂O, 280 mM NaCl, 10 mM KCl, 12 mM D(+)-Glucose, pH 7.05
- Hirt extraction buffer
 - 10 mM Tris/HCl pH 7.4, 10 mM EDTA pH 8.0, 0.6 % SDS
- PBS-MK
 - 137 mM NaCl, 2.7 mM KCl, 8.1 mM Na₂HPO₄, 1.15 mM KH₂PO₄ pH 7.3, 1 mM MgCl₂ and 2.5 mM KCl
- VTE
 - 50 mM Tris/HCl, pH 8.7, 0.5 mM EDTA
- RIPA buffer
 - 150 mM NaCl, 10 mM Tris, 1 mM EDTA, 1 % [v/v] NP40, 0.5 % [w/v] Sodium deoxycholate, 0.1 % [w/v] SDS
- Running buffer SDS Page
 - 200 mM Glycin, 25 mM Tris, 0.1 % SDS

- Western blot buffer 1
 - 300 mM Tris, 20 % methanol
- Western blot buffer 2
 - 25 mM Tris, pH 10.4, 20 % methanol
- Western blot buffer 3
 - 40 mM Norleucine, 25 mM Tris
- 10X SSC
 - 1.5 M NaCl, 170 mM $C_6H_5O_7^{3-}$
- Hybridisation buffer
 - 3x SSC, 1 % SDS, 10 x Denhardtts Solution [50 x Denhardtts Solution: 5 % BSA, 5 % Ficoll, 5 % Polyvinylpyrrolidone ad 500 ml H₂O], 5 mM EDTA, 100 ng/ml herring-sperm DNA
- Neutralisation buffer
 - 1.5 M NaCl, 0.5 M Tris/HCl pH 7.2, 1 mM EDTA
- Denaturation buffer
 - 1.5 M NaCl, 0.5 M NaOH
- Washing buffer I
 - 3 x SSC, 1 % SDS
- Washing buffer II
 - 0.3 x SSC, 1 % SDS
- HEPES-buffered saline solution
 - 156 mM NaCl, 2 mM KCl, 2 mM CaCl₂, 1 mM MgCl₂, 10 mM HEPES, 0.001 mM glycine and 15 mM glucose, pH 7.3
- 0 Calcium (Calcium imaging)
 - 156 mM NaCl, 2 mM KCl, 1 mM MgCl₂, 15 mM glucose, 10 mM HEPES
- Control (Calcium imaging)
 - 156 mM NaCl, 2 mM KCl, 1 mM MgCl₂, 2 mM CaCl₂, 15 mM glucose, 10 mM HEPES
- 10K (Calcium imaging)
 - 146 mM NaCl, 10 mM KCl, 1 mM MgCl₂, 2 mM CaCl₂, 15 mM glucose, 10 mM HEPES

2.1.10 Plasmids

- pSar1-dn, pSar1-wt as described in Bär et al. 2013 (Bär et al., 2013)

- pdBMVp (“pMVMwt”) as described in Kestler et al. 1999 (Kestler et al., 1999)
- H1 helper (Kestler et al., 1999)
- pGFP by addgene
- pBS_UF3revYFP (pYFP)

2.1.11 Primer

2.1.11.1 RT-qPCR primer

- Fw: 5'-GCGCGGCAGAATTCAAACT-3'
- Rev: 5'-CCACCTGGTTGAGCCATCAT-3'
- qPCR probe: 5'-6-FAM-ATGCAGCCAGACAGTTA-MGB-3'

2.1.11.2 Mutagenesis primer

- pSUPER
 - SUPER_left_fw: AACCAAGCGCGCTTTTGCAC
 - SUPER_fw: CTGCACAGTAAAGCAGTCAAACCATGGCACCAGCCAACCTGAC
 - SUPER_rev: GTCAGGTTGGCTGGTGCCATGGTTTGACTGCTTTACTGTGCAG
 - SUPER_right_rev: TTTGGTGTCTCTACCTGAAC
- pMyc-SUPER
 - Myc-SUPER_fw: ATGGAACAAAACTCATCTCAGAAGAGGATCTGATGGCATGAC
 - Myc-SUPER_rev: CAGATCCTCTTCTGAGATGAGTTTTTGTTCATGGTTTGACTGC TTTACTGTGCAG
- pMVM-Myc-SAT-wt
 - Myc-wt_fw: CAGTAAAGCAGTCAAACCATGAGTGATGGAACAAAACTCATC
 - Myc-wt_rev: GATGAGTTTTTGTTCATCACTCATGGTTTGACTGCTTTACTG
- pMVM-V5-SAT-wt

- V5-wt_fw:


```
ATGGGTAAGCCTATCCCTAACCCCTCTCCTCGGTCTCGATTCTAC
GATGGCACCAGCCAACCTGAC
```
- V5-wt_rev:


```
CGTAGAATCGAGACCGAGGAGAGGGTTAGGGATAGGCTTACC
CATCACTCATGGTTTGACTGCTTTGCTGTG
```
- N5S
 - N5S_rev: GTTCCGCTGTCAGGGAGGCTGGTG
 - N5S_fw: CACCAGCCTCCCTGACAGCGGAAAC
- SAT_KR48/49AA
 - KR48/49AA_rev: GAATCTATAATGGCGGCGATTATCATAAG
 - KR48/49AA_fw: CTTATGATAATCGCCGCCATTATAGATTC
- SAT_GG31/35LL
 - G3135L_fw: CTCTGCGTGCTAGCTCTGGCGCTGGTGGGGTTG
 - G3135L_rev: CAACCCACCCAGCGCCAGAGCTAGCACCCCCAGAG
- T23A
 - T23A_fw: CAGAGCCTCCAGGGCGGCCAGCTGCTCGTTC
 - T23A_rev: GAACGAGCAGCTGGCCGCCCTGGAGGCTCTG
- E26A
 - E26A_fw: GACGGCCCTGGCCGCTCTGG
 - E26A_rev: CCAGAGCGGCCAGGGCCGTC
- GxxxG/AxxxA
 - G31A/G35A-fw:


```
CTCTGGGGGTGGCCGCTCTGGCCGCCGTTGGGGTTG
```
 - G31A/G35A-Rev


```
CAACCCACCGCCGCCAGAGCGGCCACCCCCAGAG
```
- L33E
 - Fw: CTCTGGGGGTGGGGGCTGAAGCGGGGGTGGGGTTG
 - Rev: CAACCCACCCCGCTTCAGCCCCACCCCCAGAG
- LVFLL38/39/40/41/42AAAAA
 - Fw: GCTGCAGCCGCTGCCGGTCTTATGATAATC
 - REV: GGCAGCGGCTGCAGCCCCAGCCCCGCCAGAG
- F40G
 - F40G_fw: GTTGGTGGGCCTACTGGGTC

- F40G_rev: GACCCAGTAGGCCACCAAC
- M45G
 - M45G_fw: CTGGGTCTTGGCATAATCAAAC
 - M45G_rev: GTTTGATTATGCCAAGACCCAG
- I46G
 - I46G_fw: GTCTTATGGGCATCAAACGC
 - I46G_rev: GCGTTTGATGCCCATAAGAC
- D52A
 - D52A_rev:

AAAGTCGACCTACCCAGCCGTCACCCAAGAGGCTATAATGCGTT

T
- W54G
 - W45G_rev: AAAGTCGACCTACCCAGCCGTCACGCCAGAATC

2.1.11.3 Primer for pNS1, pSAT, pMyc-SAT, pCFP

- pNS1
 - NS1_fw: AAAGCGGCCGCATGGCTGGAAATGCTTACTC
 - NS1_rev: AAAGTCGACTTAGTCCAAGTTCAGCGGCTC
- pSAT
 - SAT_fw: AAAGCGGCCGCATGGCACCAGCCAACCTGAC
 - SAT_rev: AAAGTCGACCTACCCAGCCGTCACCCAAG
- pMyc-SAT
 - MycSAT_fw:

AAAGCGGCCGCATGGAACAAAACTCATCTCAGAAGAGGATCT

GATGGCACCAGCCAACCTGACAG
 - MycSAT_rev: AAAGTCGACCTACCCAGCCGTCACCCAAG
- pSAT-Myc
 - SAT-Myc_fw: AAAGCGGCCGCATGGCACCAGCCAACCTGAC
 - SAT-Myc_rev:

AAAGTCGACCAGATCCTCTTCTGAGATGAGTTTGTGTTCCATCC

CAGCCGTCACCCAAG
- pCFP
 - CFP_fw: AAAGCGGCCGCATGGTGAGCAAGGGCGAGGAG
 - CFP_rev: AAAGTCGACCTACTTGTACAGCTCGTCCATG

- pFlag-SAT
 - MycSAT_fw:


```
AAAGCGGCCGCATGGACTACAAAGACGATGACGACAAGATGGC
ACCAGCCAACCTGACAG
```
 - FlagSAT_rev: AAAGTCGACCTACCCAGCCGTCACCCAAG

2.1.11.4 shRNA primer

- pshRNA2-SAT
 - 2CTCGAGfw:


```
CCGGCTCAGCTGCAAGAGTTGAACTCGAGTTCAACTCTTGCAGC
TGAGTTTTTG
```
 - 2CTCGAGrev:


```
AATTCAAAAACCTCAGCTGCAAGAGTTGAACTCGAGTTCA
ACTCTTGCAGCTGAG
```
- pshRNA6-SAT
 - 6TTCAAGAGAfww:


```
CCGGCTCAGCTGCAAGAGTTGAATTCAAGAGATTCAACTCTTGC
AGCTGAGTTTTTG
```
 - 6TTCAAGAGArevv:


```
AATTCAAAAACCTCAGCTGCAAGAGTTGAATCTCTTGAATTCAAC
TCTTGCAGCTGAG
```

2.1.12 Technical equipment

- | | |
|--|------------------|
| ● ECL Chemocam imager | INTAS |
| ● UV-table for crosslinking N 90 LW 366 | Konrad Benda |
| ● RT-qPCR cycler: realplex 2, Mastercycler ep gradient S | Eppendorf |
| ● Spectrophotometer ND-1000 | NanoDrop |
| ● UV-Transilluminator Gel IX | INTAS |
| ● FACS Guava easyCyte4HT | Merck |
| ● Epifluorescent microscope BZ9000 | Keyence |
| ● Confocal microscope | Leica TCS SP5 II |
| ● Cell Observer.Z1 (time lapse) | Zeiss |

- Ultracentrifuge, Optima LE-80K Beckman
- Diagnostic microscope slides 10 well 6.7 mm diameter Thermo Scientific
- QuickSeal tube Beckmann

2.2 Methods

2.2.1 Construction and production of plasmids

2.2.1.1 Production of pSUPER, pMyc-SUPER, pMVM-Myc-SAT-wt, pMVM-V5-SAT-wt

For the production of the DNA of pSUPER, pMyc-SUPER, pMVM-Myc-SAT-wt and pMVM-V5-SAT-wt chimeric PCRs were conducted. In this assay a mutation, deletion or insertion is inserted into an existing DNA sequence. The assay is depicted in figure 12. First, a left and a right PCR product are made with primers containing a mutation, deletion or insertion. These two products are mixed together and a second PCR is conducted yielding the final PCR product.

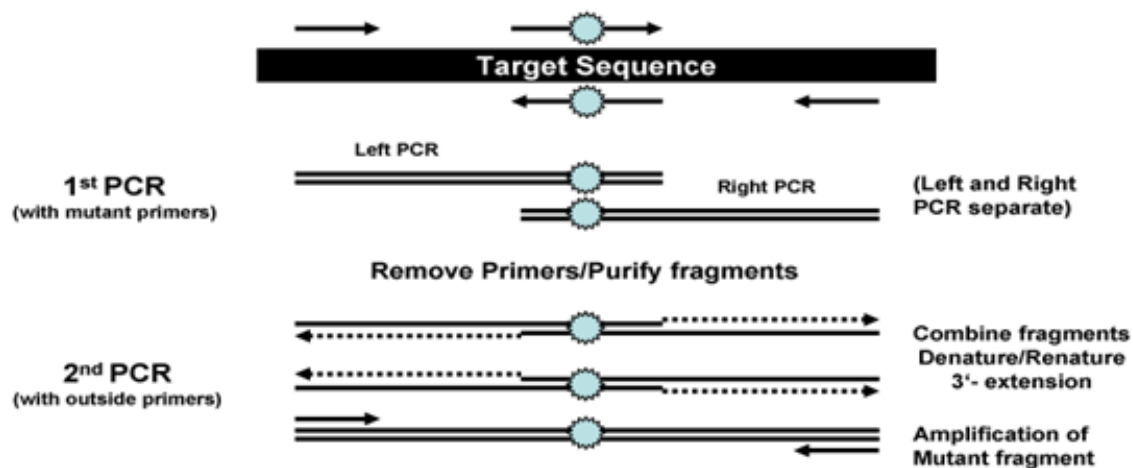


Figure 12: Schematic overview over a chimeric PCR. Blue stars indicate mutations.

The left PCR product was produced using the SUPER_left_fw primer and the SUPER_rev, Myc-SUPER_rev, Myc-wt_rev or V5-wt_rev primer. For the right PCR product the SUPER_right_rev primer together with the SUPER_fw, Myc-SUPER_fw, Myc-wt_fw or V5-wt_fw primer were used. The pMVMwt plasmid containing the whole MVMp genome

was used as a template. Primers, template and the 2X Q5 Master mix were mixed and the PCR program was started. The following list shows the used volumes of the reagents:

- Primer fw (10 μ M) 1.25 μ l
- Primer rev (10 μ M) 1.25 μ l
- DNA template (1 ng/ μ l) 1 μ l
- H₂O 9 μ l
- Q5 2X Master mix 12,5 μ l

The following PCR program was run:

1. 98°C 30 s
2. 98°C 10 s
3. 55°C 30 s
4. 72°C 20–30 s/kb

Repeat steps 2 to 4 35 times.

5. 72°C 2 min

The PCR products were run on a 1 % agarose gel containing Midori Green (1:20,000) and cut out under a UV light. The cut-out DNA fragments were purified using the gel extraction kit (Qiagen). The second PCR was conducted with the PCR products of the first PCR as templates and the primers SUPER_left_fw and SUPER_right_rev.

- SUPER_left_fw 1.25 μ l
- SUPER_right_rev 1.25 μ l
- left PCR product 5 μ l
- right PCR product 5 μ l
- Q5 2X Master mix 12,5 μ l

The same PCR program was used for the second PCR as for the first PCR. The product was run on a agarose gel, cut out and purified as described for the first PCR. The PCR product and 1 μ g of vector DNA (pMVMwt) was cut with the restriction enzyme HindIII (NEB) using the NEB 2 buffer according to the manufacturer's protocol. The digested PCR product was heated to 80°C for 20 min to inactivate the HindIII enzyme. From the vector

DNA the larger fragment was cut out after running it on a 1 % agarose gel and purified as described before. The vector fragment was dephosphorylated using the alkaline phosphatase (Roche) according to the manufacturer's protocol. Afterwards, the dephosphorylated vector and the PCR product were ligated at 16°C overnight. The ligation mixture is listed below:

- PCR product 37.5 ng
- Vector 50 ng
- 10X T4 ligation buffer 2 µl
- T4 ligase 1 µl
- H₂O ad 20 µl

SURE bacteria were transformed with these plasmids.

2.2.1.2 Production of pNS1, pSAT, pMyc-SAT and pCFP

The genes for NS1, SAT, MycSAT and CFP were cloned into the vector pBS_UF3revYFP (pYFP). The vector contains a CMV promoter that regulates the expression of the transgene. The PCR was conducted using the primer pairs SAT_fw and SAT_rev, MycSAT_fw and MycSAT_rev, NS1_fw and NS1_rev, and CFP_fw and CFP_rev. pMVMwt served as a template for NS1, SAT and MycSAT. A CFP-containing plasmid was used as a template for CFP. The mixes were prepared as follows:

- Primer fw (10 µM) 1.25 µl
- Primer rev (10 µM) 1.25 µl
- DNA template (1 ng/µl) 1 µl
- H₂O 9 µl
- Q5 12.5 µl

The following program was run:

1. 98°C 30 s
2. 98°C 10 s
3. 55°C 30 s
4. 72°C 20–30 seconds/kb

Repeat steps 2-4 35 times.

5. 72°C 2 min

The PCR products were run on a 1 % agarose gel containing Midori Green (1:20,000), cut out under UV-light and purified using the gel extraction kit. The PCR products and the vector were cut using NotI (NEB) and SalI (NEB) with the NEB buffer 3 according to the manufacturer's protocol. The PCR products were treated with 65°C in order to inactivate the restriction enzymes. The vector was run on an agarose gel and the larger fragment was cut out and purified using the gel extraction kit. The ligation was conducted as described in chapter 2.2.1.1 "Production of pSUPER, pMyc-SUPER, pMVM-Myc-SAT-wt, pMVM-V5-SAT-wt".

2.2.1.3 Production of plasmids containing mutant versions of SAT

For the production of plasmids of mutant versions of SAT chimeric PCRs were conducted as described in chapter 2.2.1.1 "Production of pSUPER, pMyc-SUPER, pMVM-Myc-SAT-wt, pMVM-V5-SAT-wt". The SAT_fw primer was used with a mutant SAT reverse primer and the SAT_rev was used with a mutant SAT forward primer. pdBMV served as a template. The first and second PCRs were run. The PCR products and the vector were cut using NotI (NEB) and SalI (NEB) with the NEB buffer 3 according to the manufacturer's protocol. The PCR products were treated with 65°C in order to inactivate the restriction enzymes. The vector was run on an agarose gel and the larger fragment was cut out and purified using the gel extraction kit. The ligation was conducted as described in chapter 2.2.1.1 "Production of pSUPER, pMyc-SUPER, pMVM-Myc-SAT-wt, pMVM-V5-SAT-wt".

2.2.1.4 Production of pMVM-Myc-SAT-KR58/59AA, pMVM-Myc-SAT-GG31/35LL, pMVM-V5-SAT-KR58/59AA and pMVM-V5-SAT-GG31/35LL

For the production of pMVM-Myc-SAT-KR58/59AA, pMVM-Myc-SAT-GG31/35LL, pMVM-V5-SAT-KR58/59AA and pMVM-V5-SAT-GG31/35LL the SUPER_fw primer was used together with the mutant reverse primer, and the SUPER_rev primer was used with the mutant forward primer. pMVM-Myc-SAT-wt and pMVM-V5-SAT-wt served as templates. The first and second PCRs were run as described in chapter 2.2.1.1 "Production of pSUPER, pMyc-SUPER, pMVM-Myc-SAT-wt, pMVM-V5-SAT-wt". The PCR products and the vector DNA pMVMwt were cut using HindIII (NEB) with the NEB buffer 2 according to the manufacturer's protocol. The digested PCR product was heated to 80°C

for 20 min to inactivate the HindIII enzyme. From the vector DNA the larger fragment was cut out after running it on a 1 % agarose gel and purified as described before. The vector fragment was dephosphorylated using the alkaline phosphatase (Roche) according to the manufacturer's protocol. Afterwards, the dephosphorylated vector and the PCR product were ligated at 16°C overnight.

2.2.1.5 Production of shRNA

We followed the protocol supplied by Addgene for the construction of shRNAs with the vector pLKO.1 – TRC: <https://www.addgene.org/tools/protocols/plko/>

We used two different hairpin regions for our constructs: CTCGAG and TTCAAGAGA.

2.2.1.6 Transformation of bacteria and production of plasmids

Transformation of SURE bacteria was conducted via heat shock treatment. 50 µl of bacteria were taken from the -80°C freezer and thawed on ice. Bacteria were mixed with a few µl of DNA solution and incubated on ice for 10 min. The bacteria were heated to 42°C for 30 seconds and subsequently chilled on ice for one minute before adding 400 µl LB medium and incubating them at 37°C for 45 min. Bacteria were spun down at 6,000 g for 3 min, 300 µl of supernatant were removed and the remaining LB was mixed with the bacterial pellet. This solution was dispersed onto an agar plate containing 50 mg/l ampicillin. After 24 h of incubation at 37°C colonies were picked from the agar plates. For the analysis of the DNA minipreparation were conducted using the QIAprep Spin Miniprep Kit according to the manufacturer's protocol. The plasmids were sequenced with the sequencing-service of GATC. For the production of larger amounts of DNA, Maxi preparations were conducted using the Plasmid Maxi Prep according to the manufacturer's protocol.

2.2.1.7 Minipreparation and Maxipreparation

Amplification and purification of plasmids was conducted using the QIAprep Spin Miniprep Kit and the Plasmid Maxi Kit from Qiagen. Protocols were conducted according to the manufacturer's instructions. Mini-preparations were eluted in 50 µl millipore water. Pellets of Maxipreparations were dried by removing the remaining ethanol with a glass pipette and a pump and then resuspended in 1 ml millipore water.

2.2.2 Handling of and experimenting with eukaryotic cells

2.2.2.1 Culture of eukaryotic cells

A9 cells and HEK293T cells were cultivated in DMEM containing 10% FCS, 1% Penicillin/Streptomycin and 1% glutamate. Cells were kept in flasks or dishes at 37°C, 5% CO₂, and 95% humidity. Cells were split when they reached confluency using trypsin.

2.2.2.2 Transfection with calcium-phosphate

The standard protocol of calcium-phosphate transfection was modified in order to increase transfection efficiency. The following protocol is described for a 24-well.

560,000 HEK293T cells were seeded in one well of a 24-well dish. The transfection was conducted 5 h later. 2.5 µg DNA were mixed with 4.11 µl CaCl₂ (2M) and filled up to 41.1 µl H₂O. A glass pipette and a pipet boy were used to blow bubbles into the solution. During this process 41.1 µl 2X HBSS was slowly added to the solution. The mixture was vortexed for 5 s and incubated at room temperature (RT) for 7 min before applying the transfection-mix dropwise on top of the medium of the cells. The cells were incubated for 3 h at 37°C. Afterwards, the cells were carefully washed three times with PBS to remove the remaining transfection mix. Fresh growth medium was added to the cells and the cells were incubated at 37°C.

2.2.2.3 Fura-2-AM staining

HEK293T cells were seeded on coverslips in a 24-well dish and transfected 24 h later with Lipofectamine 3000 according to the manufacturer's protocol. The next day cells were treated with Fura-2-AM for 30 min in HEPES-buffered saline solution at RT. The cells were analysed in a perfusion chamber under a fluorescent microscope. Single cells that were positive or negative for GFP-expression were selected for the recording process. Fura-2-AM was excited at 357 nm or 380 nm wavelengths. The fluorescence was measured between 500 nm and 540 nm at a frequency of 0.5 Hz. The change in intracellular [Ca²⁺] is presented as the change in the fluorescence ratio obtained at the two excitation wavelengths (F₃₅₇/F₃₈₀). Averages of fluorescence intensity from somatic regions were chosen for quantification (≈50–80 pixels) and analysed off-line with routines written in Igor Pro

transfection mix was added dropwise to the cells. After two to three days the cells were harvested, pelleted and the cells of ten 15-cm dishes were resuspended in 4 ml VTE. After three freeze-thaw cycles at -80°C and RT the solutions were centrifuged at 1,000 g and the supernatants containing the virus transferred to new tubes. Afterwards, the viruses were purified. The MVMP-wt and SAT-ko viruses were purified with caesium-chloride, the pSUPER and pMyc-SUPER viruses were purified with iodixanol.

For the purification using caesium-chloride, 5 ml CsCl_2 solution (50 g CsCl_2 in 90 ml VTE, $\delta=1.4\text{ g/cm}^3$) was filled in a centrifugation tube. 1 ml saccharose solution (1 M, in VTE) was carefully layered above. 5 ml of virus solution was put on top of the layers. The tube was centrifuged at 30,000 k for 24 h at 10°C . Afterwards, a hole was created at the bottom of the tube using a syringe and the virus was collected in about 25 Eppendorf cups with each cup containing 4 drops of virus solution. The aliquots were measured with a refractometer. Aliquots with a refraction index of 1.44 - 1.39 were pooled. These aliquots contained the full capsids. Afterwards, the virus stock was dialysed using a dialysis chamber. The chamber was placed in 1 l of VTE and incubated at 4°C overnight. The dialysed virus stock was taken out of the dialysis chamber and stored at 4°C .

For the purification using iodixanol, iodixanol was diluted with PBS-MK to 15%, 20%, 40% and 60% solutions. $0.01\text{ }\mu\text{g / ml}$ phenol-red was added to the 20% and 60% solutions. 1.5 ml of each solution was pipetted at the bottom of a QuickSeal tube (Beckmann) in the sequence 15%, 20%, 40% and 60%, the 60% solution being the lowest layer. This gradient was covered with 5 ml virus solution. The tubes were centrifuged at 50,000 rpm in a 50.2Ti-Rotor (Beckman) for 2.5 h hours at 10°C . The 40% iodixanol solution was recovered with a syringe.

2.2.3.2 Plaque assay

To analyse the plaque-forming phenotype plaque assays were performed on 6 cm dishes or 15 cm dishes. In the following paragraph the protocol is described for 6 cm dishes. Numbers in brackets account for 15 cm dishes.

A9 cells were seeded at a number of 250,000 (1,710,000) cells per dish. At the next day, infections were done in a dilution series in a volume of 400 μl (5 ml). The dishes were incubated for one hour at 37°C and slightly tilted in every direction every 10 minutes to

evenly disperse the virus solution over the cells. Afterwards, the virus solution was discarded and 8 ml (30 ml) of a agar cover was mixed by adding 5 ml (18.7 ml) preheated 2xMEM and 3 ml (11.3 ml) preheated 2% agar. After five days 1.41 ml (7.03 ml) 2xPBS, 0.125 ml (0.94 ml) neutral red and 1.41 ml (7.03 ml) preheated 2% agar solution were mixed and added on top of the previous agar cover. The next day plaques were counted. Optionally, the agar covers were removed and the cells were fixed with 4 % paraformaldehyde (PFA).

2.2.3.3 RT-qPCR

RT-qPCR analyses were conducted to count viral genomes. In a first step virus samples were treated with benzonase in order to remove unpackaged viral DNA. 200 μ l virus sample was mixed with 4 μ l benzonase (diluted 1:100 in PBS) and 0.2 μ l 2 M MgCl₂ and incubated for 30 min at 37°C. The viral DNA was then extracted using the MiniElute Virus Spin Kit by Qiagen according to the manufacturer's protocol. The viral DNA was eluted in a final volume of 40 μ l water. For the RT-qPCR a master mix was prepared containing 1.3 μ l forward primer (10 pmol/ μ l), 1.3 μ l reverse primer (10 pmol/ μ l), 1.3 μ l Taqman probe, 23.4 μ l reaction mix (TaqMan Universal PCR Master Mix 2x, Applied Biosystem) and 13 μ l water. 6.7 μ l of sample or standard plasmid was added to 40 μ l master mix and 20 μ l were added to one well of a 96-well PCR plate in duplicate. The standard plasmid was a serial dilution of a plasmid containing pMVM- Δ 800 of a known concentration. The plate was sealed with a transparent adhesive cover and centrifuged 5 min at 3,000 rpm. The cycling conditions are listed below:

Step	Temperature	Time	Number of cycles
#1	50°C	120 s	1
#2	95°C	600 s	1
#3	95°C	15 s	40
#4	60°C	60 s	40

2.2.3.4 Preparation of the radioactive probe

10 µg pMVMwt was digested with EcoRI-HF (NEB) and XhoI (NEB) in NEB buffer CutSmart according to the manufacturer's protocol. After 1 h at 37°C the DNA was separated on a 1.5 % agarose gel containing Midori Green (1:20,000). The band at about 1 kb was cut out and purified using the gel extraction kit (Qiagen). The DNA was radioactively labelled using the Megaprime kit according to the manufacturer's protocol (Amersham).

2.2.3.5 Infectious center assay

In order to conduct an infectious center assay A9 cells were seeded and infected as described in the chapter 2.2.3.2 "Plaque assay". However, the cells were not covered with an agar cover but cultured in growth medium. 24 h post infection supernatants were removed and the cells were washed in PBS. Nitrocellulose filters were placed on top of the cells which transferred the cells to the filters. The filters were taken off the dish and turned on their backside on a whatman paper, cells facing upside. The following steps were conducted in this orientation. The filters were transferred to a Whatman paper that had been soaked with denaturation buffer. After 12 min, the filters were transferred to a Whatman paper that had been soaked with neutralisation buffer and incubated for 12 min. The filters were transferred to a dry Whatman paper and baked at 80°C for 2 h. Filters were incubated in hybridisation-buffer at 65°C for 2 h. The radioactive sample (see chapter 2.2.3.4 "Preparation of the radioactive probe") was added to hybridisation buffer and incubated overnight. Afterwards, the solution was discarded and the filters were washed two times with washing buffer I and one time with washing buffer II at 65°C for 30 min each. The filters were dried on Whatman paper and autoradiography was conducted using an X-ray film.

2.2.3.6 Southern Blot

350,000 A9 cells were seeded on 6 cm dishes and infected 24 h later. After a certain amount of time cells were harvested. The cells were taken up in 1 ml PBS and spun down at 800 g for 6 min. The pellets were lysed in Hirt extraction buffer for 3 min and subsequently treated with 5 µl RNase A (100 µg), gently mixed and incubated for 1 h at 37°C. Proteins were digested by adding 20 µl Proteinase K (10 mg /ml). The solutions were gently mixed and incubated at 37°C for 6 h or longer. 120 µl 5 M NaCl was added and mixed by

inversion. The solution was incubated on ice overnight. Samples were centrifuged at 13,000 rpm at 4°C for 1 h. Supernatants were transferred to a 2 ml Eppendorf cup. 625 µl Phenol/Chloroform/Isoamylalcohol (Ph/C/I) (25/24/1) was added and vortexed for 15 s. Samples were centrifuged at full speed for 10 min at 4°C. The upper water phase was transferred to a new 2 ml Eppendorf cup. The Ph/C/I-extraction was repeated one more time. 1,250 µl ice-cold ethanol (100%) was added and vortexed slowly. The solution was incubated overnight at -20°C. Solutions were centrifuged at full speed at 4°C for 1 h. Supernatants were discarded and the pellet was dried before being resuspended in 100 µl TE (pH 8). The samples were run on a 1% agarose gel in TAE buffer. The gel was treated with denaturation buffer for 30 min and washed in VTE-water. Afterwards, the gel was treated two times with neutralisation buffer for 20 min. Three Whatman papers were equilibrated first in Millipore water and then in 10 x SSC solution. The nitrocellulose membrane was equilibrated in VTE water and 10X SSC. The Whatman papers were placed on a tray, both ends hanging in tanks filled with 10X SSC. The gel was placed upside down on top of the stack of Whatman papers. The nitrocellulose membrane was placed on top of the gel. Another stack of equilibrated Whatman papers was added and a 5-8 cm tall stack of dry paper tissues were placed on top of it. Weights were positioned on top of this stack. The next day the membrane was dried and fixed at 80°C for 2 h. From here on the same steps were conducted as previously described in chapter 2.2.3.5 “Infectious center assay” from the step on following the procedure of 2 h of baking the filter.

2.2.4 Protein analytics

2.2.4.1 SDS-Polyacrylamide electrophoresis (SDS-PAGE)

SDS-PAGE was performed to separate proteins depending on their molecular weight. The gel-chambers were sealed at their bottom with 1% agarose. 10%/12%/15% separating gels were mixed as follows in the given order:

10% Separating gel

1. H ₂ O	4 ml
2. 1.5 M Tris pH 8.8	2.5 ml
3. 30% Acrylamide mix	3.3 ml
4. 10% SDS	100 µl
5. 10% APS	100 µl

6. TEMED	10 μ l
----------	------------

12% Separating gel

1. H ₂ O	3.3 ml
2. 1.5 M Tris pH 8.8	2.5 ml
3. 0% Acrylamide mix	4 ml 3
4. 10% SDS	100 μ l
5. 10% APS	100 μ l
6. TEMED	10 μ l

15% Separating gel

1. H ₂ O	2.3 ml
2. 1.5 M Tris pH 8.8	2.5 ml
3. 30% Acrylamide mix	5 ml
4. 10% SDS	100 μ l
5. 10% APS	100 μ l
6. TEMED	10 μ l

The gels were poured into the chambers and covered with 200 μ l isopropanol. When the gels were solid, the isopropanol was discarded and the stacking gels were mixed as follows:

1. H ₂ O	3.55 ml
2. 0.5 M Tris pH 6.8	1.25 ml
3. 30% Acrylamide mix	0.75 ml
4. 10% SDS	50 μ l
5. 10% APS	50 μ l
6. TEMED	5 μ l

Samples were mixed with 5x Laemmli and heated to 65°C for 5 min. The gels were run at 120-140 Volts.

2.2.4.2 Western Blot

Western Blots were conducted with gels of the SDS-PAGE. Whatman papers were soaked with transfer buffer 1, 2 or 3 according to figure 13. Western blots were run at 25 V and 250

mA for 2 h. The membranes were blocked in 10% milk in PBS for 30 min. Afterwards, the first antibody was added in a 10 % milk in PBS solution and incubated for one hour. The membrane was washed three times with PBS for 3 min. The secondary antibody was added in 10% milk in PBS for one hour. The membranes were washed three times in PBS for 3 min. The membranes were treated with PLUS-ECL solution according to the manufacturer's protocol and analysed in the ECL Chemocam imager.

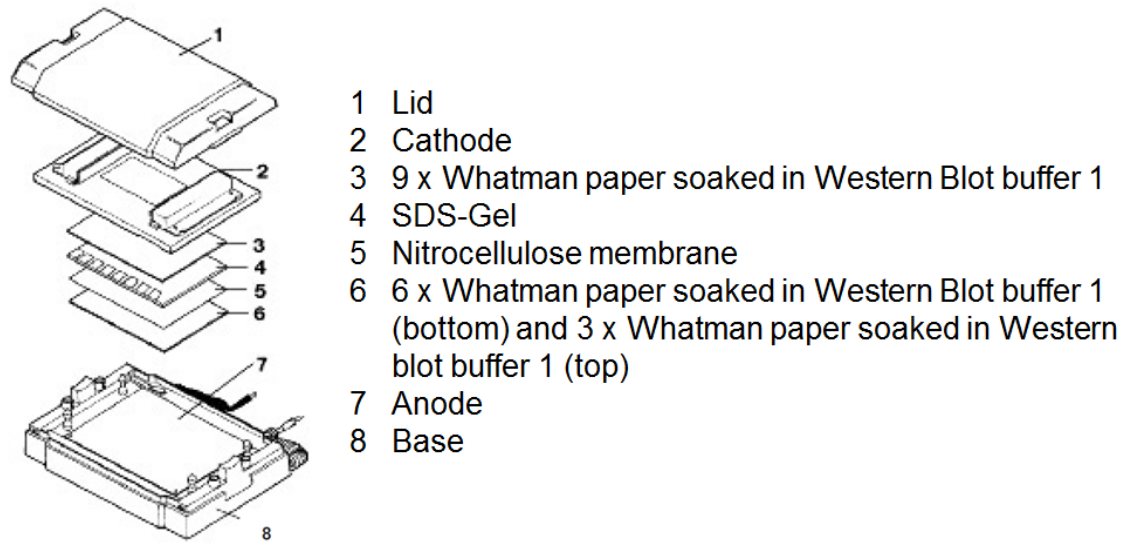


Figure 13: Installation of a Western Blot.

2.2.4.3 Crosslinking of proteins using disuccinimidyl suberate or paraformaldehyde

17,000,000 HEK293T cells were seeded on two 15-cm dishes. 24 h post transfection cells were transfected using calcium-phosphate transfection (chapter 2.2.2.2 “Transfection with calcium-phosphate”). The next day the cells were harvested and washed two times in cold PBS. The cells were divided in aliquots, treated with different concentrations of disuccinimidyl suberate (DSS) or 4% PFA and incubated for 2 h at 4°C. In order to quench the reaction Tris pH 7.5 was added to a final concentration of 20 mM. After 30 min of incubation at 4°C, Triton X-100 was added to a final concentration of 1%. Afterwards the samples were centrifuged at 15,000 g for 15 min at 4°C. The supernatants were transferred to new tubes.

2.2.4.4 Crosslinking of proteins using photo-leucine

The photoreactive amino acid photo-leucine was used in order to crosslink proteins. The amino acid is incorporated in proteins and binds non-specifically with neighbouring molecules under UV-irradiation.

For this experiment 7,000,000 HEK293T cells were seeded on 6 cm dishes. 5 hours later the culture medium was replaced by medium lacking leucine and substituted with 4 mM photo-leucine and dialysed FCS (“photo-leucine medium”). Subsequently, cells were transfected with pMVM-Myc-SAT-wt using lipofectamine 3000 according to the manufacturer’s protocol. After 3 h the transfection mix was removed and fresh photo-leucine medium was added to the cells. After 24 h cells were washed with ice-cold PBS and put on ice in 4 ml of PBS. Cells were then irradiated with UV at a wavelength of 360 nm for 17.5 min. The irradiation time was determined in a pre-experiment according to the manufacturer's protocol. Subsequently, the cells were harvested and lysed in RIPA buffer. Proteins were separated on a SDS-PAGE and transferred to a nitrocellulose membrane in a Western blot. The membrane was stained with antibodies against Myc.

2.2.4.5 Immunoprecipitation

Immunoprecipitations were conducted using the magnetic beads “dynabeads” by Thermo Scientific. The beads are coated with protein G which makes them affine to many kinds of antibodies including mouse and rabbit IgGs. All washing steps were conducted using a magnetic rack to fix the beads in their position.

40 µl of dynabeads were transferred to an Eppendorf cup and the supernatant was removed with the help of the magnetic rack. Antibodies were diluted in 200 µl of PBS with 0.02% tween 20 before adding them to the beads and mixing them by pipetting up and down. The Eppendorf cups were rotated for 20 min. Afterwards, beads were washed two times in PBS with 0.02 % tween 20 and one time in PBS. 500 µl of 500 µg protein were added to the beads and mixed by pipetting up and down. The solutions were rotated for 20 min. The beads were washed three times in PBS. 100 µl PBS was added and the beads were transferred to a new Eppendorf cup in order to remove remaining contaminants. The PBS was removed and the beads resuspended in 16.8 µl of a 50 mM glycine solution (pH 2.8)

and 4.2 μ l 5x Laemmli. Solutions were heated to 65°C for 5 min and afterwards transferred to a SDS-PAGE for further analysis.

2.2.4.6 Hygromycin B Assay

The Hygromycin B assay was performed to analyse the permeability of the plasma membrane of SAT-expressing cells. HEK293T cells were seeded on a 6-well dish with 3,000,000 cells per well. 5 hours later cells were transfected with pYFP and pMVMwt or pSAT-ko using calcium-phosphate. After 24 h 400 μ g/ml Hygromycin B was added to the cells for 30 min. Cells were washed two times with PBS and methionine-deficient medium containing 50 μ Ci [³⁵S] methionine. 10% dialysed FCS and 400 μ g/ml Hygromycin B was added to the cells. Cells were then incubated for 3 h at 37°C under light shaking of the dishes. Afterwards, cells were collected and lysed in RIPA buffer. Immunoprecipitations with an anti-GFP antibody were performed followed by SDS PAGE and Western blot. Irradiation was detected by subjecting an X-ray film to the Nitrocellulose membrane. A graphic illustration of the method can be found in chapter 3.10 “SAT makes the plasma membrane permeable to Hygromycin B”.

2.2.4.7 Immunofluorescence staining

Immunofluorescence studies were conducted on diagnostic microscope slides. Cells were fixed using 4% Paraformaldehyde for 20 min, followed by permeabilization with 0.5% Triton X-100 in PBS for 10 min. After five washing steps in PBS, cells were blocked in 20% FCS in PBS for 30 min. Cells were washed three times in PBS and then incubated with the first antibody in a volume of 20 μ l of 2% FCS in PBS for one hour. The first antibody was removed and the spots were washed six times in PBS. The second antibody was added in 20 μ l 2% FCS in PBS for one hour. The second antibody was removed and the cells were washed six times in PBS. Finally, diagnostic microscope slides were mounted by elvanol and by a cover slip.

For cell surface stainings the cells were put on ice for 10 min. The first antibody was directly added to the medium and mixed by very carefully by pipetting up and down. The cells were washed three times with cold PBS and afterwards fixed in 4% PFA for 20 min. 20% FCS in PBS was added for 20 min before adding the secondary antibody in 2% FCS in PBS. After 1 hour, the cells were washed five times in PBS. If additionally an intracellular staining was

conducted, the cells were permeabilised using 0.5% Triton in PBS. The following steps are outlined in the previous protocol.

2.2.4.8 Proximity ligation assay

Fluorescent staining of protein interactions was achieved using the Duolink proximity ligation kit by Sigma. 10,000 HEK293T cells were seeded on diagnostic microscope slides and transfected the next day using lipofectamine 3000 according to the manufacturer's protocol. The protocol for the proximity ligation assay followed the same steps of a usual fluorescent staining procedure including the incubation of the cells with the first antibody. The following steps were conducted as suggested by the manufacturer.

2.2.4.9 Preparation of samples for FACS

3,000,000 HEK293T cells were seeded on a 6-well dish. 5 h later the cells were transfected using calcium-phosphate. 20 h post transfection, cells were detached using trypsin and collected in 4 ml medium. Cells were spun down at 800 g for 5 min, the supernatant was removed and the pellet was resuspended in ice-cold PBS and transferred to an Eppendorf cup. The following steps were conducted at 4°C and centrifugation steps were carried out at 800 g for 5 min. Cells were spun down and resuspended in 200 µl of 10% FCS in PBS containing the first antibody. After 30 min, cells were pelleted and washed two times in PBS, resuspending the cells at each washing step. The pellet was taken up in 500 µl of PBS and while slowly vortexing, 500 µl of 4% PFA was added dropwise. After 30 min PFA was removed and the cells washed two times in PBS. 10% FCS in PBS was added for 30 min. Then, the secondary antibody (Alexa fluor 488) was added in 10% FCS in PBS for 30 min. The secondary antibody was removed and the cells were washed two times in PBS. Cells were resuspended in 1x BD Perm/Wash buffer (P/W buffer) and incubated for 15 min on ice. Then, the first antibody was added in 200 µl P/W buffer. The next day the first antibody was removed and the cells were washed two times in P/W buffer. Afterwards, cells were treated with the secondary antibody for 30 min and washed twice in P/W buffer. The pellet was taken up in 600 µl PBS and filtered through a nylon mesh. Samples were analysed on a GUAVA 4HT FACS machine.

2.2.5 Preparation and implementation of coarse-grained molecular dynamics simulation

In order to follow potential self-assembly events of putative oligomers of SAT we prepared and implemented a coarse-grained molecular dynamics simulation of 20 initially separated monomers of the full length protein.

As the structure of SAT is unknown, the secondary structure prediction server PredictProtein (<https://www.predictprotein.org/>) (Yachdav et al. 2014) was first used to predict an all-atom structure of the full sequence (residues 1-58). This predicted two helical conformations, the first one from residues 1-28 and the second from residues 32-56. The transmembrane helix was predicted from residues 27-47. The Modeler 9.10v software was used to model the helical conformations using restraints applied in the above-specified regions, using the `automodel.special_restraints()` option and the entire SAT sequence was consequently modelled as a contiguous helix structure. Taking this initial all-atom monomer structure, a grid of 5x4 monomers with a spacing of 5 nm was generated using an internally-developed tcl script in VMD.

The latest version of the MARTINI force-field (MARTINI version 2.2) was used for subsequent coarse-grained (CG) system preparation. The all-atom system consisting of the 5x4 SAT monomer grid was converted to a CG model by using the `martinize.py` script (<http://cgmartini.nl>) with elastic network restraints on backbone atoms with a force constant set to 500 kJ.mol⁻¹.nm⁻². The elastic bond cutoff was set as 0.9 nm for the upper limit and 0.5 nm for the lower limit. The `martinize` script generated the martini topologies for the proteins. The CG protein model was then inserted into a lipid bilayer consisting of 2914 POPC lipid molecules using the `insane.py` script with a box size of 32,27.7 and 15.2, nm in the x,y and z dimensions respectively. The protein-membrane system was then solvated using the MARTINI standard water model (NPW) (Jong et al. 2013) with 72,352 water particles and 60 Na⁺ ions were added to electrically neutralize the system. This generated a complete CG model system consisting of 112,414 particles.

A CG molecular dynamics (MD) simulation was then prepared. All preparatory and production phases of the simulation were carried out using the GROMACS MD software (Gromacs 5.0x). A more detailed description of the general simulation procedure applied is

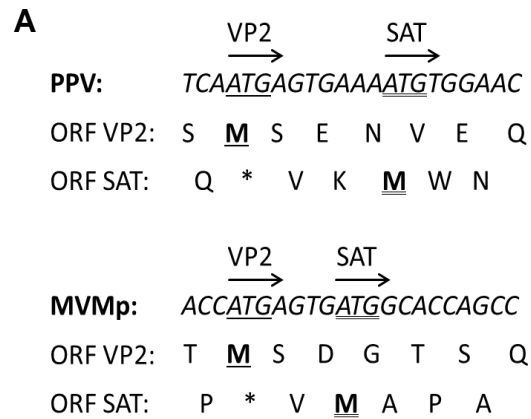
described in (Mustafa et al. 2015). Specifically, the simulation preparation procedure started with steepest descent energy minimization followed by NPT equilibration with a constant temperature of 310 K using a velocity rescale (v-rescale) thermostat. Separate groups were defined for protein, POPC, and solvent for thermostat coupling with a coupling constant of 1 ps. Berendsen weak coupling was used in the initial equilibration step with a coupling constant of 2.0 ps and a reference pressure of 1 bar.

A CG MD production simulation of approximately 1.5 μ s was then performed. During the production simulation, a Parrinello-Rahman barostat with a coupling constant of 12 ps was used. Semi-isotropic pressure coupling was used with a compressibility of 3.0×10^{-5} and the time step was set to 20 fs. As implemented in the new version of Gromacs (Gromacs 5.0x), non-bonded interactions were calculated by the RF (reaction field) approach and cut-off methods when calculating the Coulomb and VDW interactions, respectively. Simulation results were visually analyzed for oligomer formation. Several frames of the simulation (frame 520 and 551) were back-converted to all-atom models using the backward.py script in MARTINI in order to inspect various interactions at the atomic level.

3 Results

3.1 Sequence comparison of SAT between MVMp - PPV

Both MVMp and PPV belong to the group of autonomous replicating parvoviruses and share a common genomic structure. Zádori and coworkers showed that PPV expresses the small protein SAT in an alternative reading frame within the coding sequence of VP2. By sequence comparison they found a similar genomic pattern in MVMp and other Protoparvoviruses. In MVMp the *SAT*-gene is 177 bps long and starts four base-pairs after the start codon of VP2 (figure 14A). A global alignment of the SAT proteins of MVMp and PPV showed a sequence identity of 30.3% and a sequence similarity of 39.5% (figure 14B). Both protein sequences contain a section of highly hydrophobic residues. Since the SAT protein of PPV was found to be located within membranes we used the TMHMM Server v. 2.0 to predict transmembrane helices in SAT (Figure 14C). The SAT proteins of MVMp and PPV were predicted to harbour a single transmembrane helix. The N-terminal part of SAT was predicted to be located outside, the C-terminal part inside. For the SAT protein of PPV this orientation was predicted to be reversed. However, the developers of the prediction tool advise the users of the tool that the quality of the predicted orientation of single-pass transmembrane helices might be questionable.

**B**

MVMp SAT: -MAPANLTAETLSTQLQELNEQLTALEALGVG-ALAGV----GLVFLGLMIKRIIDSWVTAG-----
|...:|...||:| |||| |:||| |||.|.|.|||:..:|.|.|.

PPV SAT: MWNNNTLLMQALNCLQQEMN-----LGVGAAVAGVGLGGLVCLQVLSIIKQNFNTWGRAWLESLHTHQDSYI

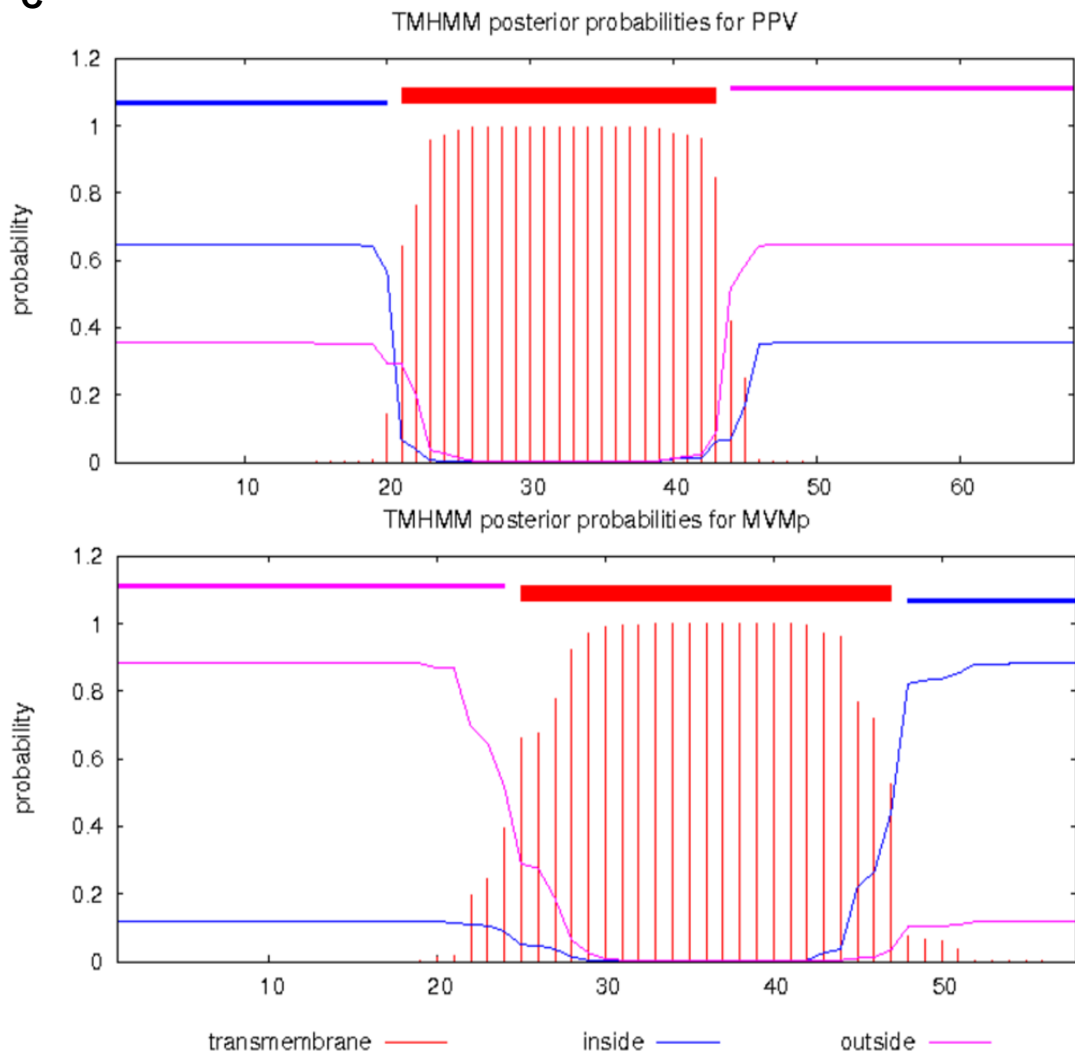
C

Figure 14: Sequence-comparison of SAT in the porcine parvovirus (PPV) and prototypic minute virus of mice (MVMp) (A) Transcription start site of VP2 and SAT in the PPV and the MVMp. The genomic sequence is written in italic. The amino acid sequence for the open reading frame (ORF) of VP2 and SAT is written below in roman. The transcription and translation start sites of VP2 and SAT are underlined with a single or a double line, respectively. (this figure was adapted from Zádori et al. 2005) (B) Global sequence alignment of SAT of PPV and MVMp. The EMBOSS Needle algorithm for a pairwise sequence alignment was used. The BLOSUM62 scoring matrix was used with a gap open penalty of 10, a gap extend penalty of 0.5 and no gap end penalty. (C) Prediction of transmembrane helices in SAT of PPV and MVMp. The TMHMM Server v. 2.0 was used to predict transmembrane helices. The x-axis shows the amino acid number, the y-axis shows the probability of a transmembrane helix. The pink and blue curves show the probability of the non-transmembrane regions to be outside or inside the cytoplasm, respectively.

3.2 The SAT-knockout virus produces smaller plaques than the wild type virus

SAT of PPV was shown to be involved in the lytic process and the spreading of progeny viruses (Mészáros et al., 2017). In order to determine these features for MVMp, SAT-knockout (SAT-ko) viruses were produced which carried two mutations that blocked the translation of SAT (figure 15A). These mutations did not affect the integrity of VP2. Plaque assays were performed with A9 mouse fibroblasts. The plaques formed by the SAT-ko virus were significantly smaller than plaques formed by the wild type MVMp virus (MVM-wt) which implies a reduced spreading capacity of the SAT-ko virus (figure 15B, 15C). Next, we titrated the MVM-wt and SAT-ko virus in an RT-qPCR and in an infectious center assay (ICA) (figure 15D, table 1). For the RT-qPCR, viral genomes were extracted from viral stocks and a Taqman RT-qPCR was conducted with primers against the *NS1*-gene. For the ICA, A9 cells were seeded and infected with the two different viruses. 24 h post infection, the cells were fixed and stained with a radioactive probe against the *NS1*-gene. An autoradiograph revealed the number of *NS1*-positive cells. When the two obtained titers were analysed, the ratio of infectious particles to viral genomes revealed that the infectivity of the SAT-ko virus was reduced. We assumed that the titer obtained by the plaque assay was deceiving. Some plaques of the SAT-ko virus might have been too small to see them with the naked eye and therefore we think that only a fraction of the plaque forming units could be counted for this mutant virus using this method. In order to circumvent this limitation, we used the titer obtained by the ICA for infecting cells in the subsequent experiments.

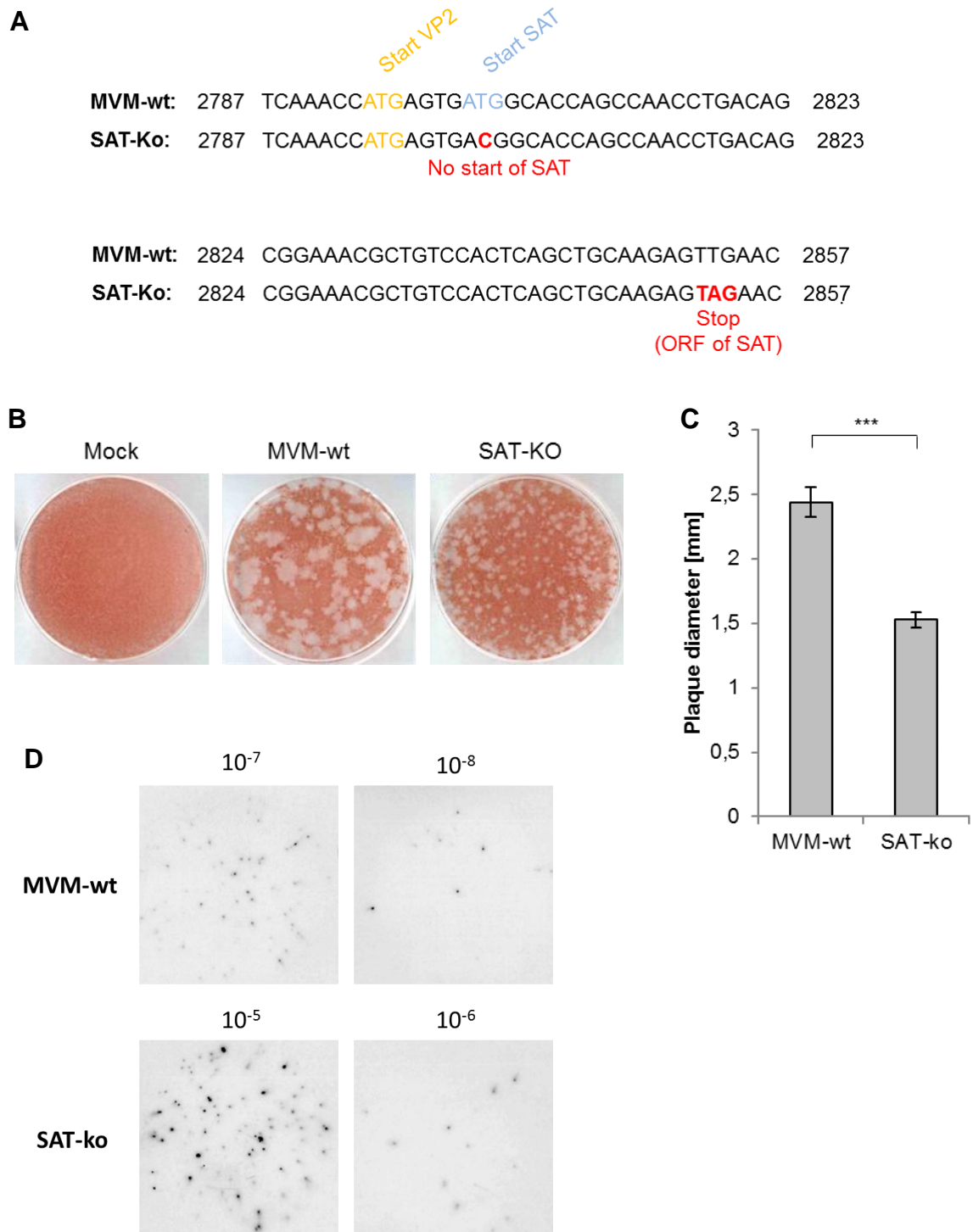


Figure 15: Infections with the SAT-ko virus lead to the formation of small plaques. (A) Comparison of the genomes of wild type and SAT-ko. The translation initiation sites are coloured in orange and blue, respectively. The two mutations in the SAT-ko are coloured in red. (B/C) Comparison of plaque sizes in MVM-wt- and SAT-ko-infected A9 cells. Standard plaque assays were conducted and the cells were fixed with 4% PFA. Photos were taken of 6 cm dishes (B) and plaque diameters counted for 100 plaques on 15 cm dishes (C). *** $p < 0.001$ as calculated by two sample t-test. (D) An infectious center assay with MVM-wt virus and SAT-ko and different virus dilutions was conducted. A sequence of the *NS1*-gene served as a radioactive probe.

Table 1: The SAT-ko virus shows a reduced ICA/qPCR titer. The titer of the MVM-wt virus and SAT-ko virus was assessed by RT-qPCR. The ratio of the titers acquired by the ICA and the RT-qPCR was calculated.

	ICA [infectious centers/ml]	RT-qPCR [genomes/ml]	Ratio ICA / qPCR
MVM-wt	3.00×10^9	4.08×10^{11}	73.5×10^{-4}
SAT-ko	4.50×10^7	1.11×10^{11}	4.1×10^{-4}

3.3 The SAT-ko virus is not inhibited in its replication

The reduced plaque size of SAT-ko suggests that the virus was defective in a crucial step of its life cycle. The ICA, that utilised a probe against the *NS1*-gene, did not show significant differences between wt- and SAT-ko-infected cells regarding the size of the dots seen in the autoradiograph. Therefore, we assumed that the SAT-ko virus had no defect in its DNA replication. A potential defect in its replicating ability would have led to a reduced copy number of *NS1* and subsequently to a reduced size of the dots seen in the autoradiograph. To confirm this hypothesis, we conducted a Southern blot analysis. A9 cells were infected with SAT-ko or MVM-wt virus at an MOI of 0.01, 0.1 or 1 and harvested after 24 h, 48 h or 72 h. The lysates were subjected to a Southern blot and analysed with a radioactive probe against the *NS1*-gene (figure 16). By this approach the different forms of the viral genome should become visible as distinct bands (see chapter 1.6.2 “The replication process”). The autoradiograph showed that viral replication was taking place in the SAT-ko- and the MVM-wt-infected cells. At 24 h the monomeric, dimeric and tetrameric replicative DNA-forms were clearly visible. Differences between SAT-ko and MVM-wt-infected samples were small except for the lowest MOI of 0.01. At 48 h and 72 h the monomeric and dimeric form of the SAT-ko virus were very strong, whereas the bands in the MVM-wt-infected cells became weaker, probably due to the massive cell death that had already occurred in these samples.

It should be mentioned that under the conditions how the DNA preparations were performed no visualisation of the single-stranded (ss) viral DNA was possible. The ssDNA

indicates that progeny viruses are produced since this form of parvoviral DNA only exists in encapsidated virions. This form was most likely lost during the DNA purification processes, which is frequently seen for MVMp. Nevertheless, the monomeric, dimeric and tetrameric forms demonstrate that viral DNA amplification was taking place in the SAT-ko-infected cells. Additionally, the plaque assay implied that progeny viruses of SAT-ko were formed since the formation of small plaques was observed.

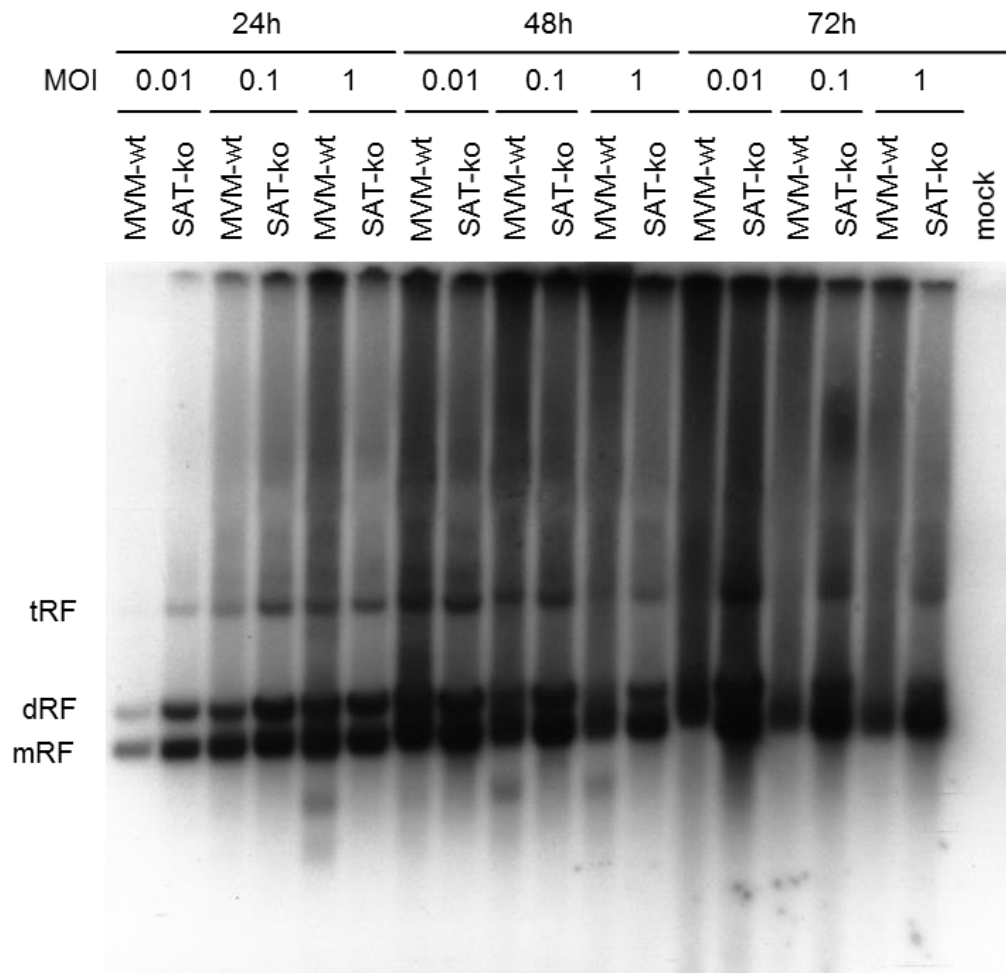


Figure 16: The SAT-ko virus replicates in A9 cells. A9 cells were infected with MVM-wt virus or SAT-ko virus for 24 h, 48 h and 72 h with an MOI of 0.01, 0.1 or 1 or mock-infected for 72 h. A Southern blot analysis was conducted using a probe against the *NS1*-gene. The monomeric, dimeric and tetrameric replicative forms are indicated (mRF, dRF, tRF, respectively).

3.4 The spreading capacity of the SAT-ko virus is restrained

The results of the plaque assay suggested that the SAT-ko virus was inhibited in its spreading capacity. In order to test this hypothesis, A9 cells were infected with MVM-wt or SAT-ko virus with an MOI of 1. 4 h, 24 h and 48 h post infection viral genomes were isolated from infected cells and their supernatants and the genomes were counted using RT-qPCR. Neuraminidase was added after 6 h to inhibit reinfections. This enzyme cuts off sialic acid moieties from cell surface proteins including the receptor for MVMp which inhibits MVMp from binding to it (figure 17A). At 4 h post infection about ten times more viral genomes of SAT-ko virus was seen inside the cells compared to the MVM-wt-infected cells underscoring the reduced infectivity of the SAT-ko virus. After 24 h SAT-ko- and MVM-wt-infected cells comprised almost the same number of viral genomes. However, the supernatant of MVM-wt infected cells carried ten times more viral genomes than the supernatant of SAT-ko infected cells. After 48 h the number of released viruses was about the same for MVM-wt- or SAT-ko-infected cells. The SAT-ko virus seemed to be inhibited in its ability to spread while the replication of the genome stayed unaffected. The experiment was also conducted with an MOI of 0.1 which led to a similar result (figure 17B).

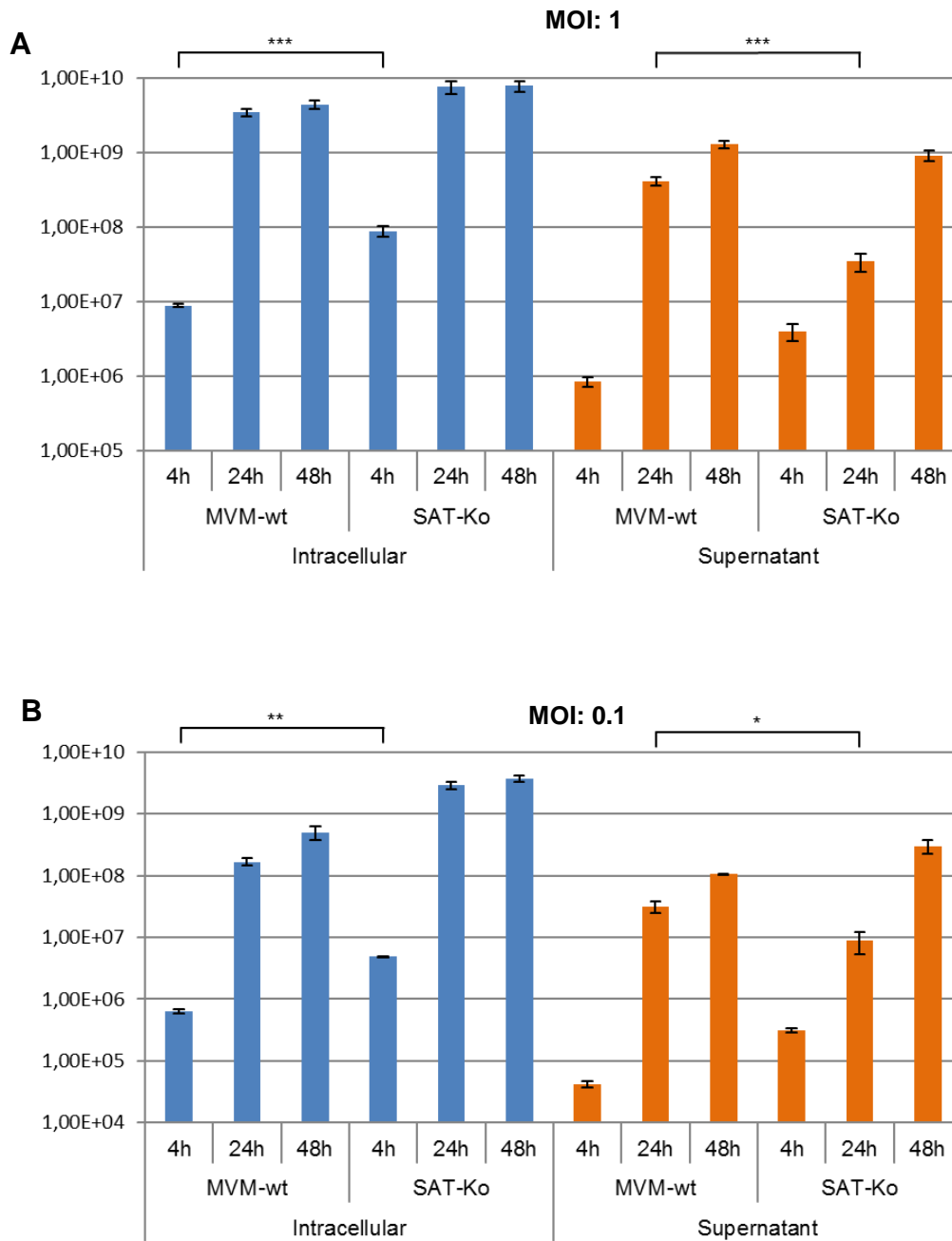


Figure 17: The release of progeny viruses is inhibited in SAT-ko-infected cells. A9 cells were infected with MVM-wt or SAT-ko with an MOI of 1 (A) and 0.1 (B). After 4 h, 24 h and 48 h cells and their supernatants were harvested and quantitatively analysed for viral genomes using RT-qPCR. * $p < 0.05$, ** $p < 0.01$, *** $p < 0.001$ as calculated by two sample t-test.

3.5 A knockout of SAT decreases the lytic activity of MVMp and inhibits the release of HMGB1

The knockout of SAT was shown to reduce the spreading capacity of the virus. For PPV it was suggested that this phenotype was caused by a reduced lytic potential of the mutant virus. Without SAT the cell would not be lysed and therefore the progeny viruses would be trapped within the cell and would not be released from it (Mészáros et al., 2017). In order to test if SAT of MVMp acts in the same lytic way, A9 cells were infected with either MVM-wt or SAT-ko virus with an MOI of 0.1 and stained for dead cells using PI after 24 h, 48 h or 72 h (figure 18A). The SAT-ko virus showed a reduced lytic potential especially after 48 h and 72 h. Even after 24 h slight differences in the amount of dead cells could be observed between MVM-wt- and SAT-ko-infected cells. The experiment was also conducted with an MOI of 0.01 and 1 which led to similar results.

To confirm that the SAT-ko virus was not inhibited in its expression of NS1, A9 cells were infected with different MOIs of MVM-wt or SAT-ko virus and harvested after 16 h, 24 h, 48 h or 72 h. The lysates were analysed for NS1 expression in a Western blot. MVM-wt- and SAT-ko-infected cells showed similar levels of NS1 accumulation (figure 18B).

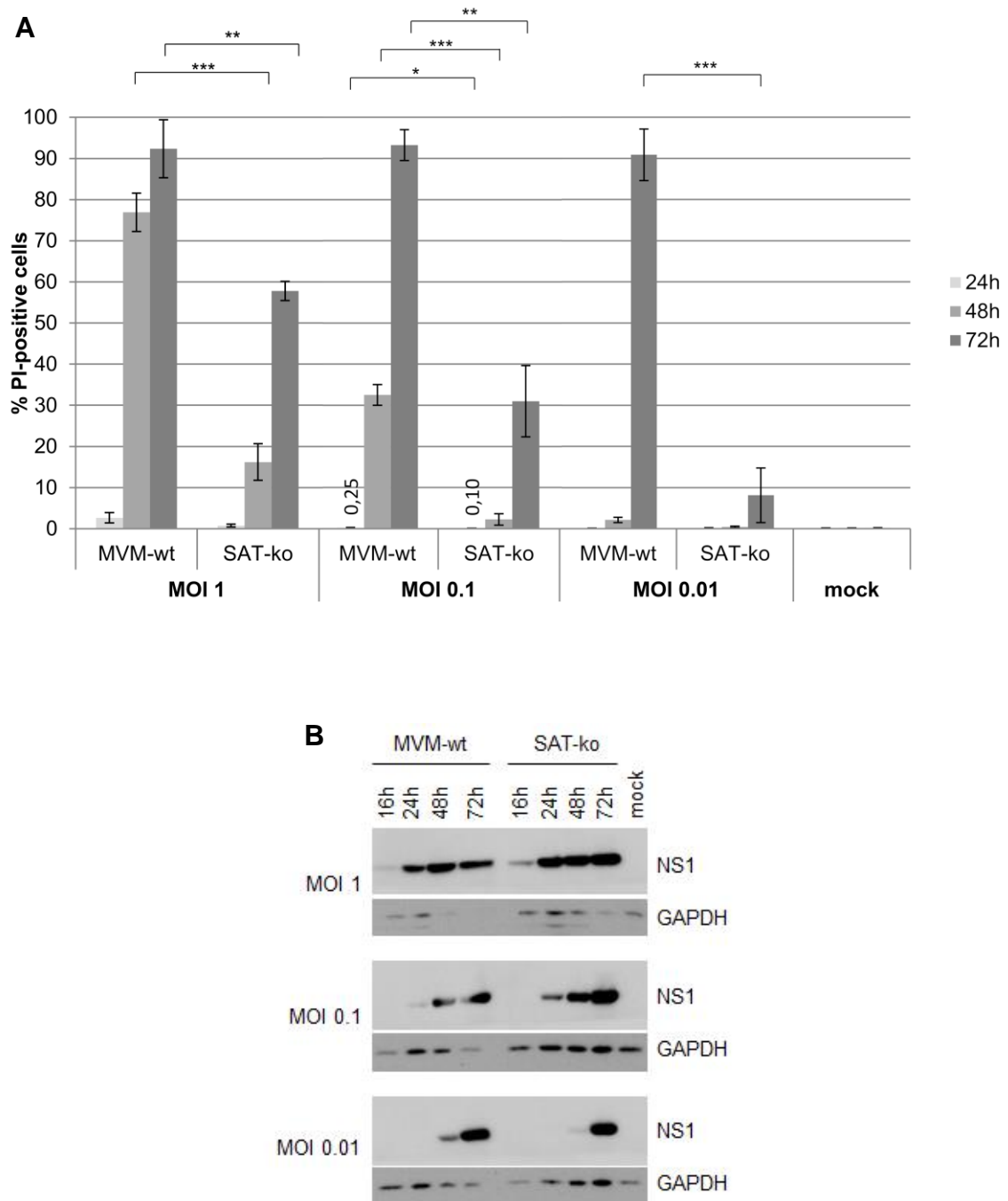


Figure 18 Cell-lysis is reduced in SAT-ko-infected cells while the expression of NS1 is similar to MVM-wt-infected cells. **(A)** A9 cells were infected with MVM-wt- or SAT-ko-virus with an MOI of 1, 0.1 or 0.01 or were mock-infected for 24 h, 48 h or 72 h. Dead cells were stained with PI and counted under the microscope. Hoechst 33342 was used for counterstaining. * $p < 0.05$, ** $p < 0.01$, *** $p < 0.001$ as calculated by two sample t-test. **(B)** A9 cells were infected with MVM-wt- or SAT-ko-virus with an MOI of 1, 0.1 or 0.01 for 16 h, 24 h, 48 h or 72 h or mock-infected for 72 h. Cell lysates were analysed on a Western blot with antibodies against NS1 and GAPDH.

Furthermore, we wanted to test if the knockout of SAT affects the immunogenic features of the virus. In oncolytic therapy a strong immunogenic response of the patient is desirable.

The cellular protein HMGB1 can give a first hint towards this question. HMGB1 is usually located in the nucleus and binds DNA non-specifically (Janko et al., 2014). During necrosis HMGB1 is released from the cells and acts as an immunostimulatory signal to trigger inflammation (Rovere-Querini et al., 2004; Scaffidi et al., 2002). A9 cells were infected with MVM-wt or SAT-ko and 24 h and 48 h later the cells and the supernatants were collected and analysed in a Western blot with antibodies against HMGB1 (figure 19). The release of HMGB1 was stronger in the MVM-wt-infected cells compared to the SAT-ko-infected cells which underscores the importance of SAT in the release of HMGB1.

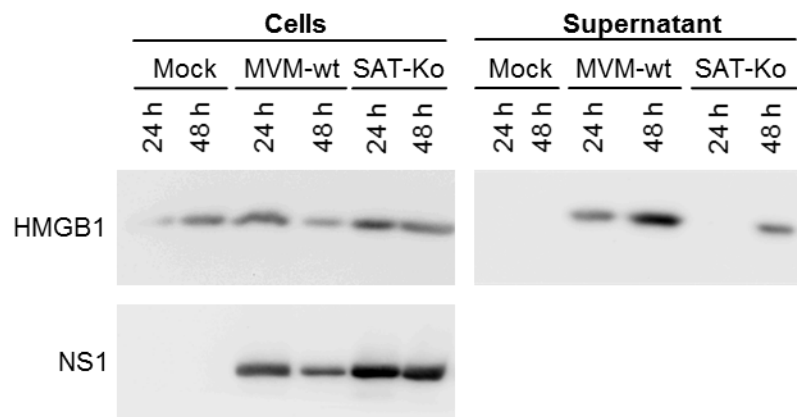


Figure 19: MVM-wt-infected cells release greater amounts of HMGB1 than SAT-ko-infected cells. A9 cells were infected with MVM-wt or SAT-ko. 24 h and 48 h post infection supernatants and cells were harvested and analysed on a Western blot with antibodies against NS1 and HMGB1.

3.6 The SAT protein has a higher lytic potential than NS1

The knockout of SAT in MVMp led to a strong reduction of its capacity to lyse cells and subsequently it led to a reduced spread of progeny viruses. A similar phenotype was observed for the SAT-knockout in PPV. However, it is noteworthy that the expression of NS1, which has been frequently reported in the past to have cytotoxic activities, was not inhibited in the SAT-ko virus. Still, only a small number of cells were lysed after infection with the SAT-ko virus. The striking difference in the lytic abilities of MVM-wt and SAT-ko led us to directly compare the lytic capacity of NS1 and SAT. To this end, the *NS1*-gene or the *SAT*-gene were cloned into an expression vector under the control of a CMV-promoter (pNS1, pSAT, respectively). The constructs were transfected into HEK293T cells. 24 h post transfection lysed cells were stained with PI and counted under the microscope. As a non-toxic control, cells were transfected with the expression vector containing the sequence for

CFP under the control of a CMV-promoter (pCFP). CFP also served as a marker for the amount of transfected cells (figure 20A). Transfection of pSAT induced a strong lytic effect. About 20% of the cells were PI-positive. pNS1-transfected cells were indistinguishable from pCFP-transfected cells regarding the amount of PI-positive cells. Even after 48 h and 72 h the amount of dead cells after pNS1-transfection did not significantly increase (data not shown). In order to confirm the expression of NS1 and SAT, transfected cells were lysed and analysed on a Western Blot for protein expression. Since no antibody for SAT was available, the *SAT*-gene was tagged with the Myc-epitope (Myc-SAT) (figure 20B). pNS1 and pMyc-SAT showed robust levels of protein expression. The two bands of SAT were likely a result of a glycosylation event, since the mutation of a putative glycosylation site in the N-terminus of SAT eliminated the upper band in a Western blot (Supplementary figure 1). It is noteworthy, that the transfection of HEK293T cells with pMyc-SAT killed even more cells than the native pSAT. We believe that the Myc-tag might have a stabilising effect on the SAT protein. The experiment showed that the sole expression of SAT had a strong lytic effect on cells, even in the absence of any other parvoviral factor.

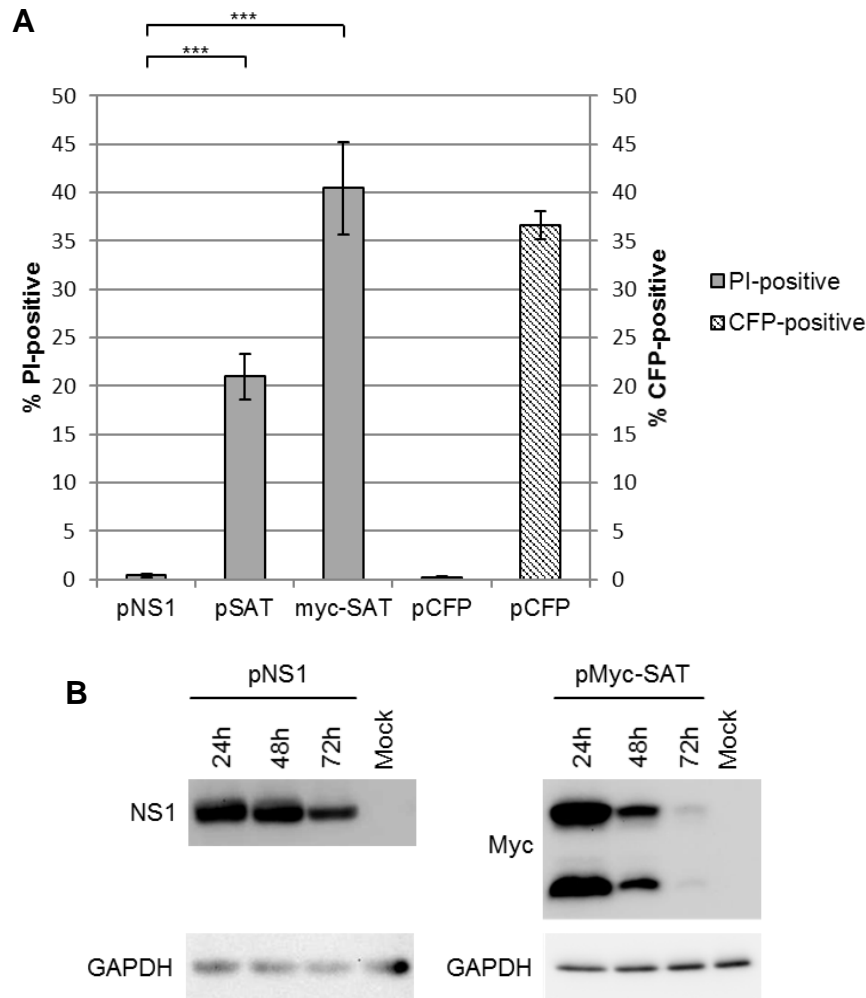


Figure 20: The SAT protein is more potent in killing cells than NS1. **(A)** HEK293T cells were transfected with pNS1, pSAT, pMyc-SAT or pCFP. 24 h post transfection dead cells were stained with PI and counted under the microscope. Hoechst 33342 was used as a counterstaining. CFP-positive cells were counted as well. *** $p < 0.001$ as calculated by two sample t-test. **(B)** HEK293T cells were transfected with pNS1 or pMyc-SAT for 24 h, 48 h or 72 h. Cell lysates were analysed on a Western blot using antibodies against NS1, Myc and GAPDH.

3.7 The SAT protein of MVMp is transported to the plasma membrane and its lytic potential depends on this transport

Mészáros and coworkers already showed that the SAT protein of PPV is located in the ER and they suggested that it confers its lytic capacity by inducing an irreversible stress in the endoplasmic reticulum (Mészáros et al., 2017; Zádori 2009). We wanted to test if the SAT protein of MVMp is transported from the ER to the plasma membrane and if this transport is involved in cell lysis. To this end, plasmids were produced carrying the Myc sequence

fused to either the 5'- or the 3'-end of the *SAT*-gene (pMyc-SAT or pSAT-Myc, respectively). The constructs were transfected into HEK293T cells. After 24 h living cells were stained with a Myc-antibody and a fluorescent secondary antibody. This staining-approach allows the potential detection of the Myc-epitope at the surface of the cells since the antibodies used for the detection cannot enter living cells under the chosen conditions. Afterwards, the cells were fixed in 4% PFA, permeabilized and stained again with a Myc-antibody and a fluorescent secondary antibody (figure 21). This approach makes the intracellular and extracellular distribution of Myc-SAT and SAT-Myc visible. pSAT-Myc-transfected cells showed an intracellular localisation of SAT-Myc whereas cells transfected with pMyc-SAT were additionally stained at the plasma membrane. Myc-SAT seems to be transported to the plasma membrane and its N-terminus is likely to be located extracellularly while its C-terminus lies within the cell.

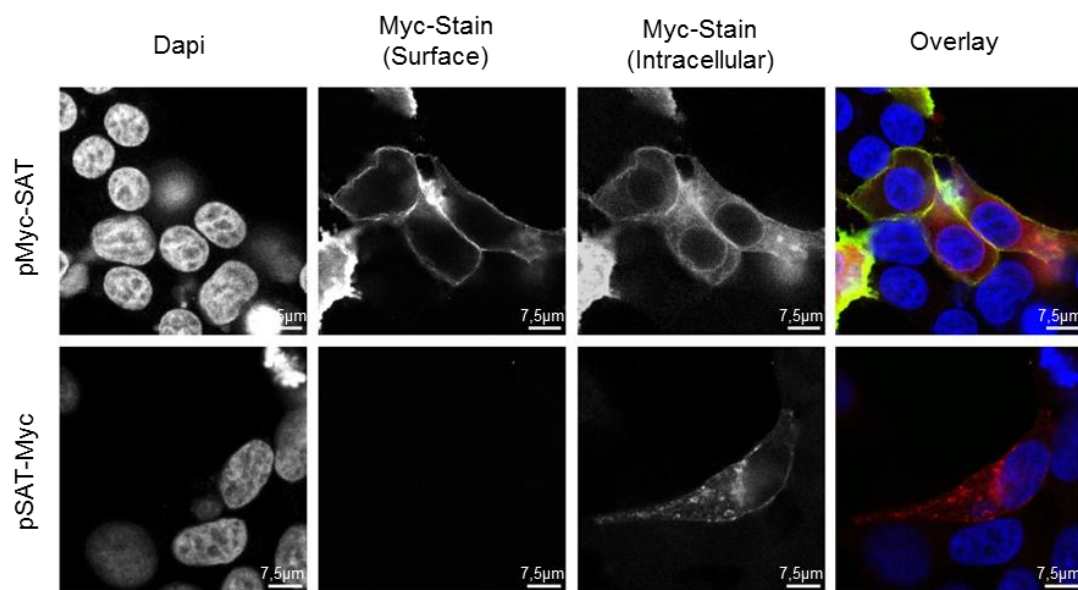
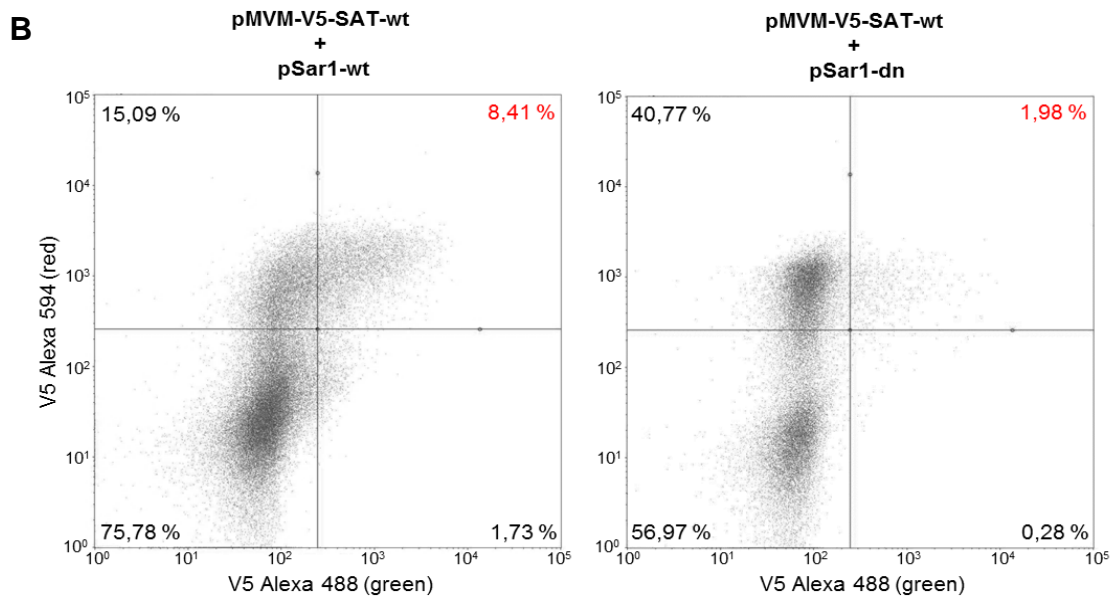
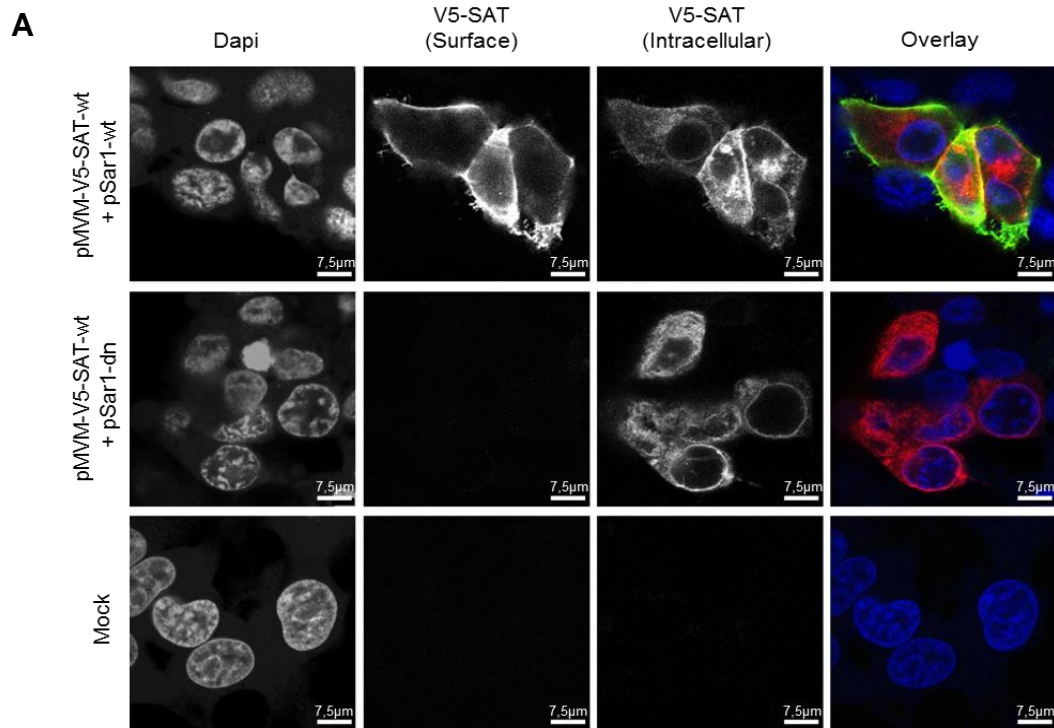


Figure 21: Myc-SAT is transported to the plasma membrane. HEK293T cells were transfected with plasmids encoding for SAT which was N- or C-terminally fused to the sequence of Myc (pMyc-SAT, pSAT-Myc, respectively). 24 h post transfection live cells were stained with Myc-antibodies and secondary antibodies coupled to Alexa 488 (Surface). Subsequently, cells were fixed, permeabilised and stained with Myc-antibodies and secondary antibodies coupled to Alexa 594 (Intracellular). Dapi was used for nuclear staining. Images were taken with a confocal microscope.

We wanted to further investigate if the transport of SAT to the plasma membrane correlates with its lytic potential. To this end, the *SAT*-gene within the viral genome was fused to the sequence of the V5 epitope (pMVM-V5-SAT-wt). These constructs were co-transfected with plasmids expressing dominant negative Sar1 (pSar1-dn) or its wild type counterpart

(pSar1-wt) into HEK293T cells. In both cases the sequences of *Sar1*-wt and *Sar1*-dn were fused to the sequence of the Myc-epitope. Sar1 is involved in the vesicular transport of cargo proteins from the ER to the Golgi. This small GTPase is part of the COPII complex which orchestrates the formation and cargo-loading of budding vesicles from the ER (UniProt: the universal protein knowledgebase; accession number Q9NR31). Sar1 binds GTP and releases GDP to exert its function. The dominant negative form of Sar1 carries a mutation in its nucleotide-binding site at position K38 (K38M) and is therefore inhibited in its function. In the past this mutant was already shown to reduce the vesicular transport from the ER to the plasma membrane. In these experiments the secretion of Gaussia luciferase from transfected cells was strongly inhibited by this mutant (Bär et al., 2013).

Live cells were first stained with V5-antibodies and fluorescent secondary antibodies, subsequently permeabilized and stained with V5-antibodies and fluorescent secondary antibodies again. Cells were then analysed in IF and FACS. As shown in figure 22A, B and C transfection of pSar1-dn clearly reduced the surface translocation of V5-SAT. Next, HEK293T cells were co-transfected with pMVM-V5-SAT-wt and pSar1-dn or pSar1-wt. 24 h post transfection the amount of dead cells was analysed (figure 22 D). Co-expression of Sar1-dn strongly reduced the lytic potential of V5-SAT. These data indicate that the translocation of V5-SAT to the plasma membrane is a crucial process for the induction of cell lysis.



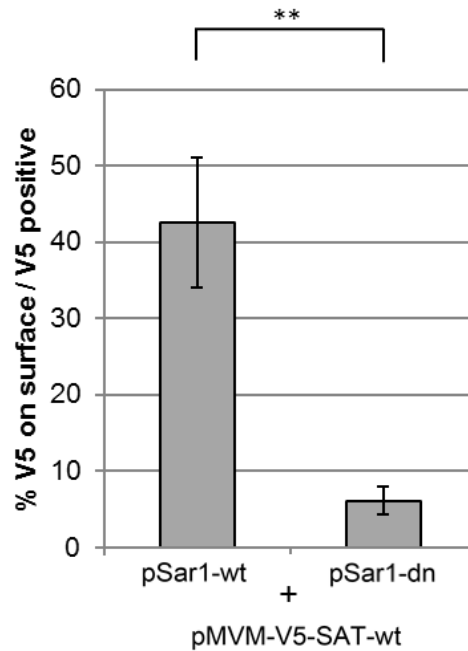
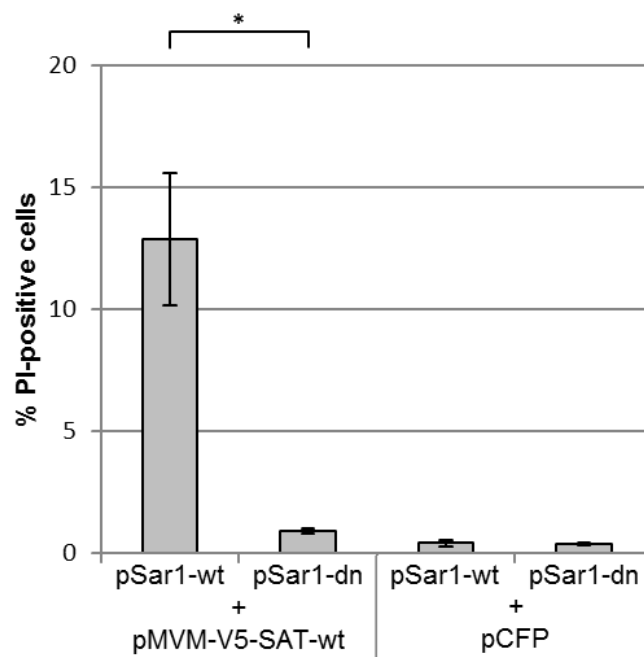
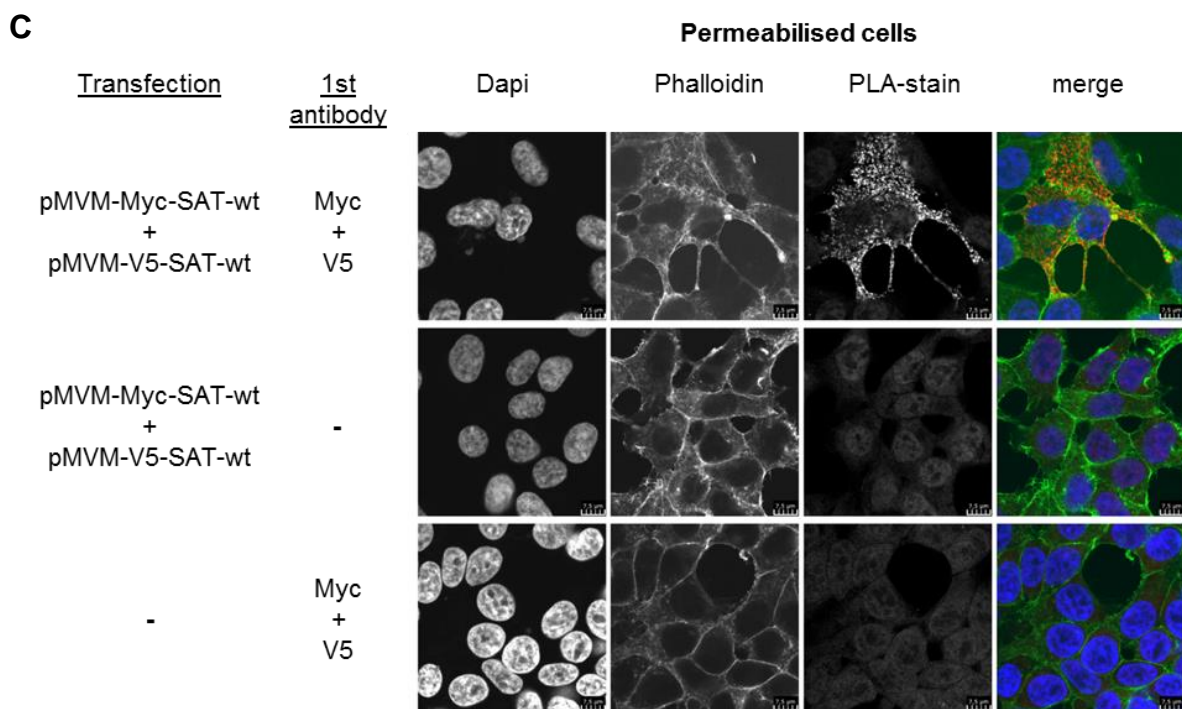
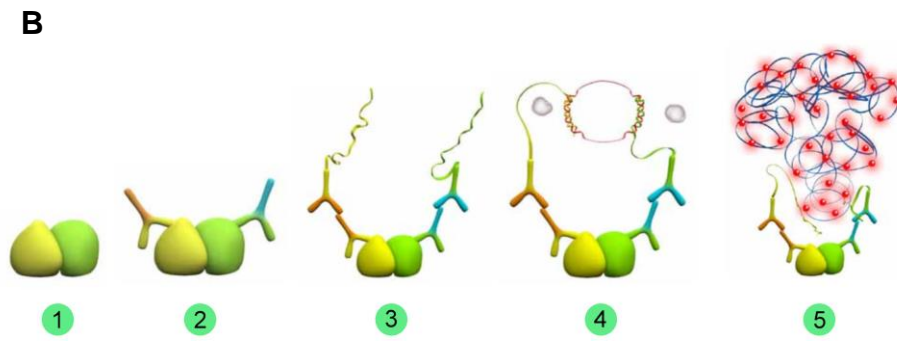
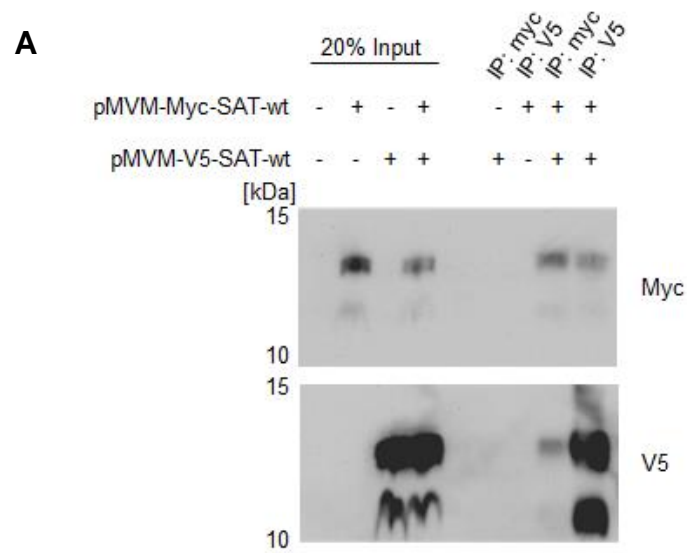
C**D**

Figure 22: The transport of SAT to the plasma membrane is essential for its lytic property. (A/B/C) Sar1-dn reduces the transport of V5-SAT to the plasma membrane. HEK293T cells were co-transfected with pMVM-V5-SAT-wt and pSar1-dn or pSar1-wt. 24 h post transfection live cells were stained with V5-antibodies and secondary antibodies coupled to Alexa 488 (Surface (A) / V5-Alexa 488 (B)). Subsequently, cells were fixed, permeabilised and stained with V5-antibodies and secondary antibodies coupled to Alexa 594 (Intracellular (A) / V5-Alexa 594 (B)). (A) Cells were stained with DAPI and analysed under a confocal microscope. (B) Cells were analysed with a FACS machine. (C) The ratio between the number of cells that were positive for V5 on their surface and the number of cells that were positive for V5 intracellularly and on their surface was calculated. (D) HEK293T cells were co-transfected with pMVM-V5-SAT-wt or pCFP and pSar1-wt or pSar1-dn. 24 h post

transfection dead cells were stained with PI and counted. Hoechst 33342 was used as a counterstaining. * $p < 0.05$, ** $p < 0.01$ as calculated by two sample t-test.

3.8 Monomers of SAT form stable interactions with each other

The SAT protein comprises basic characteristics of a viroporin: It is short, it has a transmembrane domain and it can induce cell lysis. Another characteristic of viroporins is their ability to form homo-oligomers within membranes to form pores that are permeable to small molecules and ions. In order to find a homo-oligomerising activity of SAT, immunoprecipitations (IP) were conducted. To this end, the *SAT*-gene within the genome of MVMp was fused to the sequence of Myc or V5 (pMVM-Myc-SAT-wt, pMVM-V5-SAT-wt respectively). HEK293T cells were transfected with these constructs and harvested the next day. Co-immunoprecipitations were conducted with antibodies against Myc and V5 (figure 23A). Myc-SAT was co-immunoprecipitated by V5-antibodies and vice versa, indicating that the two SAT-monomers specifically interacted with each other to form stable oligomers. In order to confirm this observation proximity ligation assays (PLA) were conducted. This approach allows for the direct localisation of protein-protein interaction within the cell. A graphic illustration of the method can be seen in figure 23B. HEK293T cells were transfected with pMVM-Myc-SAT-wt and pMVM-V5-SAT-wt and PLAs were conducted with cells that were permeabilised with Triton X-100 or not (figure 23C/D). Permeabilised cells showed mainly cytosolic oligomerisation, non-permeabilised cells showed oligomerisation on their plasma membrane. These results demonstrate the ability of SAT monomers to homo-oligomerise both intracellularly and at the plasma membrane.



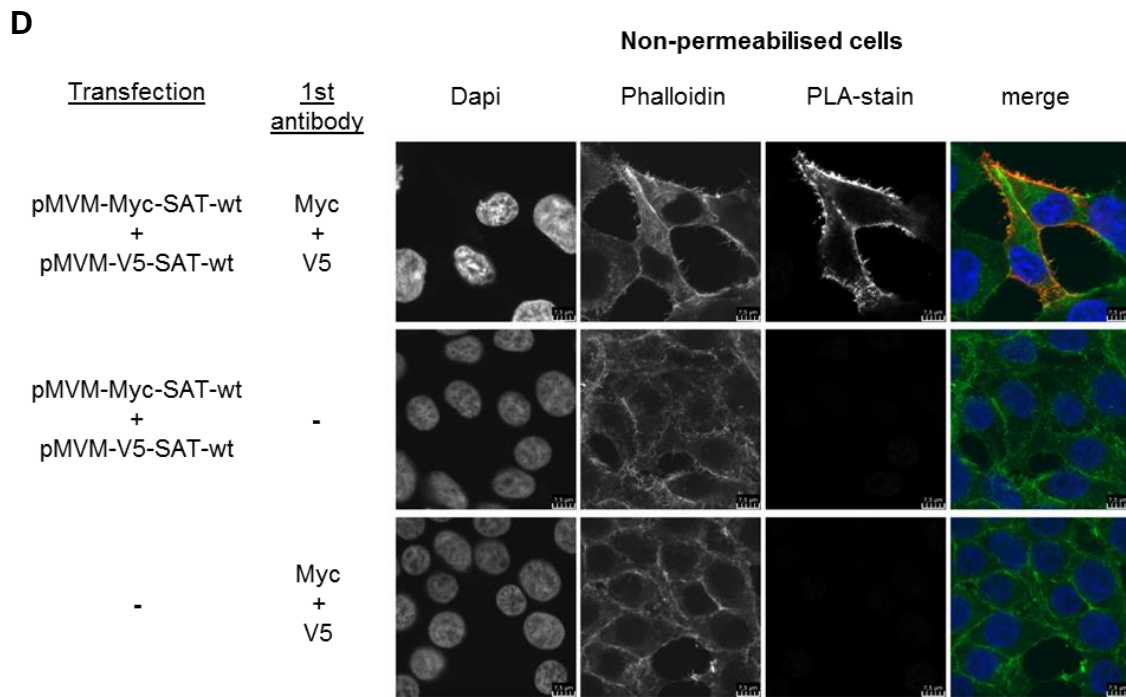


Figure 23: SAT monomers homo-oligomerise at the plasma membrane. **(A)** HEK293T cells were transfected with pMVM-Myc-SAT-wt and pMVM-V5-SAT-wt. Co-immunoprecipitations were conducted with the cell lysates with antibodies against Myc or V5. Western blots were stained with antibodies against Myc and V5. **(B)** Schematic overview of a proximity ligation assay. 1.) Two proteins bind to each other. 2.) Antibodies are added and bind to the proteins. 3.) Probes that are attached to DNA-oligomers are added. 4.) Additional oligomers hybridise to the probes with the help of a ligase (grey spheres) to form a DNA circle. 5.) The amplification mix is added consisting of nucleotides, polymerase and fluorescently labeled oligonucleotides. The polymerase multiplies the DNA in a rolling circle amplification and the fluorescent oligomers hybridise to the product. (https://www.sigmaaldrich.com/content/dam/sigma-aldrich/docs/Sigma-Aldrich/General_Information/1/duolink-short-protocol.pdf) **(C/D)** Proximity ligation assays were conducted with HEK293T cells transfected with pMVM-Myc-SAT-wt and pMVM-V5-SAT-wt. Cells were either permeabilized with Triton X-100 **(C)** or not **(D)**. Red staining indicates protein-protein interaction. Cells were additionally stained with Dapi and Phalloidin.

Typical viroporins are formed by at least four monomers. The previous experiments showed that SAT monomers are able to homo-oligomerise. However, these experiments can only show dimerisation. In order to overcome this limitation and to determine the number of monomers forming one pore, crosslinking experiments were conducted. This approach takes advantage of crosslinking molecules that introduce covalent connections between multiple proteins that are in close proximity to each other. HEK293T cells were transfected with pMyc-SAT or pFlag-SAT. After 24 h cells were treated with disuccinimidyl suberate (DSS) or formaldehyde and the lysates were analysed on a Western blot with

antibodies against Myc or Flag (figure 24). The monomeric form of SAT was clearly visible. However, no multimeric forms were detected with this approach.

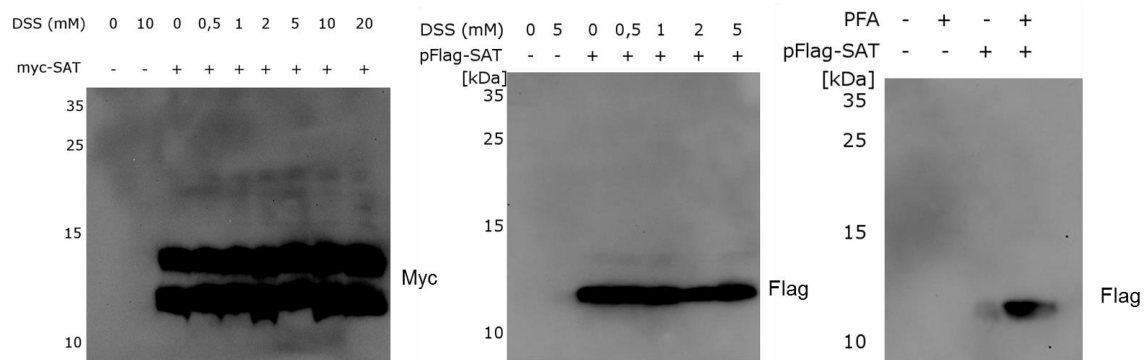


Figure 24: Crosslinking of SAT monomers. HEK293T cells were transfected with pMyc-SAT or pFlag-SAT and crosslinked with different concentrations of DSS or 4% PFA and analysed on a Western blot with antibodies against Myc or Flag.

DSS and Formaldehyde are able to crosslink primary amines that are only present at two residues in the SAT protein. Therefore, the failure of the approach to crosslink monomers of SAT was not surprising. To circumvent this problem, we turned to photo-leucine as a crosslinking reagent which is a photoreactive amino acid that is incorporated into proteins and crosslinks to nearby molecules upon UV-radiation. HEK293T cells were transfected with pMVM-Myc-SAT-wt and photo-leucine was added to the medium. The photoreactive amino acid is then incorporated by the cells during the translation of new proteins. Irradiation of cells was performed 24 h post transfection and cell lysates were analysed on a Western blot using anti-Myc antibodies (figure 25). Monomeric Myc-SAT was found at a molecular weight of about 13 kDa. Two additional species were found at higher molecular weights of about 20 kDa and 40 kDa. We suspect these to represent dimers and tetramers of Myc-SAT. The multimeric bands did not look as sharp as the monomeric bands. This effect was probably caused by the low power of the UV lamp (15 watts) that was used in this experiment. The manufacturer of photo-leucine recommends using UV-lamps with an output between 15 watts to 200 watts. It should be also considered that the UV-irradiation is likely to induce the formation of various differently crosslinked SAT species. The crosslinking might appear at different sites of SAT since the protein sequence contains 12 leucine residues, and therefore 12 potential sites of crosslinking. These different species are likely to show slightly different migration behaviours in the SDS-gel leading to a cloudy appearance of the multimeric protein bands.

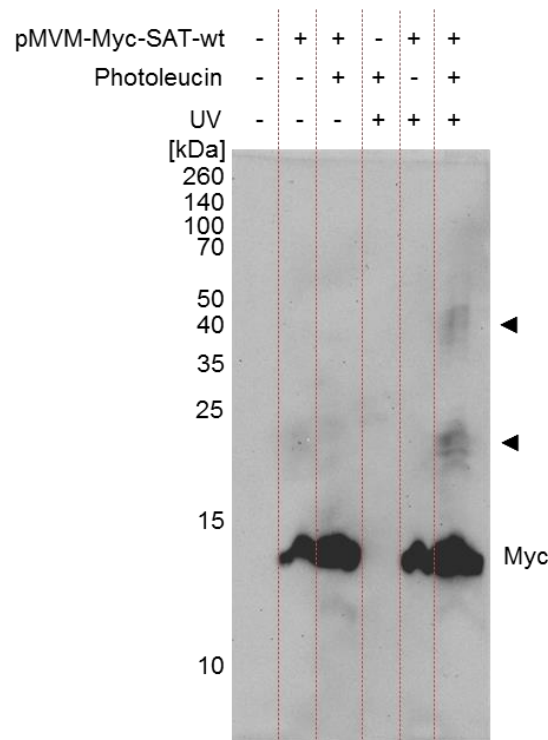


Figure 25: Photo-leucine crosslinks monomers of Myc-SAT. HEK293T cells were transfected with pMVM-Myc-SAT-wt and fed with photo-leucine for 24 h. Cells were irradiated with UV and cell-lysates were analysed on a Western blot with antibodies against Myc. Oligomers are indicated with black arrowheads.

3.9 Mutations in its transmembrane domain abolish the killing potential of SAT but do not inhibit its homo-oligomerisation

To substantiate our findings, we performed site-directed mutagenesis of SAT within its transmembrane helix. We suspected this domain to be important for the oligomerisation of SAT. Mutagenesis of important residues in the transmembrane domain might prevent its oligomerisation and therefore might have negative effects on the lytic potential of SAT. The transmembrane domain of SAT is located between amino acids 27 and 47. At its C-terminal end two basic residues can be found: K48 and L49 (figure 26A). An arginine and a lysine residue were previously found next to the transmembrane domain of agnoprotein of the JC virus which also acts as a viroporin. Mutations of these amino acids abolished the function of agnoprotein as a viroporin (Suzuki et al., 2010). In analogy, we replaced K48 and R49 of SAT with two alanines and transfected the constructs into HEK293T cells. 24 h

post transfection the lytic potential of the wild type and mutant protein was analysed using PI-staining (figure 26B). Indeed, the mutation strongly inhibited the capacity of SAT to lyse the transfected cells. A similar phenotype was observed when two glycines at position 31 and 35 within the transmembrane domain were mutated to leucines. The glycines were assumed to form a GxxxG motif, a common motif in transmembrane helices frequently seen to be important for helix-helix interactions. Further mutations were tested out (figure 26C). However, they showed less dramatic negative effects than the mutations described above. Some of these mutations such as F40G and M45G actually boosted the lytic effect (figure 26D). The reasons for these effects are unknown to us.

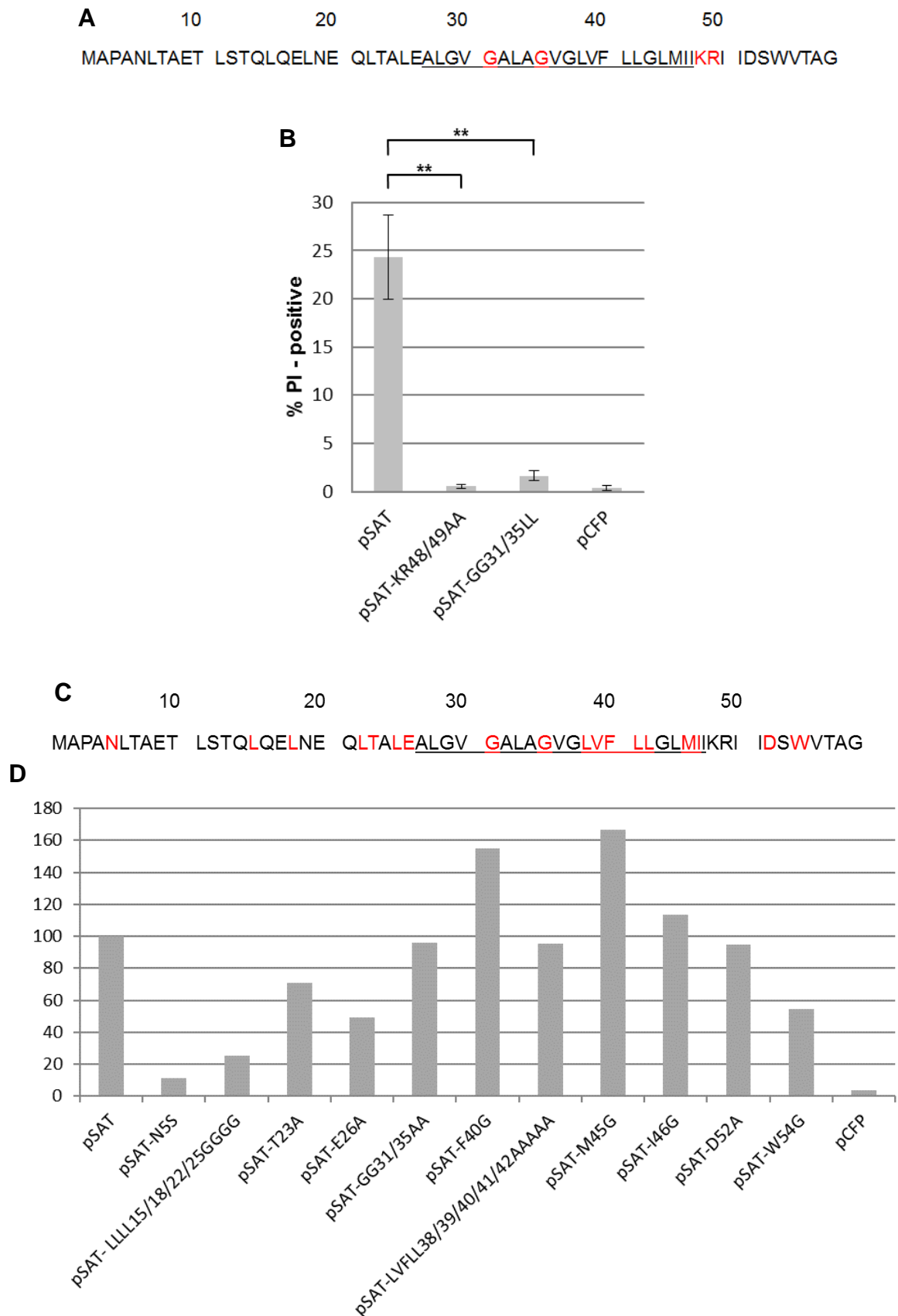


Figure 26: Mutations at the transmembrane domain of SAT eradicate the lytic function of SAT. (A) The amino acid sequence of SAT is depicted with its transmembrane domain underlined. The introduced mutations GG31/35 and KR48/49 are indicated in red. (B)

HEK293T cells were transfected with pSAT, pSAT_KR48/49AA or pSAT_GG31/35LL. pCFP served as a non-toxic control. 24 h post transfection cells were stained with Hoechst 33342 and PI and counted under a fluorescent microscope. ** $p < 0.01$ as calculated by two sample t-test. **(C)** The amino acid sequence of SAT is shown with its transmembrane domain underlined. The introduced mutations are indicated in red. **(D)** HEK293T cells were transfected with pSAT, or mutant versions of pSAT. pCFP served as a non-toxic control. 24 h post transfection cells were stained PI and positive cells were counted under a fluorescent microscope. This experiment was only conducted once.

In order to analyse if these mutations had an effect on the oligomerisation of SAT we conducted co-immunoprecipitations as described in the previous chapter. The mutations were introduced into the viral genome and SAT was fused at its 5'-end to the sequence of Myc or V5 (pMVM-Myc-SAT-KR48/49AA, pMVM-V5-SAT-KR48/49AA, pMVM-Myc-SAT-GG31/35LL, pMVM-V5-SAT-GG31/35LL) (figure 27A). Figure 27B shows that both mutants oligomerised in the α -V5 staining. However, the interaction was not seen in the α -Myc staining. Furthermore, the input controls were not seen in the α -Myc staining, but the protein could still be precipitated. GAPDH was used as a control. However, the protein was not seen in the transfections of pMVM-Myc-SAT-wt and pMVM-V5-SAT-wt. We do not know why we observed this result. The protein might have been degraded in the dying cells. It should be mentioned that after lysis of the cells the samples were stored at -80°C for about one month before conducting the co-immunoprecipitation which might have led to the degradation of proteins. Due to reasons of time management the experiment was not repeated again. Since the immunoprecipitation showed oligomerisation in the α -V5 staining we assumed that the mutations had no effect on the oligomerisation potential of SAT.

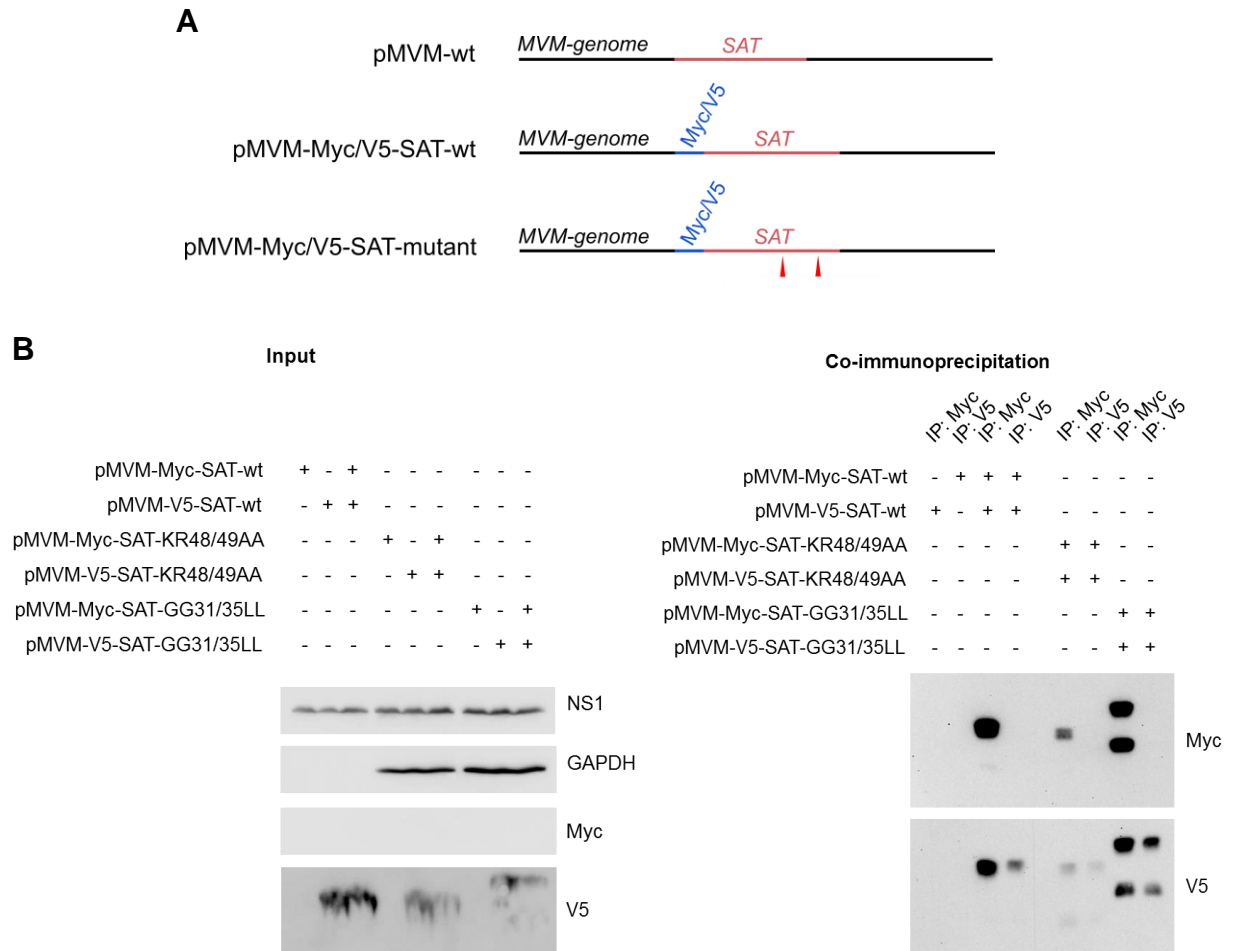


Figure 27: Mutations in SAT do not inhibit the interaction of monomers. **(A)** Graphic illustration of the DNA-constructs. The genomic area around the SAT gene within the viral genome is depicted. Red arrowheads indicate mutations. **(B)** HEK293T cells were co-transfected with pMVM-Myc-SAT-wt, pMVM-Myc-SAT-KR48/49AA or pMVM-Myc-SAT-GG31/35LL and pMVM-V5-SAT-wt, pMVM-V5-SAT-KR48/49AA or pMVM-V5-SAT-GG31/35AA. Co-immunoprecipitations were conducted with antibodies against Myc or V5. Western blot analyses were done with antibodies against Myc or V5. Input controls were additionally stained with antibodies against NS1 and GAPDH.

Additionally, we analysed the transport of the mutant SAT proteins to the plasma membrane. pMVM-Myc-SAT-GG31/35LL or pMVM-Myc-SAT-KR48/49AA were transfected into HEK293T cells. 24 h post transfection cells were either stained live with α -Myc antibodies or were permeabilised with Triton X-100 and stained afterwards with α -Myc antibodies (figure 28). Both mutants were found to be located both intracellularly and at the cell surface. The defect in the lytic capacity of the mutant SAT proteins could not be explained with a defect in their transport to the plasma membrane.

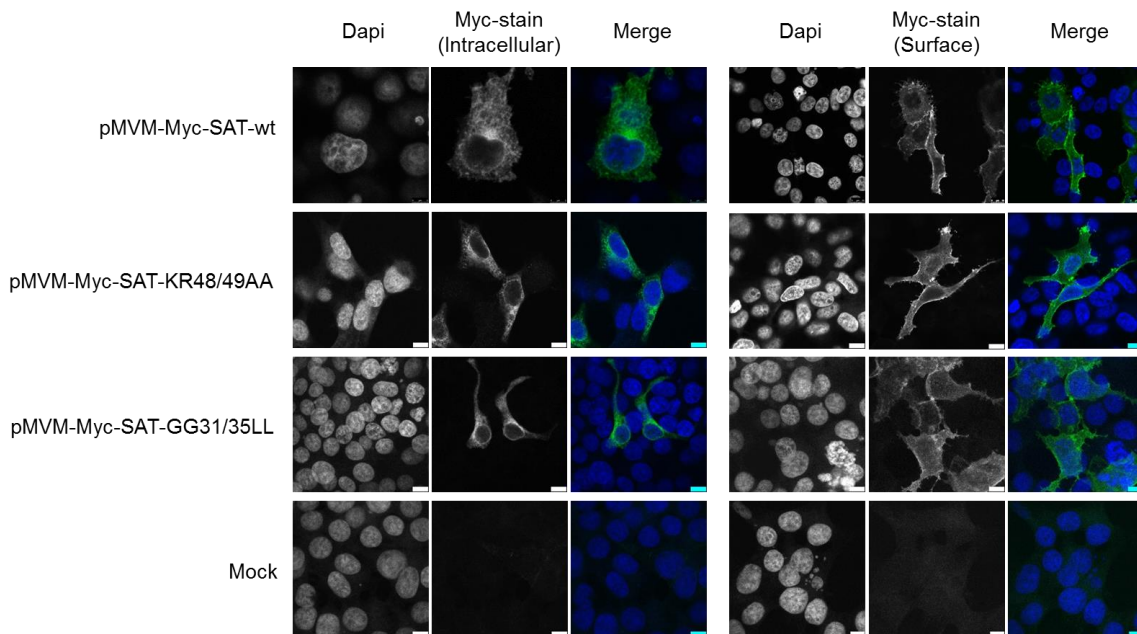


Figure 28: SAT-GG31/35LL and SAT-KR48/49AA localise to the plasma membrane. HEK293T cells were transfected with pMVM-Myc-SAT-wt, pMVM-Myc-SAT-KR48/49AA or pMVM-Myc-SAT-GG31/35LL. 24 h post transfections living cells were stained with antibodies against Myc (Myc-Stain (Surface)) or the cells were fixed and permeabilised and subsequently stained with antibodies against Myc (Myc-Stain (Intracellular)). Pictures were taken with a confocal microscope.

3.10 SAT makes the plasma membrane permeable to Hygromycin B

The main feature of viroporins is to make membranes permeable to small molecules and ions. We wanted to test this ability of SAT by conducting an assay using the small antibiotic Hygromycin B which stalls eukaryotic protein translation (Contreras and Carrasco, 1979). Hygromycin B usually takes several hours to pass through the plasma membrane of cells. Since SAT was found to oligomerise at the plasma membrane to lyse the cells, we hypothesized that SAT might increase the permeability of Hygromycin B by forming a pore. This assay was already conducted for the analysis of many other viroporins such as agnoprotein of the polyomavirus JC virus (Suzuki et al., 2010) (figure 29A). HEK293T cells were transfected both with a plasmid coding for the yellow fluorescent protein (pYFP) and the genome of MVMp (pMVM-wt), the SAT-knockout version of the genome (pSAT-ko) or no further DNA. The next day the cells were treated with Hygromycin B and fed with radioactive methionine. After 3 h of incubation the cells were harvested and an immunoprecipitation with antibodies against GFP was conducted. After a Western Blot,

autoradiograms were performed to analyse the incorporation of radioactive methionine into YFP (figure 29B). If Hygromycin B is able to easily pass through the plasma membrane the translation of YFP was expected to be decreased. In the case of pMVM-wt-transfected and Hygromycin B-treated cells a lower amount of YFP was translated compared to untreated cells. pSAT-ko-transfected cells that were treated with Hygromycin B did not show such a reduction in signal intensity. As a control Western blots with non-labeled samples were stained with α -GFP and α -NS1 antibodies (figure 29C). The global expression of YFP and NS1 was comparable between pMVM-wt- and pSAT-Ko-transfected samples and between Hygromycin B-treated and non-treated samples. These experiments show that the expression of SAT makes the plasma membrane permeable to Hygromycin B.

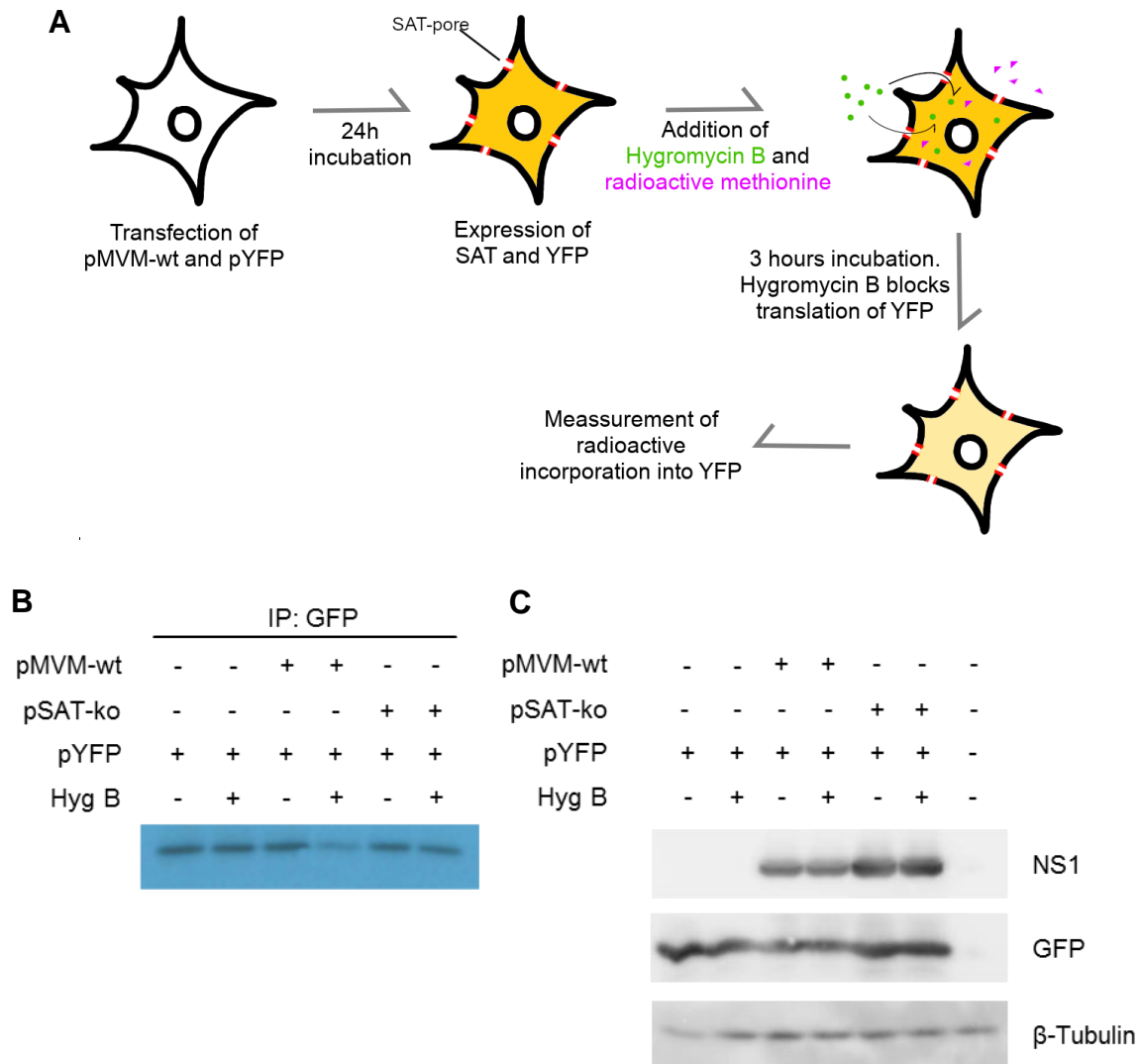


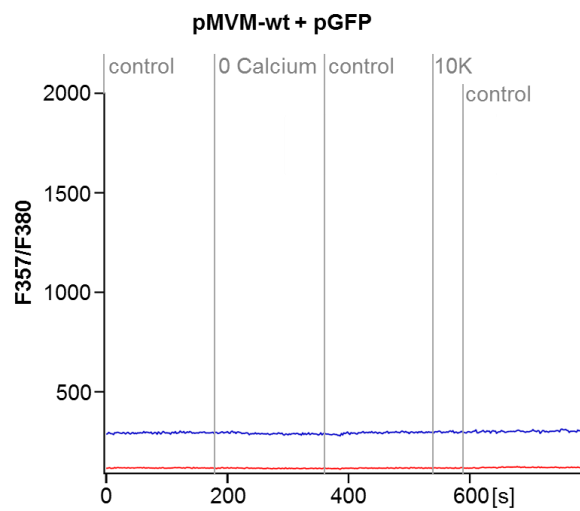
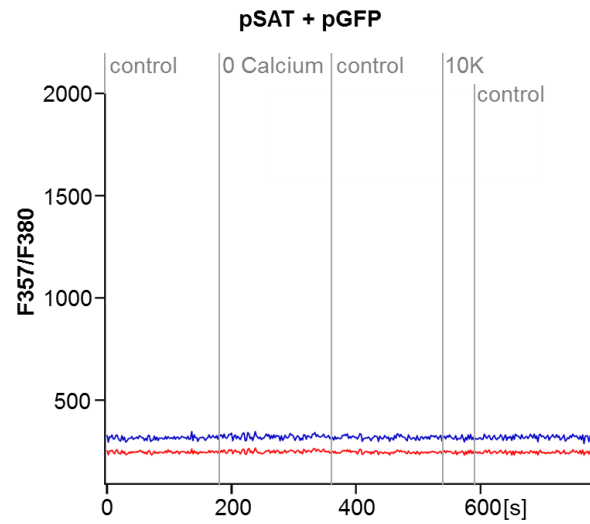
Figure 29: SAT induces changes in the permeability of the plasma membrane. **(A)** Schematic protocol of the Hygromycin B assay. Cells are transfected with pYFP and the pMVM-wt. After 24 h cells have accumulated YFP in their cytoplasm and pores are formed by SAT-oligomers at the plasma membrane. Hygromycin B is added to the cells and enters the cell through the pores. Radioactive methionine is added and incorporated in newly-synthesized proteins. After 3h the translation of YFP is inhibited by Hygromycin B. **(B)** The Hygromycin B assay was conducted and immunoprecipitations with antibodies against GFP were prepared and analysed in an autoradiogram. **(C)** The samples were analysed on a Western blot with antibodies against NS1, GFP and β -tubulin.

3.11 The SAT oligomer is not permeable to calcium or sodium ions

The experiments of the previous chapter showed that the expression of SAT leads to the permeabilisation of the plasma membrane to the small molecule Hygromycin B. Many viroporins are permeable to small ions such as calcium or sodium and allow these ions to pass through the membranous barrier. For example, Vpu which is the viroporin of HIV-1, is permeable to sodium and potassium (Ewart et al., 1996). We explored whether SAT is permeable to calcium or sodium. Both ions exist in the extracellular space in much higher concentrations than in the intracellular space (Na^+ extracellular/intracellular: 12 mM/145 mM; Ca^{2+} extracellular/intracellular: <0.0002 mM/1.8 mM) (Lodsih, 2000). An increase in the intracellular concentration of one of these ions would have dramatic effects on the cellular integrity and is likely to induce cell death.

We tested the permeability of MVM-wt- or SAT-ko-infected A9 cells for calcium using the fluorescent calcium indicator Fura-2-AM. Dr. Stefan Titz of the “Institut für Physiologie und Pathophysiologie” in Heidelberg conducted this experiment in his laboratory. HEK293T cells were transfected with pGFP and pSAT or pMVMwt and treated with Fura-2-AM 20 h post transfection. Cellular GFP-expression indicated a successful transfection and was used to identify cells that were most likely co-transfected with pSAT or pMVMwt. Twelve transfected and twelve non-transfected cells were used for the recordings. During the time course cells were placed in a perfusion chamber and treated with different solutions containing different concentrations of calcium ions. Fluorescent intensities of Fura-2-AM were recorded under a fluorescent microscope. The dye can be excited at 357 nm or 380 nm and it emits photons with a wavelength between 500 nm and 540 nm. The ratio F_{357}/F_{380} indicates the intracellular Ca^{2+} concentration. Between 0 s and 180 s the cells were perfused with control solution containing 2 mM CaCl_2 . At 180 s the cells were perfused with a solution containing no calcium ions (0 Calcium). At 360 s the cells were treated with control solution again. At 540 s cells were treated with a solution containing an increased amount of potassium ions (10K) which is thought to increase the intracellular calcium concentrations (Barish, 1991). From 590 s on the cells were perfused with control solution again. If the SAT-pore was permeable to calcium ions, we suspected the intracellular calcium concentration to react to changes in the perfusion solution. However, no changes in the calcium concentration were found in pGFP-, pSAT- or pMVMwt-

transfected cells suggesting that a putative SAT pore might not be permeable to Ca^{2+} (figure 30). The lower steady state level of transfected cells was likely affected by the expression of GFP. GFP is slightly excited at 357 nm and 380 nm with a stronger excitation at 380 nm than 357 nm. Its emitted wavelengths lie within the spectrum recorded by the microscope.



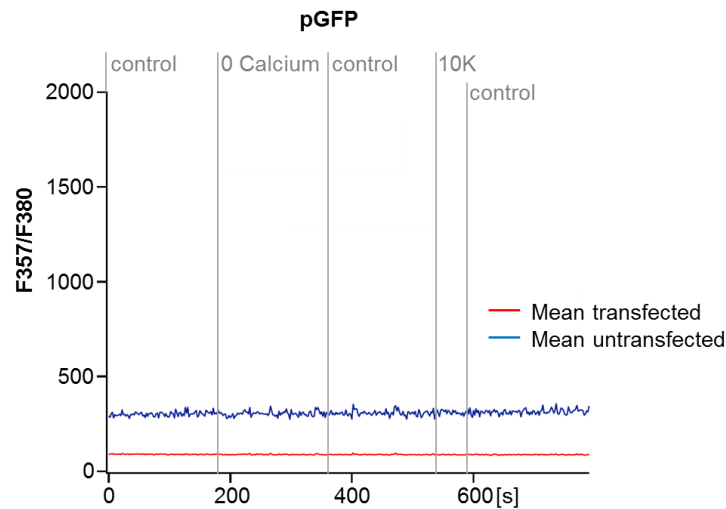


Figure 30: The expression of SAT does not affect the intracellular concentration of calcium ions. HEK293T cells were co-transfected with pGFP and pSAT or pMVMwt. 20 h post transfection cells were loaded with the calcium indicator Fura-2-AM and analysed under a fluorescent microscope (excitation: 357 nm or 380 nm; emission: between 500 nm and 540 nm; frequency of measurement: 0.5 Hz). Twelve GFP-positive and twelve GFP-negative cells were recorded. At 180 s cells were perfused with a solution containing no calcium ions (0 Calcium). At 540 s cells were treated with a solution containing an increased amount of potassium ions (10K). The left row shows the recordings of single cells, the right row shows averaged values.

Next, we tested whether the putative SAT pore was permeable to sodium ions. To this end, A9 cells were infected with MVM-wt or SAT-ko with an MOI of 5 and were loaded with Sodium Green and PI 24 h post infection. Sodium Green is an indicator for sodium ions that fluoresces green at increased intracellular sodium concentrations. The putative SAT pore was suspected to permeabilise the plasma membrane to sodium to induce cell death. The infected cells were analysed in a time lapse experiment. Every eight minutes pictures were taken with a fluorescent microscope (figure 31). Both MVM-wt- and SAT-ko infected cells did not become positive for Sodium Green before they died. The cells became first positive for PI-staining and soon later for Sodium Green-staining. At the same time the cells underwent severe morphological changes of cell lysis. No differences of any kind between MVM-wt and SAT-ko-infected cells were observed. These results suggest that the putative SAT pore is not permeable to sodium ions. However, it is questionable if the used method is appropriate to detect small changes in the intracellular sodium concentrations since the staining with Sodium Green was very hard to detect.

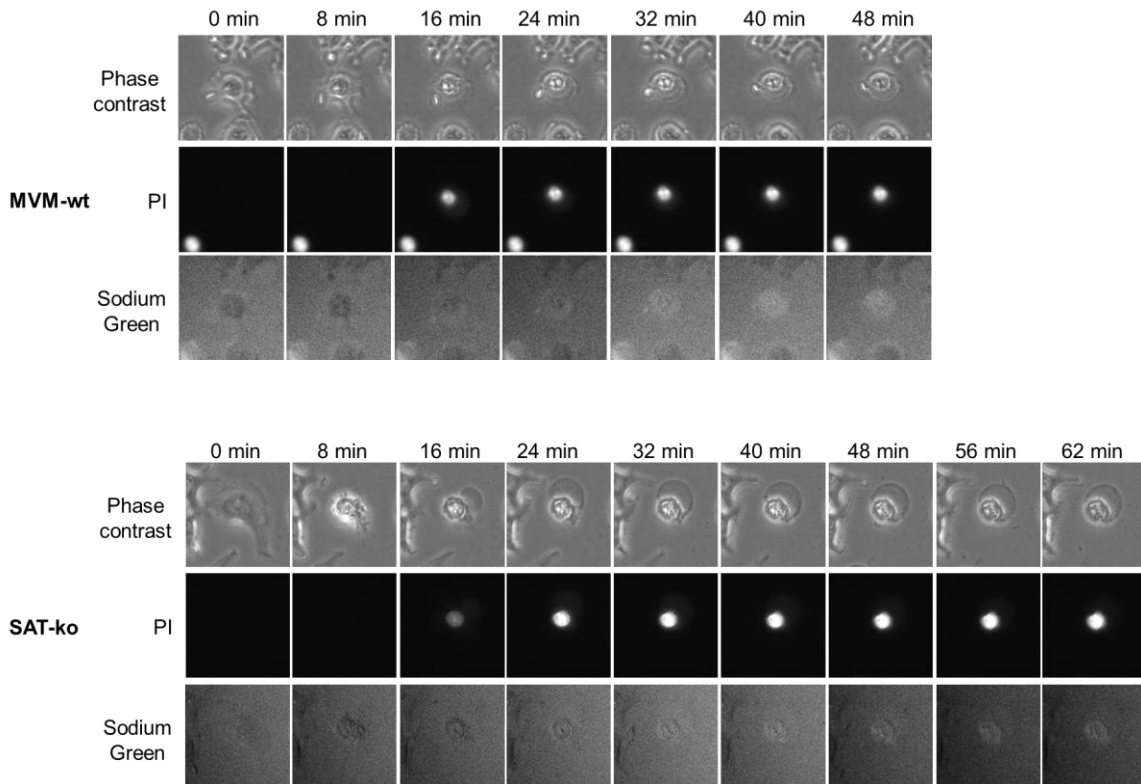


Figure 31: The expression of SAT does not change the intracellular concentration of sodium ions. A9 cells were infected with MVM-wt or SAT-ko and treated with Sodium Green and PI 24 h post infection. Cells were analysed for 24 h under a fluorescence microscope. Every eight minutes pictures were taken. The starting point “0 min” was chosen arbitrarily for both samples individually in order to analyse the point of cell lysis.

3.12 A coarse-grained computer simulation of SAT reveals oligomerisation but does not show pore-formation

In order to investigate the pore-forming activity of SAT we performed a coarse-grained computer simulation of SAT. Since no three-dimensional structure of SAT is known we performed a de novo prediction using the online tool Phyre 2 (Kelley and Sternberg, 2009). The resulting structure is illustrated in figure 32B. Phyre 2 aligns a query amino acid sequence (figure 32A) to a database of sequences with known three-dimensional structures. From these sequences the query sequence is then modeled de novo. SAT was predicted to be separated in three different helices. The middle helix matched the prediction of the transmembrane part of the protein. However, the overall confidence of the predicted model was weak.

10 20 30 40 50
 MAPANLTAET LSTQLQELNE QLTALEALGV GALAGVGLVF LLGLMIKRI IDSWVTAG

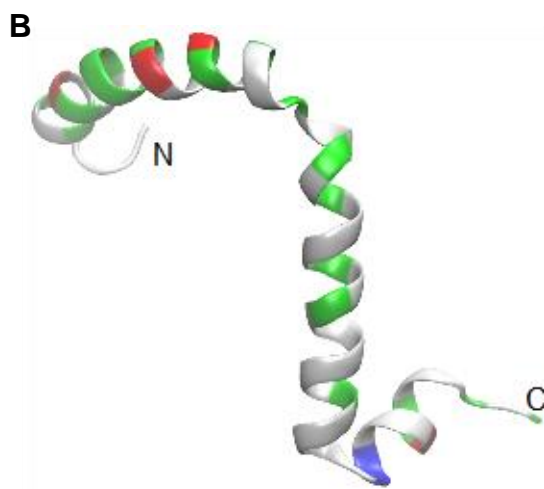


Figure 32: Prediction of the 3D-structure of SAT. **(A)** Amino acid sequence of SAT with its transmembrane domain underlined. **(B)** The structure was modelled de novo using the online tool Phyre 2. The N- and C- termini are labelled with an “N” and a “C”, respectively. Polar residues are shown in green, nonpolar in white, acidic in red, basic in blue.

Next, a coarse-grained simulation was conducted. Kashif Sadiq and Ghulam Mustafa of the HITS institute in Heidelberg conducted this simulation. A coarse-grained simulation simplifies amino acids to sphere-like structures in order to save processor performance which allows to conduct long simulation-times of a few μ seconds. An alternative to a coarse-grained simulation is an all-atoms simulation which takes each atom of the system into account. Since the confidence of the Phyre 2-predicted structure was rather low the helices of SAT were modeled de novo as one continuous helix passing through the membrane. 20 monomers of SAT were placed inside a 1-palmitoyl-2-oleoyl-sn-glycero-3-phosphocholine (POPC) membrane and the simulation was run for 2 μ s. Throughout the simulation various multimers were formed. At the end of the simulation a heptamer was the largest oligomer that was formed. The most symmetric multimers, however, were the dimers and tetramers. Therefore, we concentrated on these structures.

One dimer is shown in figure 33. The slightly bent helices were facing each other with the same surfaces and interacted with each other on their full length. One of the main characteristics were the leucine residues that paired up at the N-terminus of the protein. Leucine 11, 18, 22 and 25 interacted with the neighbouring leucines (figure 33B). This leucine zipper was the first part of the dimer that was formed. Later, parts of the

transmembrane domain interacted with each other in a very symmetrical manner. Depicted in figure 33D is the phenylalanine residue 40 (F40). F40 made contacts with the neighbouring helix. However, the two F40 residues did not contact each other. The lysine and arginine residues (K48, R49) were embedded at the edge of the membrane. They were in close proximity to the aspartic acid residue D52. The last three residues T56, A57 and G58 stuck out of the membrane whereas W54 was located inside the membrane (figure 33E). What seemed surprising to us was the orientation of G31 and G35 that formed the putative GxxxG motif. G31 and G35 were located outside of the helices not interacting with any other residues (figure 33C). This observation might explain why the mutation of these residues to leucines had no effect on the oligomerisation of the monomers (see chapter 3.9 “Mutations in its transmembrane domain abolish the killing potential of SAT but do not inhibit its homo-oligomerisation”).

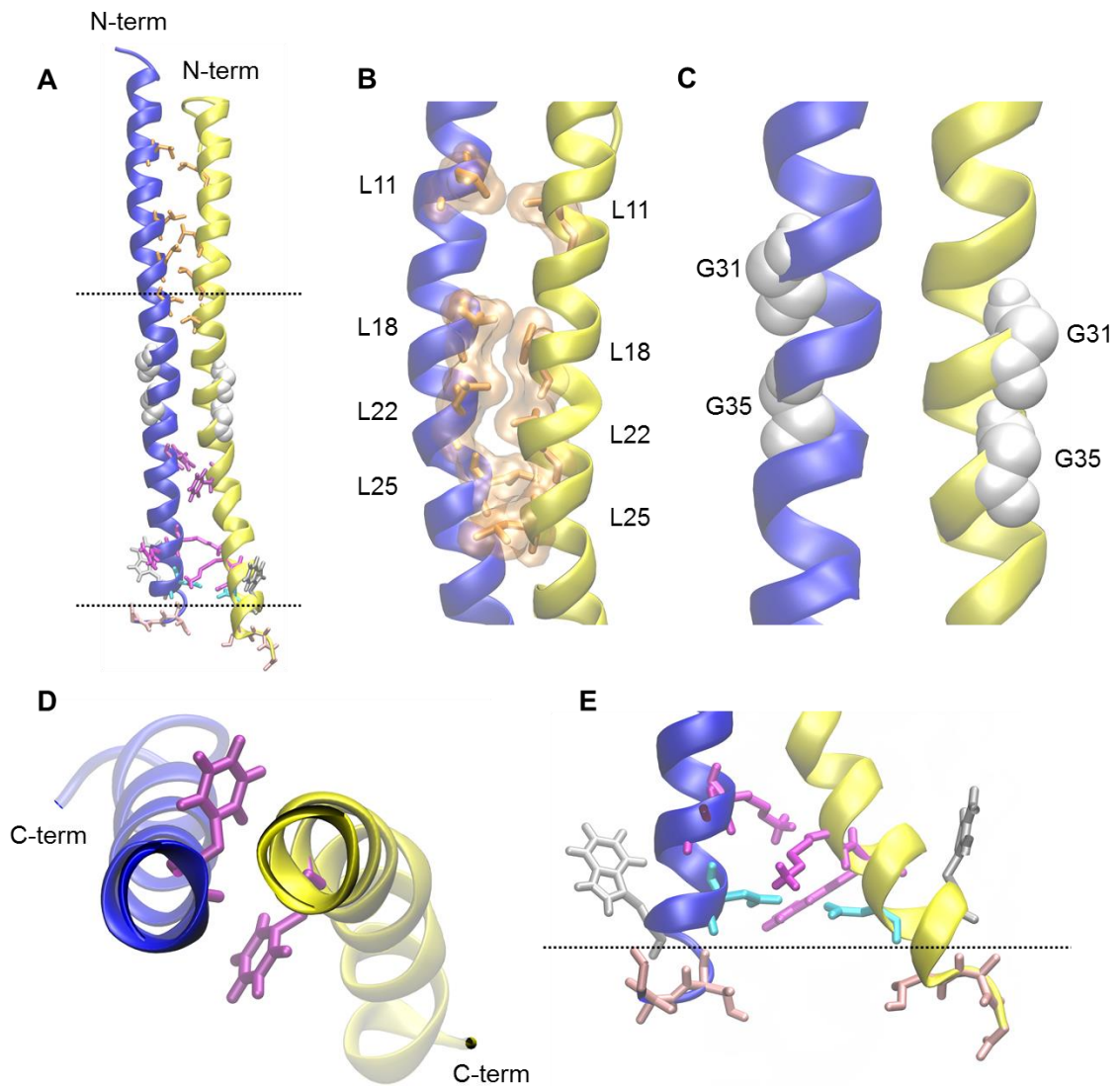


Figure 33: SAT forms dimers in a computer simulation. Two interacting SAT proteins are depicted. **(A)** Both proteins interact at their full length with each other. The edges of the membrane are shown as dotted lines. **(B)** The leucine residues L11, L18, L22 and L25 of each monomer are shown as orange sticks and their surfaces are shown transparent. **(C)** The glycine residues G31 and G35 of both monomers are shown in white with their van-der-Waals (VDW) radius. **(D)** Phenylalanine F40 of both monomers are shown as purple sticks. **(E)** The C-terminal part is depicted with the outline of the membrane shown as a dotted line. Arginine and lysine: magenta; aspartic acid: cyan; tryptophan: grey; threonine, alanine, glycine: light salmon.

One of the tetramers is depicted in figure 34A. The four helices, labeled h1, h2, h3 and h4 formed a bundle at their N-termini (figure 34C). At their C-termini the helices were more separated from each other and were lined up next to each other (figure 34B). The orientation of helix h2 and h3 was very similar to the orientation of the helices of the dimer described above. G31, G35, F40, K48, R49, D52, W54, T56, A57 and G58 adopted the same orientation and interactions that were seen in the dimeric structure. Most of the

leucines at the N-terminal bundle pointed inward the bundle. Leucine 18, 22 and 25 of helix h2 and h3 and leucine 11, 15, 18 and 22 of helix h1 and h4 pointed inwards the bundle and came into close contact with each other (figure 34D1). Helix h1 and h4 did not form interactions with each other at their C-terminal domains. G31 and G35 of all monomers were facing away from the oligomeric core (figure 34D2/3). The F40 residues of h2 and h3 adopted a similar conformation seen previously in the dimer, with one phenylalanine contacting the neighbouring helix and vice versa. However, the two F40 residues of helix h1 and h2, and helix h3 and h4 came into very close contact with each other (figure 34D4). At the C-terminal parts the helices lined up into one row which was slightly bent (figure 34B). The residues of the C-terminal part also adopted conformation which was similar to the conformation already seen in the dimeric structure (figure 34D5). The tetramers also formed an additional interaction at their C-terminal end with another helix (figure 34E). None of the observed structures resembled a pore. However, the simulation confirms the finding of oligomerisation of SAT.

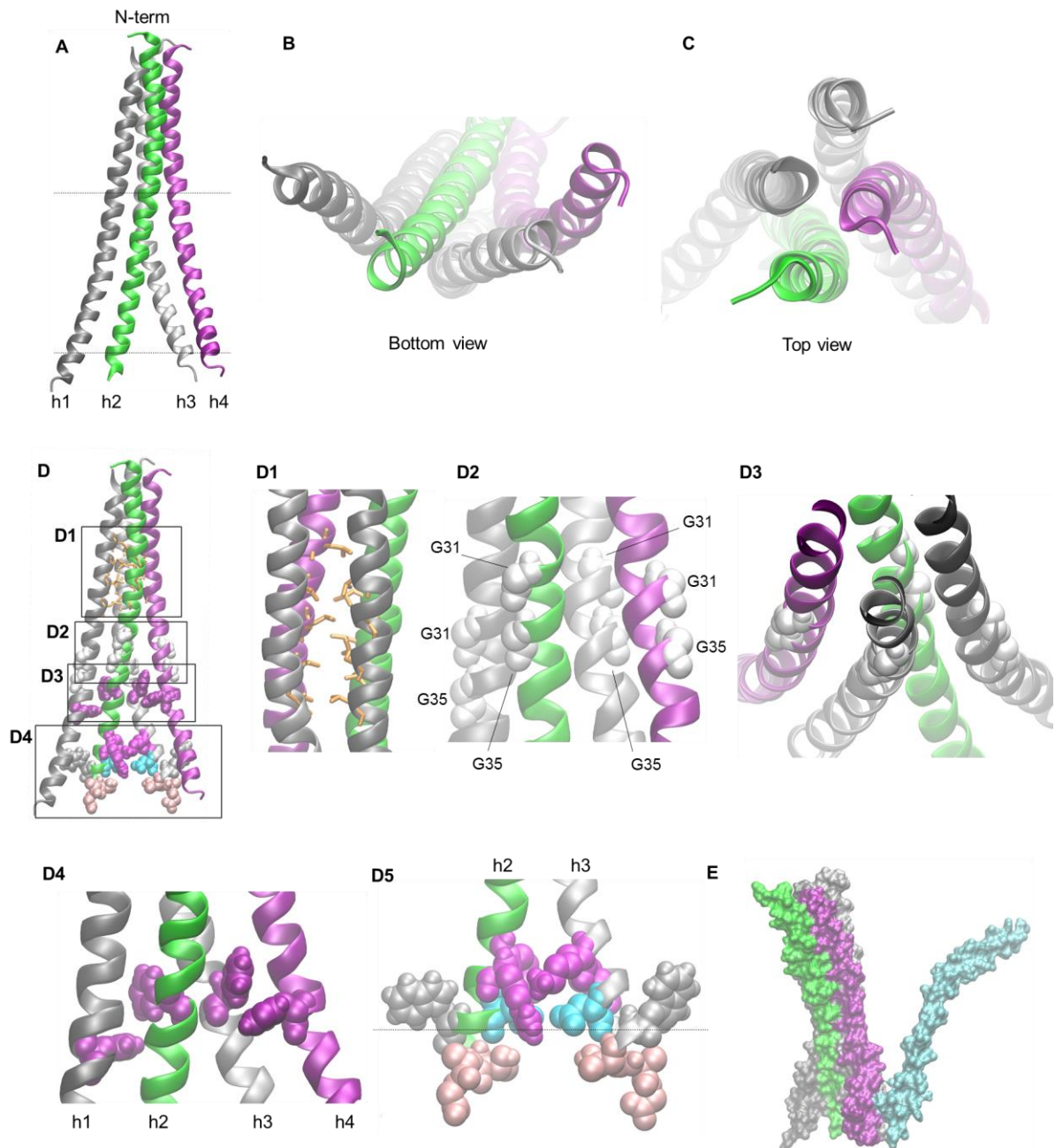


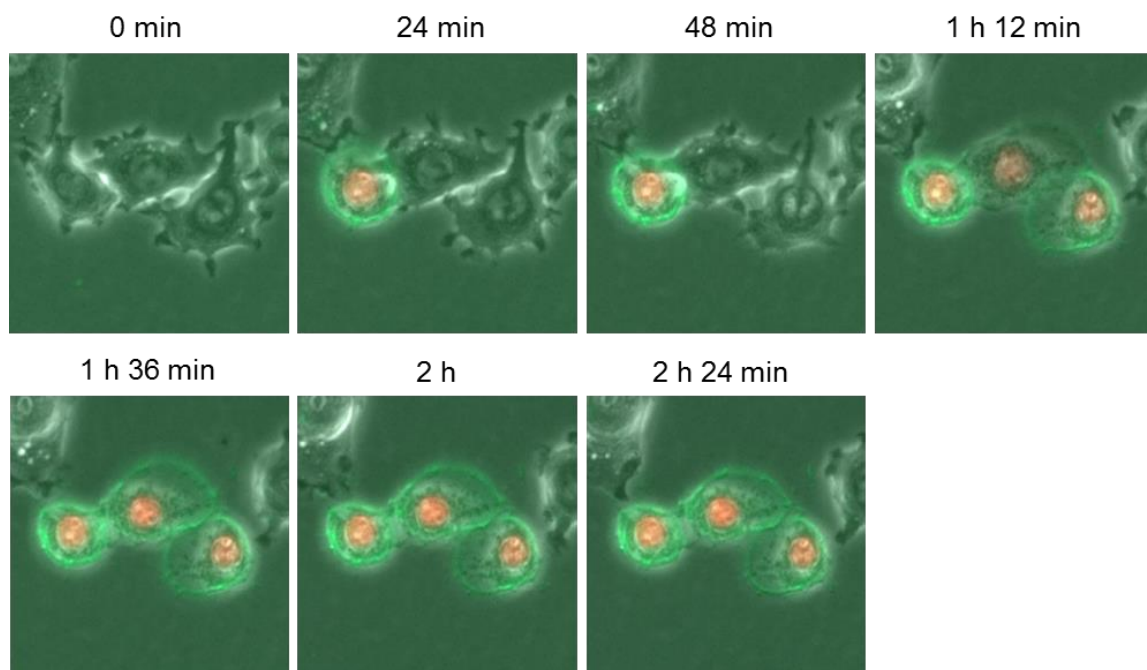
Figure 34: SAT forms tetramers in a computer simulation. **(A)** Four interacting helices of SAT are depicted, termed h1 to h4. The outlines of the membrane are shown as dotted lines. **(B)** Bottom view of the tetramer showing the C-termini of the SAT monomers. **(C)** Top view of the tetramer showing the N-terminal bundle. **(D)** Overview image of the discussed residues. **(D1)** Leucine zipper (orange sticks) at the N-terminal bundle. **(D2)** GxxxG motifs. The glycines are shown as white spheres. **(D3)** The GxxxG motif is shown from an inclined angle. **(D4)** Orientation of the Phenylalanine residues F40 (purple spheres). **(D5)** C-terminal domain of h2 and h3 with the outline of the membrane shown as a dotted line. Arginine and lysine: magenta; aspartic acid: cyan; tryptophan: grey; threonine, alanine, glycine: light salmon. **(E)** An additional helix (cyan) interacts with the tetramer. The helices are shown as surfaces.

3.13 Morphological changes of cell-death induced by SAT

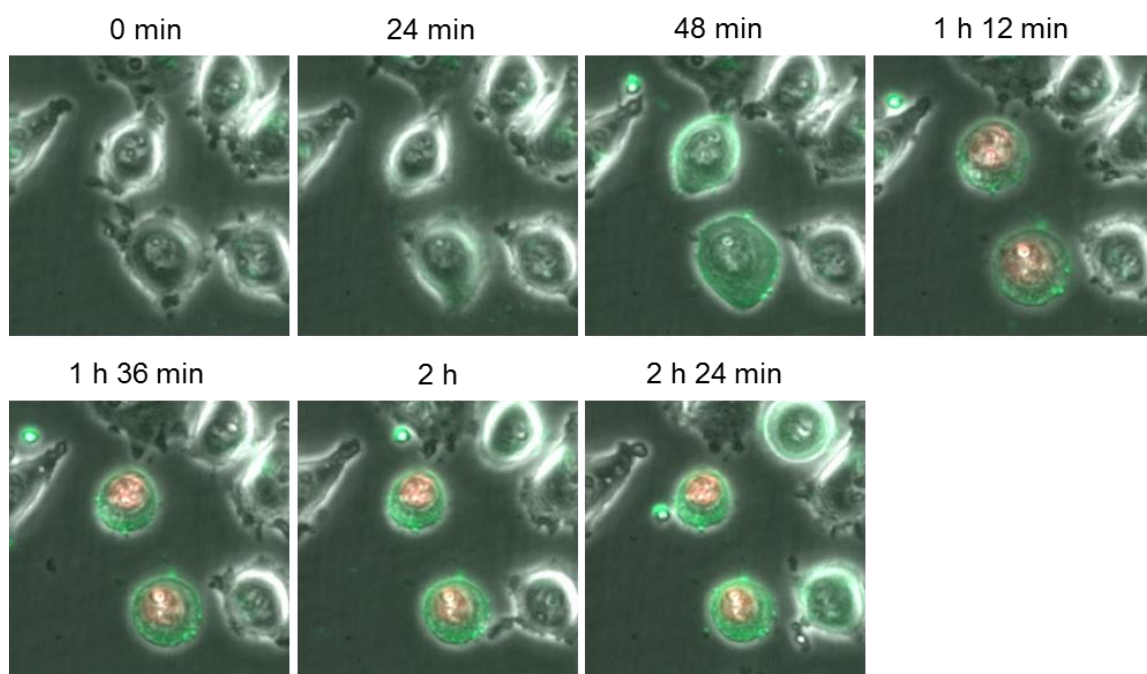
There are numerous reports about the cell-death that is induced by parvoviral infections. Signs of apoptosis have been found such as nuclear fragmentation, DNA condensation, PARP cleavage or activation of caspases (Mochler et al., 2001; Nykky et al., 2010; Ran et al., 1999; Rayet et al., 1998). However, an early disruption of the plasma membrane leading to secondary necrosis argues against a completed apoptosis (Nykky et al., 2010; Ran et al., 1999).

We wanted to investigate if SAT plays a role in the cell-death pathway. A9 cells were infected with MVM-wt or SAT-ko with an MOI of 5 and stained with Annexin V and PI. Cells were observed for 48 h under a microscope in a time lapse experiment (figure 35). Cell-death of mock-infected cells was characterised by a slow rounding up of the cells followed by a sudden swelling of the cell which is a typical sign for necrosis. Cells became simultaneously positive for PI- and Annexin V-staining. The dead cells retained a swollen plasma membrane. Cell-death of MVM-wt- and SAT-ko-infected cells became simultaneously positive for PI- and Annexin V-staining. However, there was no immense swelling of the plasma membrane seen. The cells rounded up and retracted their plasma membrane to a small sphere. There was no significant difference seen in the cell-death of MVM-wt- or SAT-ko-infected cells. The presence of SAT did not influence the cell-morphology or the staining-pattern of Annexin V and PI.

MVM-wt



SAT-ko



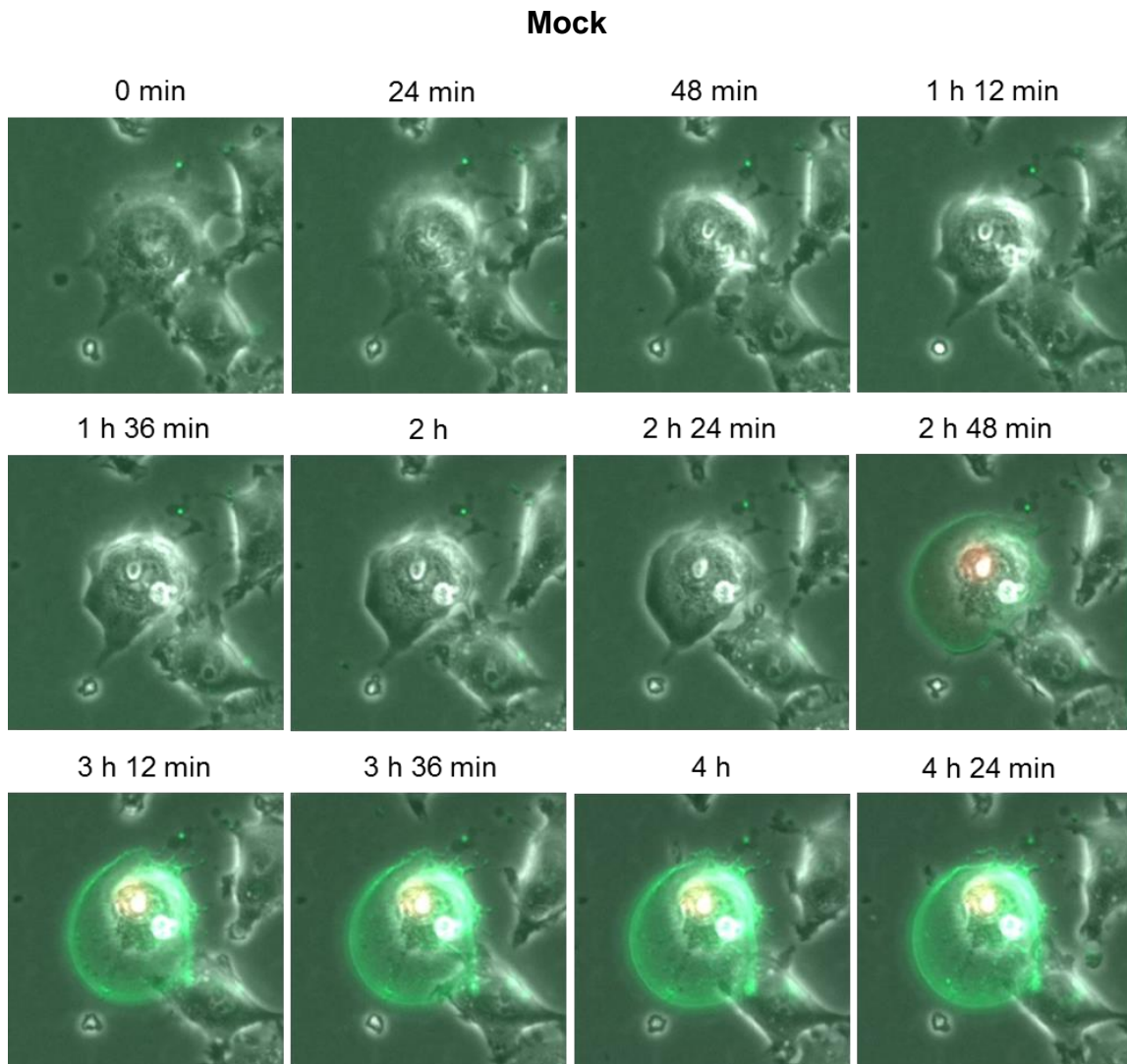


Figure 35: Annexin V-staining, PI-staining and morphological changes in MVM-wt-, SAT-ko- or mock-infected cells: A9 cells were infected with MVM-wt, SAT-ko or were mock-infected and stained with PI and Annexin V. The cells were analysed for 48 h under a fluorescent microscope. Pictures were taken every 24 minutes. The starting point “0 min” was chosen arbitrarily for the three samples individually in order to analyse the point of cell lysis.

3.14 pSUPER kills cells more efficiently than pMVM-wt

SAT is produced via the mechanism of leaky scanning. It is translated from the same mRNA as VP2, but its starting AUG is located 4 bps downstream the starting AUG of VP2. In this constellation VP2 and SAT share one mRNA for their production. The process of leaky scanning is a well-calculated process that allows the translation of the required amounts of SAT to kill the infected cell during a natural infection. However, for

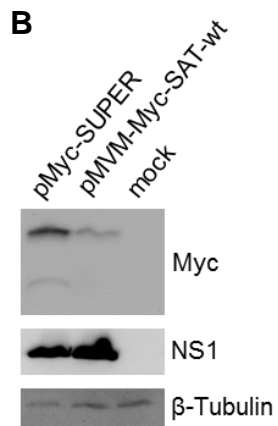
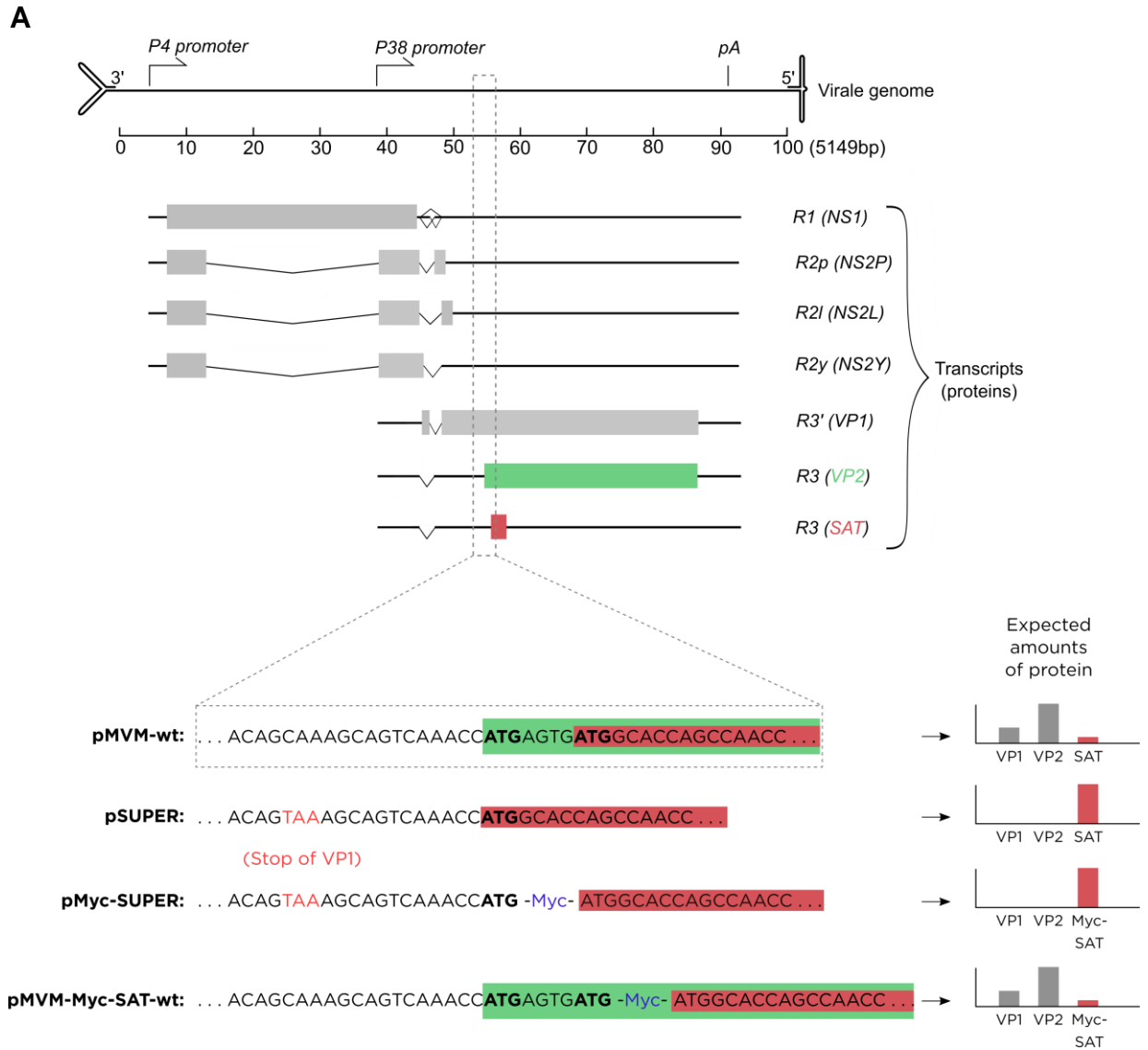
oncolytic virotherapy with parvoviruses it is beneficial to increase the toxicity of the virus. Therefore, we adjusted the position of the *SAT* gene to the starting point of the *VP2* gene in order to increase its translation (figure 36A). We suspect that an increased dose of SAT protein should kill cancer cells more efficiently. In this genomic constellation the mRNA for the translation of SAT is not shared with the sequence for VP2 anymore. This rearrangement eliminates the expression of VP2. As another modification a stop codon was introduced at the end of the N-terminal domain of VP1 in order to exclude a fusion between the N-terminal domain of VP1 and SAT. The mutated genome, termed “pSUPER”, does not allow the production of progeny viruses since the production of capsid proteins is not possible. A few considerations have to be considered here:

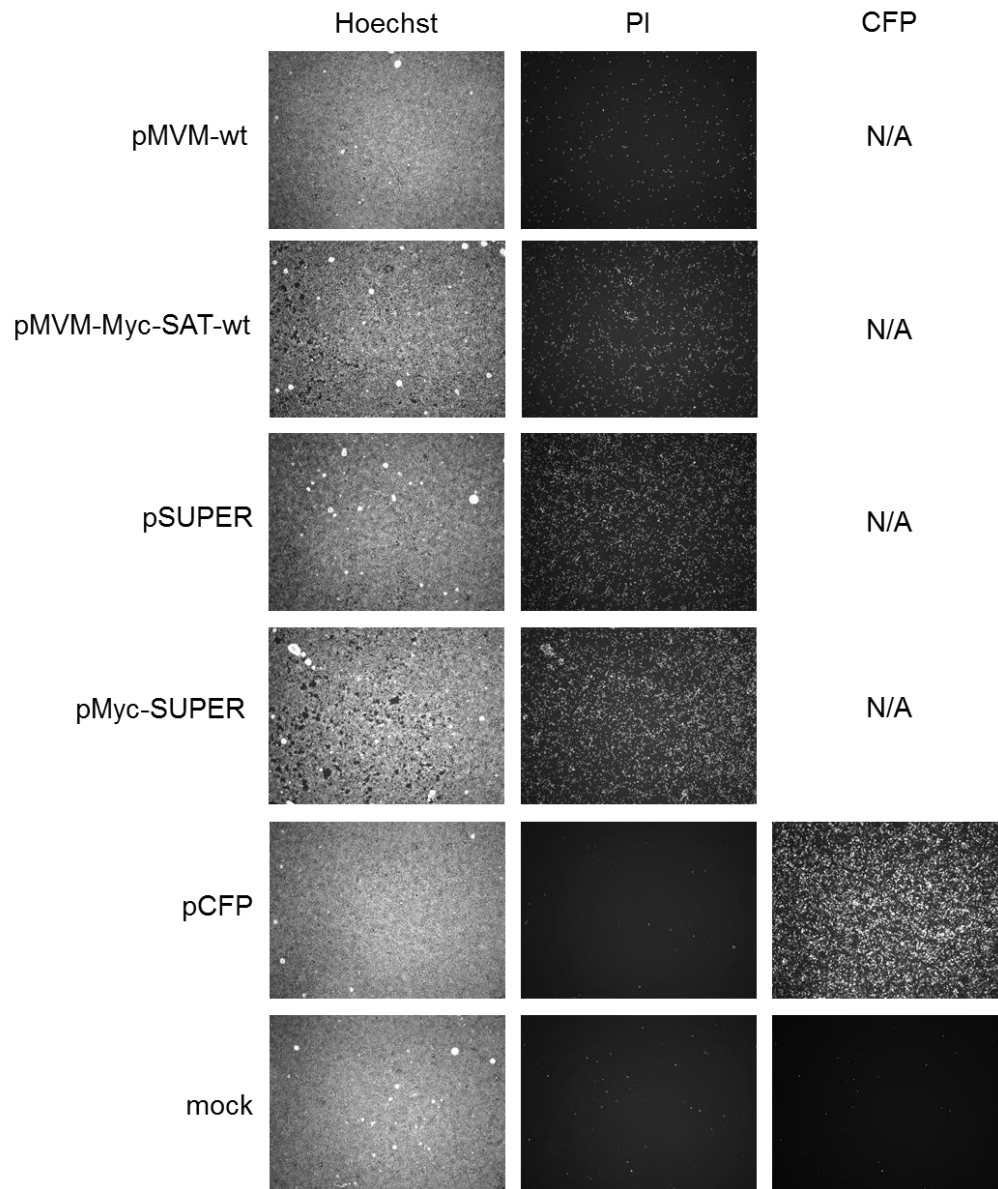
Hypothetically speaking, a single oncolytic virus should have the capability of eradicating a whole tumor by spreading of progeny viruses. However, in many preclinical studies this was not the case. The animals transplanted with tumors were often injected with multiple doses of virus but still succumbed their cancer. While some tumor cell lines gave rise to progeny viruses, others could be infected but did not produce significant amounts of progeny viruses. Moreover, the clinical data of H1-treated cancer patients did not allow to observe the production of progeny viruses, but it showed the seroconversion of the patients. Therefore, it might not be a big disadvantage for SUPER not to be able to produce progeny viruses. Many reports have emphasised the importance of the activation of the immune system for the parvoviral therapy (see chapter 1.2 “What makes Parvovirus an oncolytic virus?”). We assume that the immune activation is boosted when the toxicity of the virus is increased thereby releasing an increased amount of tumor antigen and we assume that a functional replication of the virus might not be the most important factor for the success of the therapy. We suspected that a boost in the activation of the immune system might be observed with the SUPER virus which is suspected to induce the lysis of the cells more efficiently due to its increased expression of SAT. The SUPER virus is not able to produce progeny viruses, but we suspect that its increased toxicity activates the immune system in a more efficient way than the wt-virus.

First, we investigated if pSUPER-transfected cells produce more SAT than pMVM-wt-transfected cells. Since no antibody against SAT was available, SAT was tagged N-terminally with Myc (see figure 36A) (“pMyc-SUPER” / “pMVM-Myc-SAT-wt”). HEK293T cells were transfected with these constructs, harvested after 24 h and analysed on a Western blot

with antibodies against NS1 and Myc (figure 36B). The amount of Myc-SAT was strongly increased in pMyc-SUPER-transfected cells.

Next, we analysed if the increased amount of SAT has an effect on the killing of transfected cells. HEK293T cells were transfected with constructs coding for pSUPER, the pMVM-wt, pMyc-SUPER, pMVM-Myc-SAT-wt, and pCFP. After 24 h dead cells were stained with PI and counted under the microscope (figure 36C/D). pSUPER was about 25 times more efficient than pMVM-wt in its killing potential. pMVM-Myc-SAT-wt also showed an increased lytic potential compared to pMVM-wt. This result was expected since the Myc-tag was already seen to have a boosting effect on the killing potential of SAT (see chapter 3.6 “The SAT protein has a higher lytic potential than NS1”). However, pMyc-SUPER and pSUPER showed about the same amount of dead cells. We suggest that the killing potential of pSUPER already reached such a high value that an additional amplifying effect by a Myc-tag might be difficult to see.



C

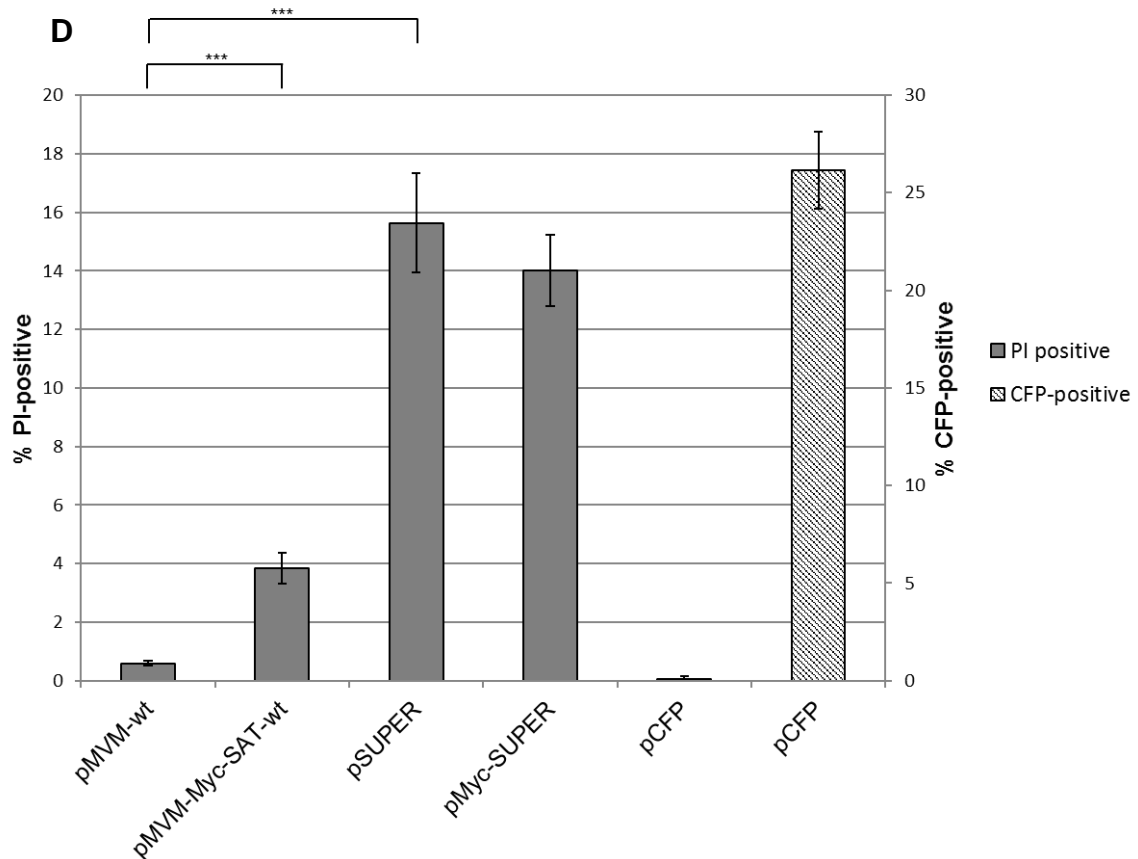


Figure 36: pSUPER and pMycSUPER are able to lyse cells more efficiently than pMVM-wt and pMVM-Myc-SAT-wt. **(A)** Graphic illustration of the different constructs used. The upper half of the graphic shows the wild type parvoviral genome with its expressed mRNAs. The lower part of the graphic concentrates on the genomic area around the Start codons of VP2 and SAT. Modifications of the wild type genome are listed below. A Stop codon was introduced in pSUPER and pMyc-SUPER in order to prevent fusions of VP1 with SAT. On the lower right side of the graphic the expected amounts of proteins are depicted as graphs. **(B)** HEK293T cells were transfected with pMyc-SUPER or pMVM-Myc-SAT-wt. 24 h post transfection cells were harvested and analysed in a Western blot with antibodies against NS1, β -Tubulin and Myc. **(C, D)** HEK293T cells were transfected with pMVM-wt, pMVM-Myc-SAT-wt, pSUPER, pMyc-SUPER or pCFP. 24 h post transfection cells were stained with Hoechst 33342 (Hoechst) and PI and counted under a fluorescent microscope. pCFP served as a non-toxic control and CFP-positive cells were counted. *** $p < 0.001$ as calculated by two sample t-test.

In an additional experiment we wanted to analyse if the cell-death of pSUPER- or pMyc-SUPER-transfected cells is more immunogenic than of pMVMwt-transfected cells. Again, we analysed the release of the immunogenic marker HMGB1 to address this question. We transfected HEK293T cells with pSUPER, pMyc-SUPER, pMVMwt or pCFP and harvested the supernatant of the cells after 24 h or 48 h. The supernatants were analysed in a Western blot with antibodies against HMGB1 (figure 37). After 24 h the levels of released HMGB1 of pSUPER, pMyc-SUPER and pMVMwt were similar with a small increase for

pSUPER-transfected cells. After 48 h pSUPER- and pMyc-SUPER-transfected cells showed an increased level of released HMGB1 compared to pMVMwt-transfected cells. Especially pSUPER-transfected cells showed a strong release of HMGB1. These experiments gave a first hint that cell-death triggered by pSUPER might stimulate the immune system more efficiently than the cell-death triggered by pMVMwt.

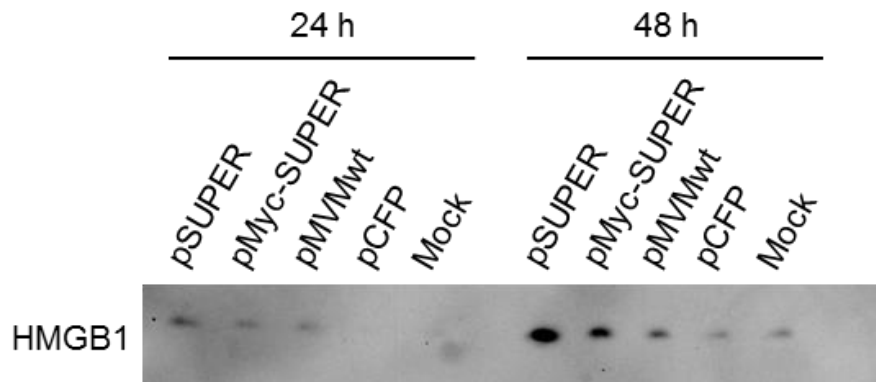


Figure 37: The release of HMGB1 is increased in pSUPER- and pMyc-SUPER-transfected cells. HEK293T cells were transfected with pSUPER, pMycSUPER, pMVMwt or pCFP. Supernatants were collected 24 h or 48 h post transfection and analysed on a Western blot with antibodies against HMGB1.

In order to continue the research on the SUPER virus and Myc-SUPER virus we tried to produce these viruses in HEK293T cells. The cells were transfected with either pMVM-Myc-SAT-wt, pSUPER, pMyc-SUPER or the pMVM- Δ 800. pMVM- Δ 800 has a deletion at the start site of VP2 of about 800 bps. It does not contain the sequence for SAT and was used in the past to insert transgenes in this area (Kestler et al., 1999) (figure 38). pSUPER, pMyc-SUPER and pMVM- Δ 800 are incapable of producing capsids. These viral genomes were co-transfected with a helper plasmid containing the capsid genes of the H1 parvovirus under the control of a CMV promoter. The capsid genes of H1 were used instead of the capsid genes of MVMP in order to prevent recombination events between the mutant genome and the helper plasmid. Such recombination events would lead to the formation of MVM-wt genomes. After transfection pMVM-wt-transfected cells are usually harvested after three days whereas MVMP- Δ 800-transfected cells are harvested after three or four days. A good indicator for the right time to harvest the cells and isolate the virus is the onset of cell lysis. The pSUPER- and pMyc-SUPER-transfected cells already started to die after two days. Given the enhanced killing abilities of pSUPER and pMyc-SUPER this result could be expected. At day two however, pMVM-wt- and pMVM- Δ 800-transfected

cells still appeared morphologically healthy. Nevertheless, all viruses were harvested at day two, purified with iodixanol and titrated using an infectious center assay. The titers of SUPER- and Myc-SUPER-virus were very low, whereas the titer of MVM-wt was about 30 times higher. MVM- Δ 800 could not be detected (table 2).

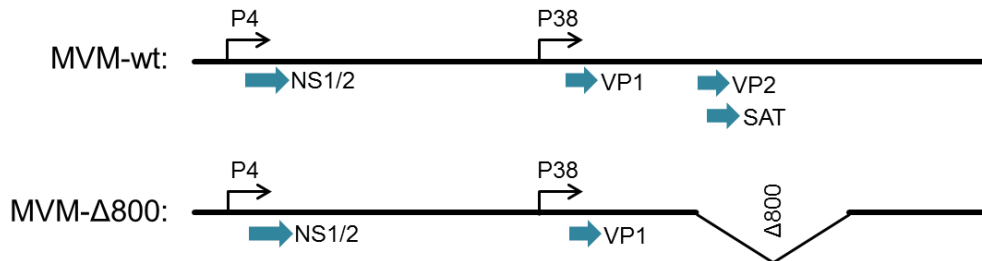


Figure 38: Genome of MVM-wt and MVM- Δ 800. The blue arrows indicate the translational start points of the respective proteins. Δ 800 indicates the deletion of about 800 base pairs from the genome.

Table 2: Different viruses were produced and their titers were measured in an infectious center assay.

Virus	Titer [infectious centers/ml]
SUPER	11.1×10^3
Myc-SUPER	6.6×10^3
MVM- Δ 800	not detected
MVM-wt	3.6×10^5

In order to increase the production rate of SUPER and Myc-SUPER we constructed shRNAs against SAT. We suspected that the accelerated cell death caused by an increased production of SAT might have negative effects on the production rate of the virus. In order to test the efficiency of the shRNAs HEK293T cells were co-transfected with pMVM-Myc-SAT-wt and the shRNA-constructs pshRNA2-SAT, pshRNA6-SAT or the empty shRNA vector (pshRNA_empty). 24 h post transfection cells were harvested and the lysates analysed on a Western blot for the expression of Myc (figure 39). The staining clearly showed a downregulation of the expression of Myc-SAT. The sequences of SAT that were used to construct the shRNAs strongly differed from the SAT sequence of H1, which is an

important feature since the mRNA of the capsid genes in the helper plasmid, would also be affected by the shRNA against SAT which would downregulate the expression of capsid proteins.

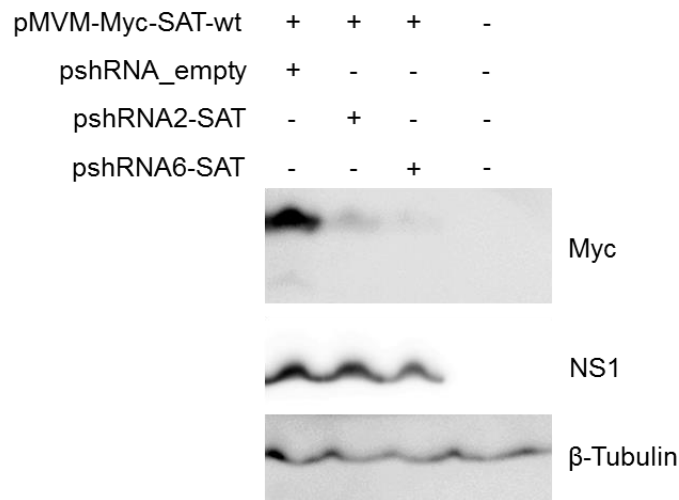


Figure 39: Knockdown of Myc-SAT. HEK293T cells were transfected with pMVM-Myc-SAT-wt and shRNA constructs against SAT (pshRNA2-SAT / pshRNA6-SAT) or the empty shRNA vector (pshRNA_empty). 24 h post transfection cells were harvested and analysed on a Western blot using antibodies against Myc, NS1 and β -tubulin.

In order to analyse if the knockdown of SAT has beneficial effects on the production rate of SUPER, HEK293T cells were co-transfected with either pMVM-wt, pSUPER or pMVM- Δ 800 and pshRNA_empty, pshRNA2-SAT or pshRNA6-SAT. As a control cells were transfected only with the viral constructs without the plasmids for shRNA production. Three days post transfection the virus was harvested and isolated from the cell debris via centrifugation. The produced virus was used to infect A9 cells on spotslides. 24 h post infection cells were fixed and stained with fluorescent antibodies against NS1 and NS1-positive cells were counted under the microscope. The results are shown in table 3. Unfortunately, the production of SUPER and MVM- Δ 800 was not successful. However, the production of MVM-wt was boosted using pshRNA_empty and pshRNA6-SAT. The reasons for this effect are obscure to us. The here-presented experimental data relies on only one single experiment and the approach should be changed in order to obtain decent amounts of SUPER virus. Due to the shortage of time these adoptions could not be done in the present work.

Table 3: Production of different viruses with the help of shRNAs. A9 cells were infected with the produced viruses and stained with fluorescent antibodies against NS1. NS1-positive cells were counted under the microscope. Titers are given in NS1-positive cells / ml.

	pshRNA_empty	pshRNA2-SAT	pshRNA6-SAT	---
MVM-wt	11.1 x 10 ⁵	1.7 x 10 ⁵	32.5 x 10 ⁵	0.36 x 10 ⁵
SUPER	0	0	0	0
MVM-Δ800	0	0	0	0

4 Discussion

The data presented in this thesis shows that SAT acts in a viroporin-like manner to induce the lysis of the cell. We show that SAT is transported to the plasma membrane where it homo-oligomerises to multimers and permeabilises the plasma membrane which eventually leads to cell lysis and virus release. Furthermore, we analysed the therapeutic potential of a modified MVMP, called SUPER, in which the *SAT* gene is translated in larger amounts. SUPER showed increased lytic activity and might be established in preclinical and clinical trials for its therapeutic potential to activate the host immune system to target cancerous tissue.

4.1 A Knockout of SAT is followed by a reduced cell lysis

In agreement with the results of Mészáros and colleagues who analysed the SAT protein of the porcine parvovirus (Mészáros et al., 2017), our findings showed that cell lysis, virus release and spreading were strongly reduced upon a knock-out of SAT in the genome of MVMP. Still, when infected with the SAT-ko virus, cells were lysed after an extended amount of time. The delayed cell death was probably caused by other cytotoxic processes such as the extensive production of viral DNA and proteins, the virus-induced DNA-damage response, cell-cycle arrest, and the cytotoxic features of NS1. Indeed, many previous reports attributed the main cytotoxicity of the virus to the NS1 protein. For example, NS1 was shown to induce the production of reactive oxygen species or to induce cell cycle arrest. However, a direct molecular mechanism of cell lysis has never been shown for NS1. We directly compared the lytic potential of NS1 with SAT and found that SAT was much more effective than NS1 in lysing cells. Although NS1 was shown to have cytotoxic activity, the wild type virus most likely gains its full lytic potential from the SAT protein. The addition of a Myc-tag to SAT further increased the killing potential of the protein. The reason for this finding is not clear, but we suspect that the Myc-tag could stabilize the SAT protein and extend its half-life. These findings have to be considered for the oncolytic therapy with parvovirus. The success of the therapy strongly depends on the activation of the immune system by the release of tumour antigens from dying cells. SAT clearly acts as a lytic protein and is likely to play a crucial role in this immunologic aspect of the therapy by releasing PAMPs (pathogen-associated molecular patterns) and DAMPs (damage-associated molecular patterns) such as HMGB1.

4.2 The transport of SAT is crucial for its lytic function

Mészáros and coworkers suggested that the SAT protein of PPV induces the lytic process by an upregulation of ER-stress (Mészáros et al., 2017). Virus-induced ER-stress is a frequent phenomenon in viral infections. The extensive production of viral proteins disturbs the homeostasis of the ER and can lead to the formation of unfolded and misfolded proteins. Different sensors in the ER such as IRE1 and PERK detect the ER-stress and initiate the so-called unfolded protein response (UPR), which is supposed to relieve the ER-stress and restore proper ER-functionality. For example, the UPR induces the production of chaperones in order to increase the folding abilities of the ER (Zhang and Wang, 2012). This process can also be exploited by viruses: Japanese encephalitis virus (JEV) and dengue viruses (DEN) trigger the UPR in order to increase the folding capacity of the ER to produce more viral proteins (Urano et al., 2000). The activation of the ER-stress sensor PERK can also lead to the phosphorylation of the translation initiation factor eIF2 α which initiates a shutdown of protein-translation. This pathway can be utilised by viruses as well: Herpes Simplex Virus (HSV) 1 induces the activation of PERK - a process that has been shown to be important for the viral replication of HSV 1. However, the viral protein γ 134.5 mediates the dephosphorylation of eIF2 α thereby preventing the shutdown of protein-translation. By this strategy, HSV1 activates the UPR and disarms it at the same time (Cheng et al., 2005; He et al., 1997).

If the UPR is unable to resolve the ER-stress, it induces the expression of CHOP which initiates apoptosis. Mészáros and coworkers could show that CHOP localised to the nucleus upon infection with the wild type porcine parvovirus (PPV-wt) which was not seen in PPV-SAT-Ko-infected cells (Mészáros et al., 2017). Nuclear CHOP is known to induce apoptosis and the researchers hypothesised that a CHOP-induced apoptosis would release the progeny viruses from the cell. However, Mészáros and coworkers could not discover a direct link between PPV SAT and the localisation of CHOP. When SAT was expressed without any other viral factor CHOP did not translocate into the nucleus. Additionally, a toxic overexpression of CHOP could not rescue the spreading capacity of the PPV-SAT-Ko virus to reach PPV-wt levels. Moreover, researchers working with West Nile Virus found out that infections with this virus led to the induction of CHOP, which initiated apoptosis. However, viral titers were significantly higher in *chop*^{-/-} cells compared to wild

type cells suggesting that CHOP-induced apoptosis might represent a cellular defense mechanism against viral infections (Medigeshi et al., 2007).

In our experiments we discovered that SAT was transported to the plasma membrane. Blocking this transport via the expression of Sar1 dn abrogated the lytic effect of SAT. This finding was not in agreement with the results of Mészáros since the expression of SAT was not reduced upon the co-expression of Sar1 dn. This experiment suggested that there might be an alternative lytic pathway triggered by SAT. However, it should not be excluded that SAT might induce an ER-stress response. Many viroporins have multiple functions and can interact with other cellular factors. The observed ER-stress might be important for other steps of the parvoviral lifecycle. For example, in our experiments we observed a decreased infectivity of SAT-ko viruses which might be the result of a missing ER-stress response.

4.3 SAT shows properties of a viroporin

Since SAT is a short viral protein harbouring a transmembrane domain we hypothesised that it might act as a viroporin. Viroporins usually homo-oligomerise within membranes to form pores that are permeable to small molecules such as ions. Some of them have also been shown to be involved in the lysis of cells. In several experiments we investigated the question if SAT could function as a viroporin:

The immunoprecipitation and proximity ligation-experiments clearly showed that SAT formed oligomers located within the cell and at the plasma membrane. The UV-induced crosslinking experiment let us to suspect that oligomers of higher-order, potentially tetramers, might exist. However, the stained protein-bands in the Western Blot did not show a sharp outline but appeared cloudy. In the future this method might be improved: Similar crosslinking experiments were already conducted with the viroporin protein p7 of HCV. In these experiments recombinant p7 protein was inserted into artificial lipid bilayers. The photoreactive amino acids photo-leucine and photo-methionine had been incorporated into the p7 protein. Following UV-crosslinking, precise bands representing multimeric states of p7 were detected in the Western blot (Soranzo et al., 2016). Such an approach might also be applicable for SAT in order to determine the oligomeric state of a potential pore.

The Hygromycin B assay demonstrated that the expression of SAT increased the permeability of the plasma membrane to small molecules. Only the cells that were transfected with pMVM-wt allowed Hygromycin B to pass through the plasma membrane which led to the downregulation of the translation of YFP. SAT might also indirectly increase the permeability of the plasma membrane to small molecules. The Hygromycin B assay was used many times to assess the increase in permeability of a membrane caused by a viroporin. However, Madan and Bartenschlager suggested that the uptake of Hygromycin B upon expression of a viroporin might be explained with an upregulated endocytosis rather than an increased permeability of the membrane (Madan and Bartenschlager, 2015). If this is the case for SAT and how this process would be able to induce cell lysis is not clear.

Viroporins are often permeable to small ions such as calcium or sodium ions. We tested if pores formed by SAT were permeable to these ions but could not find any hint supporting this idea. The time lapse experiment using Sodium Green showed that there was no increase in the intracellular sodium concentration preceding cell death and the influx of PI. However, it should be considered that the changes in the intracellular sodium concentration induced by a SAT pore might be very little. It might not be possible to detect such small changes with Sodium Green. Even in dead cells the signal of Sodium Green was very weak which let us suspect that the dye might not be sensitive enough for our purposes.

The experiment using Fura-2-AM also did not show any elevated levels of intracellular calcium ions, however, it should be considered that this experiment concentrated on a very short time period of a few minutes. The time between permeabilisation of the plasma membrane to calcium caused by a SAT pore and the event of cell-death might be very short. It has to be considered that the concentration of SAT at the plasma membrane might be a crucial factor. The more SAT monomers accumulate at the plasma membrane the more likely a pore formation becomes. Once a critical concentration of SAT is reached, permeabilisation and cell-death might occur in a very short time frame. A dying cell might become positive for Fura-2-AM-staining a short time before its cell death. Such events were not recorded.

An ideal experiment to analyse the pore formation of SAT would be a black-lipid assay. This assay uses an artificial membrane. On both sides of the membrane buffer solutions are

filled in tanks equipped with electrodes measuring currents between the two tanks. Recombinant protein such as a viroporin protein is added to the membrane. In this setting the permeability of the pores for certain ions can be analysed (figure 40) (Mueller et al., 1962). This assay already helped to study viroporins such as the p7 viroporin of HCV (Griffin et al., 2003) or the Vpu viroporin of HIV-1 (Römer et al., 2004). Another approach would be to use the patch-clamp technique that measures currents at the plasma membrane of living cells. A viroporin, embedded in the plasma membrane, should be able to change the currencies of certain ions across the plasma membrane which can be measured using this technique.

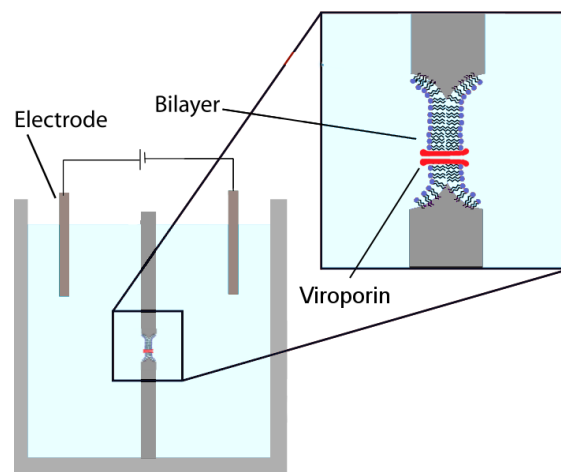


Figure 40: Schematic figure of a setup of a black lipid membrane assay. An artificial membrane is placed in a hole of a wall that separates two tanks from each other. The membrane contains a viroporin. Electrodes are submerged in both tanks and measure currents between the two chambers. (https://en.wikipedia.org/wiki/Model_lipid_bilayer; 10.06.2018)

What we found surprising was the observation that PI (668.40 Da) with a molecular weight that is only slightly bigger than Hygromycin B (527.53 Da) did not pass the membrane before cell death occurred. In the time lapse experiment we observed that the dye only entered cells that underwent severe morphological changes of cell lysis. We suspect that the charged nature of PI inhibits its translocation to the cytoplasm of living, SAT-expressing cells. The residues of the transmembrane domain of SAT are exclusively uncharged which would make the passage of charged molecules through the pore difficult. The non-polar nature of the transmembrane domain might be permeable to other molecules than ions which eventually induces cell lysis.

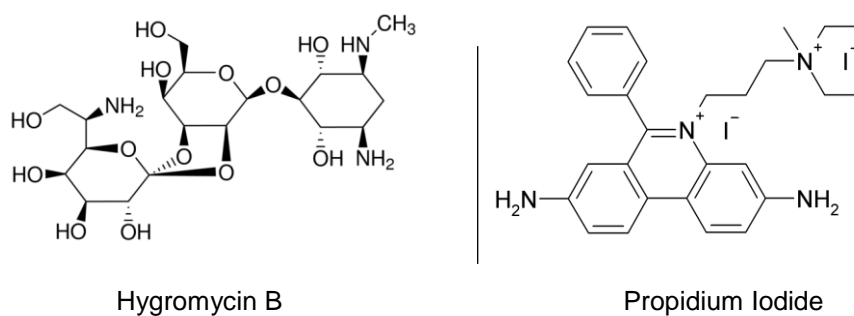


Figure 41: Schematic structures of Hygromycin B (527.53 Da) and Propidium Iodide (668.40 Da).

The coarse-grained simulation of SAT monomers in a simulated membrane did not lead to the development of pore-like structures. However, very symmetric arrangements of dimers and tetramers were observed, confirming the results of the UV-induced crosslinking experiment. Especially the leucine zipper that starts at the N-terminal domain and reaches into the transmembrane domain apparently played an important role in this process. The helices first met at their N-termini and increased their interaction surface along the leucine residues. A mutation of the leucine zipper (LLLL15/18/22/25GGGG) strongly inhibited the lytic nature of SAT.

We suspect that the tetramers might not be the final oligomeric state. The C-termini of the helices in the tetramer adopted a slightly curved configuration which let us to suspect that additional tetramers might come in to form one large pore. This would lead to the formation of structures such as a tetramer of tetramers or a pentamer of tetramers (figure 42). Furthermore, we also observed during the simulation that the C-termini of the helices of the tetramers were able to make interactions with additional monomers underscoring the possibility of larger oligomers. An extended simulation time with more monomeric helices might lead to the development of larger complexes and even pore-like structures.

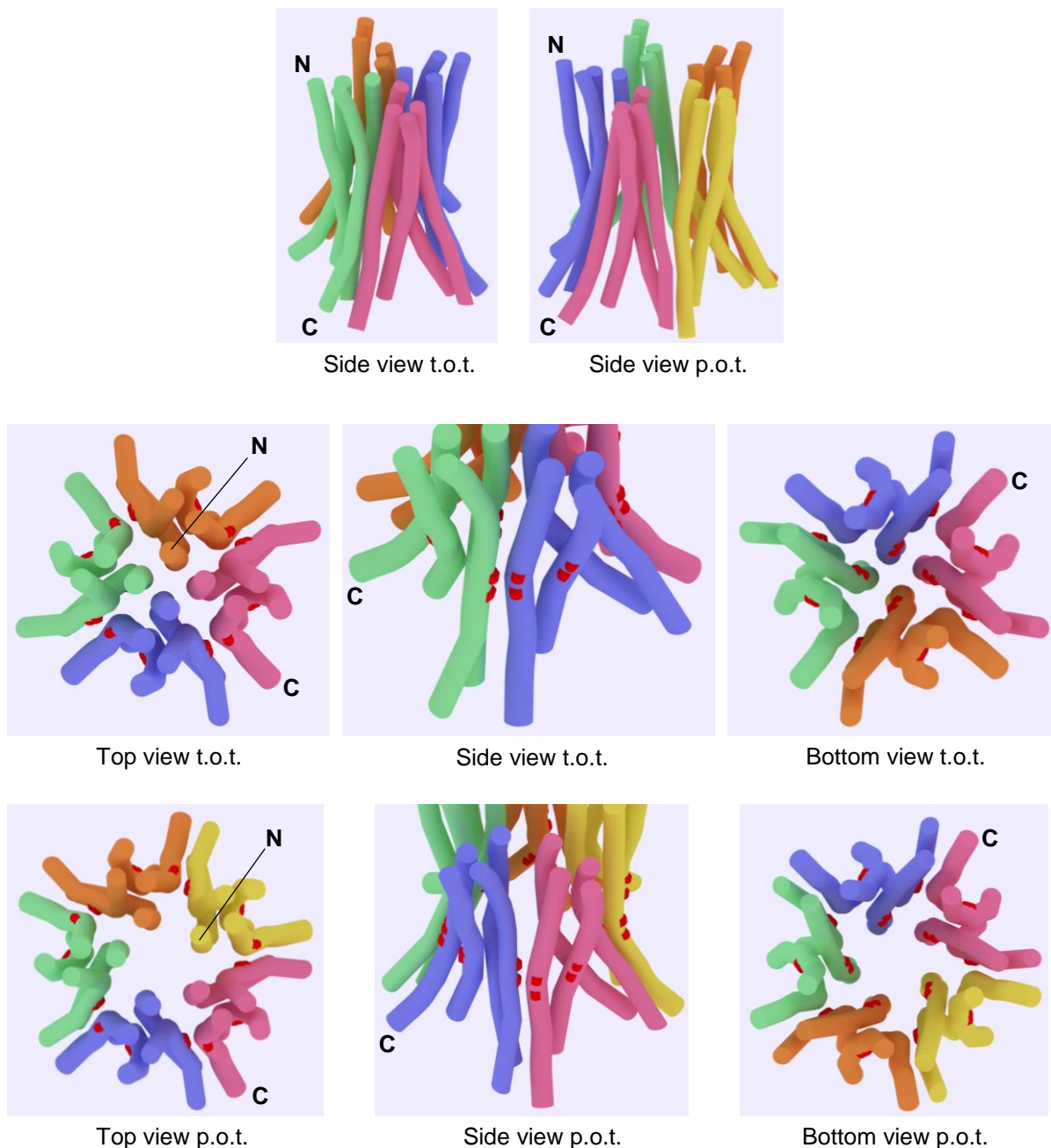


Figure 42: Potential structures of a tetramer of tetramers (t.o.t.) and a pentamer of tetramers (p.o.t.) of SAT. The tetramer that was found during the coarse-grain simulation was modelled using the modeling software blender. This tetramer was used to build large oligomeric structures of SAT with each tetramer coloured in a different colour. The glycine residues of the GxxxG motif are coloured in red (N: N-terminal end; C: C-terminal end).

Another hint came from the GG31/35LL mutations that abrogated the lytic effect of SAT. The glycine 31 and 35 were suspected to form a GxxxG motif, which is frequently seen in transmembrane proteins. In this motif the two glycines are located at the same side of the α -helix within one turn of the helix. With glycine being the smallest residue, this configuration

would allow another protein helix to come into very close contact to this site of the protein. However, glycine 31 and 35 did not fulfill this function in the simulation. They rather faced outwards of the dimers and tetramers and did not take part in the interactions of the monomers. If a large pore was formed by a tetramer of tetramers the glycine residues of adjacent tetramers would make contacts to each other. A similar configuration of the glycine residues would be found in the case of pentamers of tetramers. Additionally, in a pentameric tetramer the glycine residues of one helix of each tetramer would face inside the large pore (figure 42). This putative configuration might explain the non-lytic phenotype of the GG31/35LL mutation. The large leucine residues might inhibit the interaction of the tetramers and might reach into the center of the large pore, preventing small molecules to pass through. This assumption is also in accordance with the immunoprecipitation experiment that showed that the G31/35LL mutation did not abrogate the oligomerisation ability of SAT. The GG31/35LL mutation would not inhibit the formation of tetramers, but it would prevent the formation of larger oligomers.

The simulation could not explain the non-lytic phenotype of the KR48/49AA mutation. The residues seemed to interact with D52, but it was not clear if this interaction was crucial to the lytic nature of SAT. Residues at the C-terminal domain might be important to form interactions with other helices outside the tetramer. On the other hand, K48 and R49 might be important to stabilise the monomeric helix in its position in the membrane. The positively charged residues might interact with negatively charged head groups of the membrane molecules. The mutation of K48 and R49 to two alanines neither abolished the oligomeric state of SAT nor the transport of SAT to the plasma membrane. However, a destabilised protein might not be able to fulfill its function.

Furthermore, the simulation could not explain the increased permeability of the plasma membrane to Hygromycin B. No pore-like structure was detected that would have been big enough for Hygromycin B to fit through. A hypothetical large pore made up of multiple tetramers might provide a portal to Hygromycin B.

Another possible lytic mechanism of SAT would be the formation of a holin-like structure. Holins are expressed by bacteriophages and they include one to four highly hydrophobic transmembrane helices which locate them to the plasma membrane. These proteins are important for the lysis of the infected cell and the release of progeny phages. Holins form

large holes in the plasma membrane of the infected bacterium. Additionally, the phage expresses endolysins that pass through these holes and cleave the cell wall on the other side of the plasma membrane. By this mechanism the bacterium is lysed and the progeny phages are released (Saier and Reddy, 2015). The molecular process of the lysis by holins is still not fully understood. A hypothetical mechanism is depicted in figure 43. Due to their hydrophobic transmembrane helices holins cluster at the plasma membrane into rafts of protein that exclude lipids from their inside. At these rafts the polarised nature of the plasma membrane is locally disturbed which leads to a conformational change of the holins. Subsequently, the holins form large holes of more than 300 nm in diameter. The hydrophilic face of the transmembrane helix of the holins is facing inward the hole (White et al., 2011). Holin-like proteins have also been found in other organisms than phages. The eukaryotic proteins Bax and Bak are holin-like proteins which are involved in the permeabilisation of the mitochondrial outer membrane during apoptosis. It was shown that Bax and Bak are able to permeabilise the bacterial plasma membrane in a similar way as holins (Pang et al., 2011; Saier and Reddy, 2015). SAT might also act in a holin-like way. With its highly hydrophobic transmembrane domain it might be able to cluster into rafts at the plasma membrane of infected cells which might lead to the formation of large holes. Various substances including progeny virions would be able to pass through such a hole which would immediately lead to the cell lysis.

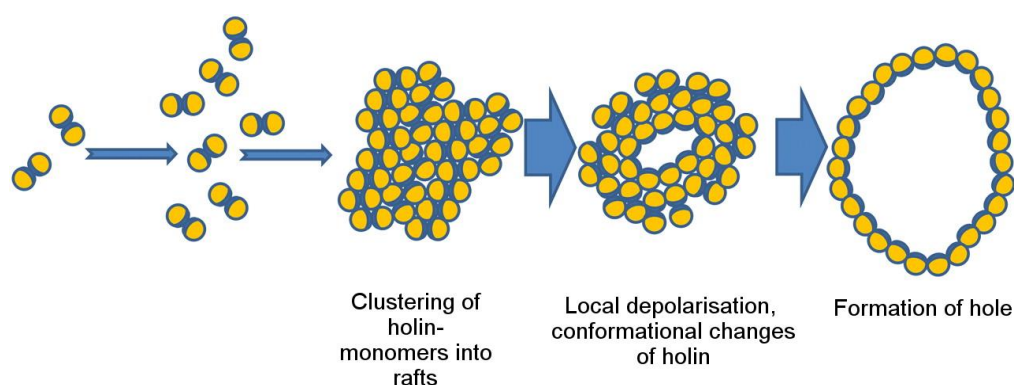


Figure 43: Top-view on the hole formation by holins at the plasma membrane. Holins cluster together to form large rafts. Local depolarisation of the plasma membrane leads to conformational changes of the holin proteins which makes the rafts transform into large holes (White et al., 2011).

It should also be mentioned in this context that parvovirus and phages are similar in other features, too. Especially the phage ϕ X174 was already found to have similar features as parvovirus. Parvovirus replicates in a rolling hairpin replication (see chapter 1.6.2 “The

replication process”), phage ϕ X174 replicates in a rolling circle replication. Both of these mechanisms are very similar to each other. Both viruses are packaged as single stranded DNAs. Furthermore, it has already been suggested in previous reports that NS1 has similarities to protein A of phage ϕ X174 (Astell et al., 1985; Nüesch et al., 1995). Both proteins contain a metal-coordination site and are involved in the replicative cycle by inducing nicks in the viral genome which covalently links them to the DNA via a tyrosine residue. These further similarities between parvovirus and phages might be a hint for a common evolutionary path between these two viruses. Parts of the phage genome might have been incorporated into the genome of parvovirus via recombination events. The *SAT* gene might be the result of such a recombination event which underscores the possibility that SAT might act similar to a phage holin.

In this work we could not deliver clear evidence that SAT forms a pore or a hole. Therefore, we also have to consider that SAT might induce cell lysis via a different pathway that does not include the formation of a pore. SAT might interact with other proteins of the plasma membrane such as ion channels, receptors or lipid-sensing proteins and influence their functionality which would eventually lead to cell lysis. Such binding partners might be found via immunoprecipitations and mass spec analysis.

4.4 Cell-death in MVM-wt or SAT-ko-infected cells and the function of SAT

The potential action of SAT as a viroporin let us hypothesise that the cell morphology might change due to osmotic pressure changes in the intracellular environment assuming that ions would cross the plasma membrane. Therefore, we performed a time-lapse experiment with MVM-wt and SAT-ko-infected cells. However, we did not observe any differences in the morphology of MVM-wt-infected cells compared to SAT-ko-infected cells. In both cases the plasma membrane collapsed towards the nucleus probably due to the degeneration of the cytoskeleton caused by the actions of NS1. Furthermore, the PI-staining and the Annexin V-staining did not show any differences between MVM-wt- and SAT-ko-infected cells. Cells became positive for these dyes when they have already undergone severe morphological changes.

If the SAT-ko virus is able to produce progeny viruses and lyse the cell, we asked ourselves what the function of the SAT protein in MVM-wt virus was. A striking difference between MVM-wt virions and SAT-ko virions was seen in the infectivity. SAT-ko virions were 18 times less infectious than MVM-wt virions. Such a reduced infectivity was also seen in the studies of Baer and coworkers, who observed a strong reduction in infectivity of progeny viruses when the vesicular transport system of the virus-producing cells had been inhibited (Bär et al., 2013). We suspect that this inhibition of the vesicular transport might have also affected the transport of SAT to the plasma membrane, leading to a reduced lysis of the virus-producing cells. The produced progeny viruses from these cells were reduced in their infectivity. Therefore, we suspect the delayed lysis of SAT-ko-infected cells to be harmful to the progeny viruses. It was shown that parvovirus can induce apoptosis which is abrogated by a disruption of the plasma membrane. A missing lytic agent might lead to a further progression of apoptosis that would be followed up by the breakdown of cellular and viral proteins and nucleic acids. It has already been shown that during the infection of tumor cells by the H1-parvovirus cathepsins are released from the lysosomes into the cytosol (Di Piazza et al., 2007). These released proteases might attack progeny viruses and reduce their infectivity. Therefore, we suggest that SAT induces the lysis of the cell in order to avoid degrading processes of the dying cell. Another possible function of SAT might be that an influx of certain ions through a pore made of SAT might support the virus in processes such as maturation. The nonstructural protein 4 (NSP4) of rotavirus, for example, is a viroporin that was found to release calcium ions from the ER. These ions induce autophagy required for viral assembly.

From the similarity of SAT to viroporins and the behaviour of SAT within the cell we assumed that SAT would act as a pore-forming protein. Viroporins are often permeable to ions. If SAT was permeable to ions, we would have expected to see differences in the morphological features of dying cells infected with either wt or SAT-ko due to osmotic changes. However, neither changes in ion concentration nor differences in the cell death were observed. Therefore, we searched for other substances than ions that might pass through a pore at the plasma membrane and induce cell death. In 1999 Ran and coworkers observed a massive drop in the intracellular concentration of nicotinamide adenine dinucleotide (NAD) after an infection with parvovirus. NAD acts as a coenzyme in redox reactions thereby transferring electrons to several proteins. It exists in an oxidized (NAD^+) and a reduced (NADH) form. When synchronized HeLa cells were infected with parvovirus

H-1 the concentration of intracellular NAD (NAD⁺ and NADH) dropped by 90% after 6 h of infection. A drop in intracellular concentration of NADP (NADP⁺ and NADPH) was also observed. Upon inhibition of NAD-consuming enzymes the early secondary necrosis which is usually observed in parvovirus-infections, was delayed and more cells showed apoptotic features. However, a stimulation of NAD production did not protect cells from death. The authors of the paper concluded that the NAD-consuming enzymes would influence the cell death pathways to induce an early necrosis thereby depleting NAD stores (Ran et al., 1999). In contrast, we hypothesise that NAD (664.43 g/mol) might pass directly through the SAT pore at the plasma membrane which would induce necrotic cell death. A few reports deliver hints that are in favor of this idea:

Bupivacaine is a local anesthetic. However, it is also neurotoxic and induces apoptosis and necrosis. It was found that the treatment of cells with bupivacaine is associated with an intracellular depletion of NAD⁺. Supplementation of NAD⁺, however, rescued the cells from cell death (Zheng et al., 2013). In a similar experimental setup, PC12 cells were treated with rotenone, which usually induces apoptosis and necrosis. Additional treatment with NAD⁺ inhibited the induction of cell death (Hong et al., 2014). The exact mechanisms of how cell death is induced when NAD stores are depleted is probably quite complex, since NAD is a universal communicator in redox biology and therefore involved in many cellular reactions. However, the flux of NAD through a SAT-pore might explain a few of the phenomena we observed during our studies. The proximity ligation experiment showed that an oligomerisation of SAT was taking place at the plasma membrane. However, we also observed oligomerisation at intracellular structures, most likely the ER and the Golgi. In these compartments high concentrations of calcium ions can be found. If SAT-pores were permeable to calcium ions the formation of a pore at the ER and the Golgi should already have led to strong cellular disturbances without the need for SAT migrating the whole way to the plasma membrane. However, an inhibition of the transport of SAT to the plasma membrane abrogated the cell death indicating that only the permeabilisation of the plasma membrane had cytotoxic effects. NAD is both present in the cytoplasm and the ER and Golgi (Dölle et al., 2010). The exact concentrations in the respective compartments are not known. However, assuming that there are no big concentration gradients between the cytoplasm and the ER or Golgi, a permeabilisation of the ER and Golgi membrane to NAD would not have a strong negative effect on the cells. However, the concentration gradient of NAD between the intracellular space and the extracellular space is large, since the

extracellular concentrations of NAD are kept low. An efflux of NAD would halt glycolysis and other important cellular processes and might induce cell death. In order to find out whether SAT has the ability to permeabilise the plasma membrane to NAD, cells could be infected with either the MVM-wt- or the SAT-ko-virus and their intracellular and extracellular NAD concentrations could be analysed.

Besides its beneficial oncolytic features, parvovirus can also infect animals and humans and lead to the development of harmful symptoms such as gastrointestinal problems. A putative pore-forming ability of SAT might be exploited by an antiviral therapy. Amantadine was shown to strongly interfere with M2, the viroporin of influenza A (Hay et al., 1985). A similar molecule might have the potential to block the permeabilisation of the plasma membrane by SAT. Such a strategy might be useful for infected canine puppies that suffer from severe symptoms of parvovirus infection such as weight loss or heart problems. Additionally, it could serve as a safety switch in the oncolytic therapy for special cases if unexpected events occur such as a cytokine storm induced by the release of tumor antigens from dying cancer cells. A SAT-blocking agent might slow down the viral life cycle and thereby reduce the speed of cell lysis.

4.5 Potential therapeutic applications of SAT

During their studies Geletneky and coworkers discovered a vaccinating effect of the oncolysis by parvovirus. Tumour-bearing mice that were treated with H1-parvovirus and survived the procedure developed an immunity against the cancer cells. A re-challenge with tumour cells did not lead to the formation of a tumour although parvovirus was not detected any more. This experiment clearly underscores the importance of the immune system in the therapeutic approach. However, it has to be considered that the oncolytic therapy with parvovirus still does not lead to a complete regression of tumours in patients. Even in preclinical trials tumour-bearing animals that were treated with a low dose of virus showed tumour growth and had to be killed eventually (figure 44).

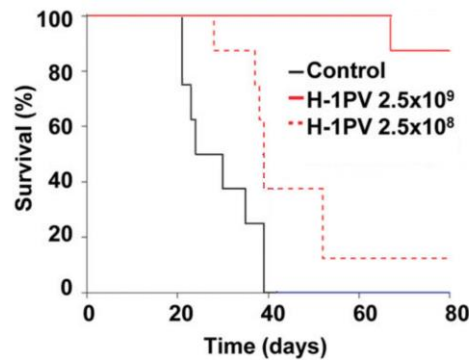


Figure 44: A low dose of H1-parvovirus cannot heal tumour-bearing rats. Tumour-bearing, immunocompromised rats were infected with two different doses of the oncolytic parvovirus H1. Survival is shown in a Kaplan-Meier plot. Figure adapted from Li et al. 2013 (Li et al., 2013)

In order to improve the oncolytic virotherapy we wanted to utilize the SAT protein to make the virus more toxic to cancer cells. Therefore, we constructed the SUPER virus. The genome of SUPER is altered in order to increase the amount of translated SAT. Since SAT is mainly responsible for the lysis of the cell we concluded that an increased expression of SAT should lead to an increased cell lysis. In a Western blot we saw that the expression of SAT could be increased in pMyc-SUPER-transfected cells compared to pMVM-Myc-SAT-wt-transfected cells. We suspect the increased amount of SAT to be responsible for the enhanced lytic potential of pSUPER and pMyc-SUPER that was observed experimentally. It should be considered that we analysed cell death after 24 h. Since the wild type virus is capable of forming progeny viruses and to spread in the cell culture it is suspected to outrun the SUPER virus on the long term regarding cell killing in *in vitro* experiments. However, we still suspect the SUPER virus to have beneficial features compared to the wild type virus. The rapid cell killing observed in pSUPER-transfected cells is suggested to lyse the cells more efficiently and to induce a stronger immune response *in vivo*.

To investigate the potential impact of SAT on the stimulation of the host immune system, we analysed the immunogenic marker HMGB1. We observed that HMGB1 was released in greater amounts from pSUPER-transfected cells than pMVM-wt-transfected cells. Additionally, MVM-wt-infected cells released a larger amount of HMGB1 than SAT-ko-infected cells underscoring the importance of SAT in this process. HMGB1 is usually bound to the DNA. In cells that undergo apoptosis HMGB1 becomes tightly bound to the DNA and is not released into the medium until secondary necrosis appears. In the case of

apoptosis HMGB1 becomes oxidised at a disulfide bond which abolishes its proinflammatory nature. Only the reduced form released during necrosis was found to activate immune cells (Dumitriu et al., 2005; Kazama et al., 2008; Rovere-Querini et al., 2004; Scaffidi et al., 2002; Venereau et al., 2012; Yang et al., 2012). As a follow-up experiment the oxidative state of HMGB1 that was released by parvovirus-infected cells should be analysed. A non-reducing SDS-PAGE has already been shown to reveal the oxidative state of HMGB1. Here, the oxidative and reduced form of HMGB1 can be separated in two distinct bands (Hoppe et al., 2006). In order to fully analyse the immunogenic potential of SUPER the direct activation of immune cells has to be analysed followed by *in vivo*-studies.

We found it quite odd that infections with parvovirus lead to an apoptosis that is interrupted by a secondary necrosis. A necrosis is usually an inflammatory event which attracts immune cells and should negatively affect the virus and its spreading capacities in a natural infection. However, the induction of apoptosis might lead to the inactivation of inflammatory messengers such as HMGB1. It would be interesting to see if SUPER might inactivate this process by speeding up the death process and inducing a more immunogenic cell death.

Tumor antigens are usually released by dying cancer cells and are taken up by immune cells which leads to their stimulation. Moehler and coworkers could show that tumor cell lysates of parvovirus-infected cancer cells were taken up by dendritic cells. The dendritic cells cross-presented tumor antigens to cytotoxic T cells and released proinflammatory cytokines (Moehler et al., 2005). We suspect that infections with the SUPER virus might improve the release of antigens and the stimulation of the immune system. We do not know if infections of actual tumors in patients with the wild type virus lead to an efficient release of tumor antigens and a strong stimulation of the immune system. We also do not know if the infected cells produce high levels of SAT to induce lysis of the cell. Almost all patients of the clinical trial succumbed to their disease. Improvements of the therapy are therefore urgently required. With the SUPER virus we hope that we have developed a powerful vector that is able to produce large amounts of SAT to lyse the infected tumor cell in a very efficient way regarding the release of tumor antigen.

One drawback of the SUPER virus is its production. Usually, HEK293T cells are transfected with the DNA of the wild type virus. Three days after the transfection the transfected cells start to die and the produced virus can be isolated from the cells. Transfection of pSUPER together with a helper-construct did not produce large amounts of virus. The transfected cells already started dying after two days. This result was expected, since SUPER produces more SAT which makes it more toxic than the wild type virus. The co-transfection with shRNAs against SAT could reduce the production of SAT, but it did not increase the production of the virus. However, this result is based on a single experiment. Modifications of the approach might help to produce robust amounts of SUPER virus.

In order to combine the ability of the wild type virus to produce progeny viruses with the ability of SUPER to induce rapid cell death the two viruses might be used simultaneously as a mixture. This approach might even allow the production of progeny SUPER viruses when a cell is simultaneously infected with the wild type and the SUPER virus. In this case the wild type virus would provide the necessary VP proteins to package progeny viruses. However, it is questionable if a cell that was infected with both viruses is still capable to produce progeny viruses in large amounts. In the wild type virus the expression of viral proteins including SAT is likely to be finely tuned in order to guarantee the production of progeny viruses. A premature cell death induced by an overexpression of SAT might not give the cells enough time to produce progeny viruses. Recombination events between the two viruses should not be problematic since the two viruses are very similar to each other and would most likely not lead to the development of new viral species that would be potentially harmful to humans.

Further improvements of the method include the production of Adenovirus-SUPER chimera. Antonio Marchini could already show that the parvoviral genome can be incorporated into the genome of adenovirus (El-Andaloussi et al., 2012). Advantages of this method include the high titers achieved during the production of viruses and efficient gene transfer of adenoviruses. In this approach the parvoviral genome was incorporated in a replication-defective, E1- and E3-deleted Ad5 vector genome. Transfection of HEK293T

cells led to the production of Adenovirus-Parvovirus chimera - parvovirus genomes packaged in adenovirus capsids. These viruses were able to infect cancer cells and they were able to produce progeny parvoviruses. The Adenovirus-SUPER chimera would require an additional segment in their genome to produce VP1 and VP2 since the genome of SUPER does not provide the expression of these proteins. Since the uptake of foreign DNA into the Ad5 vector genome is limited, sequences in the VP-coding part of the genome of SUPER should be deleted to create additional space (figure 45). It has already been shown that similar deletions of up to 800 bps in the VP-coding region (MVM- Δ 800) did not affect the life cycle of parvovirus. For the production of capsids, the VP-coding region could be added in trans (Kestler et al., 1999). However, it has to be considered that it has not been shown yet that the adenovirus-parvovirus chimera are able to produce progeny viruses in tumor xenografts and tumours of patients. If the production does not take place, the insertion of an additional VP-producing segment might be omitted.

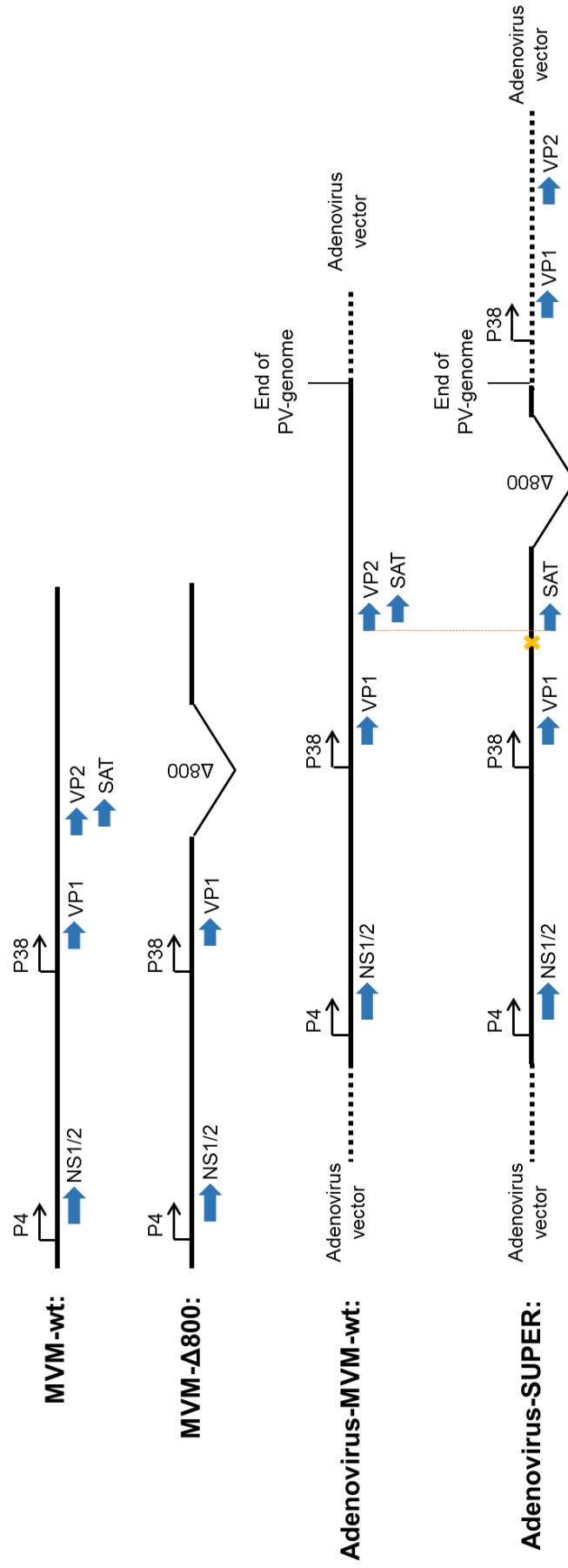
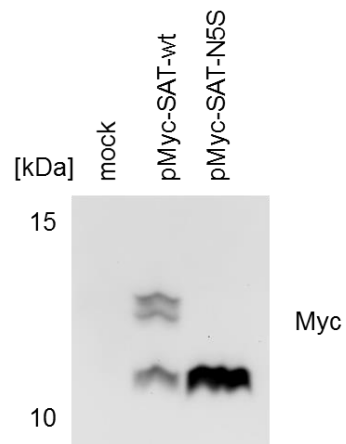


Figure 45: Genome structures of MVM-wt, MVM-Δ800, Adenovirus-MVM-wt and Adenovirus-SUPER. The blue arrows indicate translation start sites. The orange cross indicates an additional translation stop signal in the sequence of VP1.

As another improvement we consider making the expression of SAT independent from the expression of NS1. In the case of wild type and SUPER virus the expression of SAT is regulated by the P38 promoter which is transactivated by NS1. By replacing the P38 promoter of SUPER with a P4 promoter (P4-SUPER), which is generally active in proliferating cells, the expression of SAT would primarily rely on the conversion of the single-stranded viral genome to the double-stranded active form which makes transcription from the DNA possible. This conversion is only seen in proliferating cells since these cells express the required factors for this process (see chapter 1.6.2 “The replication process”). The independence of the expression of SAT from NS1 might be important since the activity of NS1 to activate the P38 promoter and hence the expression of SAT is regulated via acetylation of two residues of NS1 (Li et al., 2013). We do not know if these acetylation events also take place in the tumours of patients. In fact, it was shown that the transcriptional activity of NS1 could be improved when the cells were treated with valproic acid which strongly stimulated the acetylation of NS1 *in vitro*. Tumour-bearing mice that were treated with H1 parvovirus showed an impressive increase in the survival when they were additionally treated with valproic acid (Li et al., 2013). The study did not explicitly correlate this improvement of the therapy to the increased expression of SAT, but the expression of SAT might have been indirectly induced by valproic acid. Nevertheless, this phenomenon might be seen as a hint for our hypothesis and that the dependence of the expression of SAT on NS1 might pose a disadvantage in the oncolytic therapy. The P4-SUPER virus would be independent of acetylation events of NS1, which might or might not take place in the tumor of a patient. We suspect this virus to lyse cancer cells even in an intracellular environment that does not support the full posttranslational modification of NS1.

For these reasons we strongly believe that SUPER or any other parvovirus that increases the production of SAT should be included into the repertoire of the parvoviral treatment-strategies.

5 Supplement



Supplementary figure 1: A mutation at a putative glycosylation-site N5 abolishes bands with a higher molecular weight. HEK293T cells were transfected with pMyc-SAT-wt or pMyc-SAT-N5S. 24 h later cells were harvested and analysed on a Western blot with antibodies against Myc.

6 Abbreviations

APAR	Atonomous parvovirus-associated replication
ATM	Ataxia Telangiectasia Mutated
ATP	Adenosine triphosphate
CHOP	CCAAT-enhancer-binding protein homologous protein
Crm1	Chromosomal maintenance 1
DDR	DNA damage response
DMEM	Dulbecco's Modified Eagle's Medium
DMSO	Dimethylsulfoxid
DSS	Disuccinimidyl suberate
EDTA	Ethylenediamine tetraacetate
EMC	Encephalomyocarditis virus
ER	Endoplasmic reticulum
FCS	Fetal calf serum
GAPDH	Glycerinaldehyd-3-phosphat-Dehydrogenase
GFP	Green fluorescent protein
GppCH2p	Guanosine 5'-[α,β -methylene]triphosphate
HCV	Hepatitis C virus
HEK293T	Human embryonic kidney cells 293T
HIV	Human immunodeficiency virus
HMGB1	High-Mobility-Group-Protein B1
HRP	Horseradish peroxidase
HSV	Herpes Simplex Virus
Hyg B	Hygromycin B
IC	Infectious center
ICA	Infectious center assay
JC polyomavirus	John Cunningham polyomavirus

kb	Kilobase
M2	Matrixprotein 2
MVM	Minute virus of mice
NS1	Non-structural protein 1
NS2	Non-structural protein 2
NSP4	Nonstructural protein 4
NLS	Nuclear localisation signal
ori	Origin of replication
PBS	Phosphate-buffered saline
PFA	Paraformaldehyde
PCNA	Proliferating-Cell-Nuclear-Antigen
PCR	Polymerase chain reaction
PIF	Parvoviral initiation factor
PLA2	Phospholipase A2
PPV	Porcine parvovirus
RIPA buffer	Radioimmunoprecipitation assay buffer
RPA	Replication protein A
RT	Room temperature
SAT	Short alternatively translated
Sp1	Specificity protein 1
TBP	TATA-binding protein
TFIIA	Transcription factor II A
UPR	Untranslated protein response

7 Figures

Figure 1: Infection of a cancerous cell or a healthy cell with an oncolytic virus has two different outcomes.....	155
Figure 2: Phylogenetic tree of the family Parvoviridae based on their NS1 protein.....	199
Figure 3: Basic infectious cycle of parvovirus.....	2121
Figure 4: Molecular structure of the capsid of MVMi.....	22
Figure 5: The genome of parvovirus and the transcribed mRNAs.....	24
Figure 6: Entry mechanism of parvovirus.....	255
Figure 7: Conversion and replication of parvovirus.....	288
Figure 8: The mRNAs of the parvoviral proteins.....	3131
Figure 9: Domain structure of NS1.....	32
Figure 10: Formation of viroporins.....	366
Figure 11: The genome of SAT-ko carries two mutations.....	399
Figure 12: Schematic overview over a chimeric PCR. Blue stars indicate mutations.....	488
Figure 13: Installation of a Western Blot.....	6060
Figure 14: Sequence-comparison of SAT in the porcine parvovirus (PPV) and prototypic minute virus of mice (MVMp).....	687
Figure 15: Infections with the SAT-ko virus lead to the formation of small plaques.....	699
Figure 16: The SAT-ko virus replicates in A9 cells.....	71
Figure 17: Release of progeny viruses is inhibited in SAT-ko-infected cells.....	73
Figure 18 Cell-lysis is reduced in SAT-ko-infected cells while the expression of NS1 is similar to MVM-wt-infected cells.....	75
Figure 19: MVM-wt-infected cells release greater amounts of HMGB1 than SAT-ko-infected cells.....	766
Figure 20: SAT is more potent in killing cells than NS1.....	788
Figure 21: Myc-SAT is transported to the plasma membrane.....	799
Figure 22: The transport of SAT to the plasma membrane is essential for its lytic property.....	81
Figure 23: SAT monomers homo-oligomerise at the plasma membrane.....	84
Figure 24: Crosslinking of SAT monomers.....	86
Figure 25: Photo-leucine crosslinks monomers of Myc-SAT. HEK293T cells were transfected with pMVM-Myc-SAT-wt and fed with photo-leucine for 24 h.....	879
Figure 26: Mutations at the transmembrane domain of SAT eradicate the lytic function of SAT.....	91

Figure 27: Mutations in SAT do not inhibit the interaction of monomers.	91
Figure 28: SAT-GG31/35LL and SAT-KR48/49AA localise to the plasma membrane..	92
Figure 29: SAT induces changes in the permeability of the plasma membrane..	94
Figure 30: The expression of SAT does not affect the intracellular concentration of calcium ions	96
Figure 31: The expression of SAT does not change the intracellular concentration of sodium ions.	988
Figure 32: Predicted 3D-structure of SAT.	999
Figure 33: SAT forms dimers in a computer simulation.	101
Figure 34: SAT forms tetramers in a computer simulation.....	103
Figure 35: Annexin V-staining, PI-staining and morphological changes in MVM-wt-, SAT-ko- or mock-infected cells.....	106
Figure 36: pSUPER and pMycSUPER lyse cells more efficiently than pMVM-wt and pMVM-Myc-SAT-wt.	1119
Figure 37: The release of HMGB1 is increased in pSUPER- and pMyc-SUPER-transfected cells.	112
Figure 38: Genome of MVM-wt and MVM- Δ 800.	113
Figure 39: Knockdown of Myc-SAT.....	114
Figure 40: Schematic figure of a setup of a black lipid membrane assay..	12020
Figure 41: Schematic structures of Hygromycin B (527.53 Da) and Propidium Iodide (668.40 Da).....	121
Figure 42: Potential structures of a tetramer of tetramers (t.o.t.) and a pentamer of tetramers (p.o.t.) of SAT.....	122
Figure 43: Top-view on the hole formation by holins at the plasma membrane	124
Figure 44: A low dose of H1-parvovirus cannot heal tumour-bearing rats.....	129
Figure 45: Genome structures of MVM-wt, MVM- Δ 800, Adenovirus-MVM-wt and Adenovirus-SUPER.....	133

8 Bibliography

- Adeyemi, R. O. and Pintel, D. J.** (2012). Replication of minute virus of mice in murine cells is facilitated by virally induced depletion of p21. *J. Virol.* **86**, 8328–8332.
- Adeyemi, R. O. and Pintel, D. J.** (2014). Parvovirus-induced depletion of cyclin B1 prevents mitotic entry of infected cells. *PLoS Pathog.* **10**, e1003891.
- Adeyemi, R. O., Landry, S., Davis, M. E., Weitzman, M. D. and Pintel, D. J.** (2010). Parvovirus minute virus of mice induces a DNA damage response that facilitates viral replication. *PLoS Pathog.* **6**, e1001141.
- Agbandje, M., McKenna, R., Rossmann, M. G., Strassheim, M. L. and Parrish, C. R.** (1993). Structure determination of feline panleukopenia virus empty particles. *Proteins* **16**, 155–171.
- Agbandje-McKenna, M., Llamas-Saiz, A. L., Wang, F., Tattersall, P. and Rossmann, M. G.** (1998). Functional implications of the structure of the murine parvovirus, minute virus of mice. *Structure* **6**, 1369–1381.
- Ahn, J. K., Pitluk, Z. W. and Ward, D. C.** (1992). The GC box and TATA transcription control elements in the P38 promoter of the minute virus of mice are necessary and sufficient for transactivation by the nonstructural protein NS1. *J. Virol.* **66**, 3776–3783.
- Allaume, X., El-Andaloussi, N., Leuchs, B., Bonifati, S., Kulkarni, A., Marttila, T., Kaufmann, J. K., Nettelbeck, D. M., Kleinschmidt, J., Rommelaere, J., et al.** (2012). Retargeting of rat parvovirus H-1PV to cancer cells through genetic engineering of the viral capsid. *J. Virol.* **86**, 3452–3465.
- Andtbacka, R. H. I., Kaufman, H. L., Collichio, F., Amatruda, T., Senzer, N., Chesney, J., Delman, K. A., Spitler, L. E., Puzanov, I., Agarwala, S. S., et al.** (2015). Talimogene laherparepvec improves durable response rate in patients with advanced melanoma. *J. Clin. Oncol.* **33**, 2780–2788.
- Angelova, A. L., Geletneky, K., Nüesch, J. P. F. and Rommelaere, J.** (2015). Tumor Selectivity of Oncolytic Parvoviruses: From in vitro and Animal Models to Cancer Patients. *Front. Bioeng. Biotechnol.* **3**, 55.
- Astell, C. R., Thomson, M., Merchlinsky, M. and Ward, D. C.** (1983). The complete DNA sequence of minute virus of mice, an autonomous parvovirus. *Nucleic Acids Res.* **11**, 999–1018.
- Astell, C. R., Chow, M. B. and Ward, D. C.** (1985). Sequence analysis of the termini of virion and replicative forms of minute virus of mice DNA suggests a modified rolling hairpin model for autonomous parvovirus DNA replication. *J. Virol.* **54**, 171–177.
- Bär, S., Rommelaere, J. and Nüesch, J. P. F.** (2013). Vesicular transport of progeny parvovirus particles through ER and Golgi regulates maturation and cytolysis. *PLoS Pathog.* **9**, e1003605.
- Bär, S., Rommelaere, J. and Nüesch, J. P. F.** (2015). PKC η /Rdx-driven phosphorylation

- of PDK1: a novel mechanism promoting cancer cell survival and permissiveness for parvovirus-induced lysis. *PLoS Pathog.* **11**, e1004703.
- Barish, M. E.** (1991). Increases in intracellular calcium ion concentration during depolarization of cultured embryonic *Xenopus* spinal neurones. *J Physiol (Lond)* **444**, 545–565.
- Bashir, T., Horlein, R., Rommelaere, J. and Willwand, K.** (2000). Cyclin A activates the DNA polymerase delta -dependent elongation machinery in vitro: A parvovirus DNA replication model. *Proc Natl Acad Sci USA* **97**, 5522–5527.
- Binette, J., Dubé, M., Mercier, J., Halawani, D., Latterich, M. and Cohen, E. A.** (2007). Requirements for the selective degradation of CD4 receptor molecules by the human immunodeficiency virus type 1 Vpu protein in the endoplasmic reticulum. *Retrovirology* **4**, 75.
- Bourguignon, G. J., Tattersall, P. J. and Ward, D. C.** (1976). DNA of minute virus of mice: self-priming, nonpermuted, single-stranded genome with a 5'-terminal hairpin duplex. *J. Virol.* **20**, 290–306.
- Bowman, G. D., Nodelman, I. M., Levy, O., Lin, S. L., Tian, P., Zamb, T. J., Udem, S. A., Venkataraghavan, B. and Schutt, C. E.** (2000). Crystal structure of the oligomerization domain of NSP4 from rotavirus reveals a core metal-binding site. *J. Mol. Biol.* **304**, 861–871.
- Brownstein, D. G., Smith, A. L., Jacoby, R. O., Johnson, E. A., Hansen, G. and Tattersall, P.** (1991). Pathogenesis of infection with a virulent allotropic variant of minute virus of mice and regulation by host genotype. *Lab. Invest.* **65**, 357–364.
- Brownstein, D. G., Smith, A. L., Johnson, E. A., Pintel, D. J., Naeger, L. K. and Tattersall, P.** (1992). The pathogenesis of infection with minute virus of mice depends on expression of the small nonstructural protein NS2 and on the genotype of the allotropic determinants VP1 and VP2. *J. Virol.* **66**, 3118–3124.
- Cady, S. D., Luo, W., Hu, F. and Hong, M.** (2009). Structure and function of the influenza A M2 proton channel. *Biochemistry* **48**, 7356–7364.
- Carrasco, L.** (1978). Membrane leakiness after viral infection and a new approach to the development of antiviral agents. *Nature* **272**, 694–699.
- Chandler, D. E., Penin, F., Schulten, K. and Chipot, C.** (2012). The p7 protein of hepatitis C virus forms structurally plastic, minimalist ion channels. *PLoS Comput. Biol.* **8**, e1002702.
- Cheng, G., Feng, Z. and He, B.** (2005). Herpes simplex virus 1 infection activates the endoplasmic reticulum resident kinase PERK and mediates eIF-2 α dephosphorylation by the gamma(1)34.5 protein. *J. Virol.* **79**, 1379–1388.
- Chou, J. and Roizman, B.** (1994). Herpes simplex virus 1 gamma(1)34.5 gene function, which blocks the host response to infection, maps in the homologous domain of the genes expressed during growth arrest and DNA damage. *Proc Natl Acad Sci USA* **91**, 5247–5251.

- Christensen, J. and Tattersall, P.** (2002). Parvovirus initiator protein NS1 and RPA coordinate replication fork progression in a reconstituted DNA replication system. *J. Virol.* **76**, 6518–6531.
- Christensen, J., Cotmore, S. F. and Tattersall, P.** (1995). Minute virus of mice transcriptional activator protein NS1 binds directly to the transactivation region of the viral P38 promoter in a strictly ATP-dependent manner. *J. Virol.* **69**, 5422–5430.
- Christensen, J., Cotmore, S. F. and Tattersall, P.** (2001). Minute virus of mice initiator protein NS1 and a host KDWK family transcription factor must form a precise ternary complex with origin DNA for nicking to occur. *J. Virol.* **75**, 7009–7017.
- Contreras, A. and Carrasco, L.** (1979). Selective inhibition of protein synthesis in virus-infected mammalian cells. *J. Virol.* **29**, 114–122.
- Cotmore, S. F. and Tattersall, P.** (1986a). The NS-1 polypeptide of the autonomous parvovirus MVM is a nuclear phosphoprotein. *Virus Res.* **4**, 243–250.
- Cotmore, S. F. and Tattersall, P.** (1986b). Organization of nonstructural genes of the autonomous parvovirus minute virus of mice. *J. Virol.* **58**, 724–732.
- Cotmore, S. F. and Tattersall, P.** (1987). The autonomously replicating parvoviruses of vertebrates. *Adv. Virus Res.* **33**, 91–174.
- Cotmore, S. F. and Tattersall, P.** (1989). A genome-linked copy of the NS-1 polypeptide is located on the outside of infectious parvovirus particles. *J. Virol.* **63**, 3902–3911.
- Cotmore, S. F. and Tattersall, P.** (1990). Alternate splicing in a parvoviral nonstructural gene links a common amino-terminal sequence to downstream domains which confer radically different localization and turnover characteristics. *Virology* **177**, 477–487.
- Cotmore, S. F. and Tattersall, P.** (1994). An asymmetric nucleotide in the parvoviral 3' hairpin directs segregation of a single active origin of DNA replication. *EMBO J.* **13**, 4145–4152.
- Cotmore, S. F. and Tattersall, P.** (2003). Resolution of parvovirus dimer junctions proceeds through a novel heterocruciform intermediate. *J. Virol.* **77**, 6245–6254.
- Cotmore, S. F. and Tattersall, P.** (2007). Parvoviral host range and cell entry mechanisms. *Adv. Virus Res.* **70**, 183–232.
- Cotmore, S. F. and Tattersall, P.** (2012). Mutations at the base of the icosahedral five-fold cylinders of minute virus of mice induce 3'-to-5' genome uncoating and critically impair entry functions. *J. Virol.* **86**, 69–80.
- Cotmore, S. F. and Tattersall, P.** (2013). Parvovirus diversity and DNA damage responses. *Cold Spring Harb. Perspect. Biol.* **5**,.
- Cotmore, S. F. and Tattersall, P.** (2014). Parvoviruses: small does not mean simple. *Annu. Rev. Virol.* **1**, 517–537.
- Cotmore, S. F., Christensen, J., Nüesch, J. P. and Tattersall, P.** (1995). The NS1 polypeptide of the murine parvovirus minute virus of mice binds to DNA sequences containing the motif [ACCA]₂₋₃. *J. Virol.* **69**, 1652–1660.

- Cotmore, S. F., D'abramo, A. M., Ticknor, C. M. and Tattersall, P.** (1999). Controlled conformational transitions in the MVM virion expose the VP1 N-terminus and viral genome without particle disassembly. *Virology* **254**, 169–181.
- Crawford, L. V., Follett, E. A., Burdon, M. G. and McGeoch, D. J.** (1969). The DNA of a minute virus of mice. *J. Gen. Virol.* **4**, 37–46.
- Deleu, L., Pujol, A., Faisst, S. and Rommelaere, J.** (1999). Activation of promoter P4 of the autonomous parvovirus minute virus of mice at early S phase is required for productive infection. *J. Virol.* **73**, 3877–3885.
- Dennis, E. A.** (1997). The growing phospholipase A2 superfamily of signal transduction enzymes. *Trends Biochem. Sci.* **22**, 1–2.
- Di Piazza, M., Mader, C., Geletneky, K., Herrero Y Calle, M., Weber, E., Schlehofer, J., Deleu, L. and Rommelaere, J.** (2007). Cytosolic activation of cathepsins mediates parvovirus H-1-induced killing of cisplatin and TRAIL-resistant glioma cells. *J. Virol.* **81**, 4186–4198.
- Doerig, C., Hirt, B., Beard, P. and Antonietti, J. P.** (1988). Minute virus of mice non-structural protein NS-1 is necessary and sufficient for trans-activation of the viral P39 promoter. *J. Gen. Virol.* **69 (Pt 10)**, 2563–2573.
- Dölle, C., Niere, M., Lohndal, E. and Ziegler, M.** (2010). Visualization of subcellular NAD pools and intra-organellar protein localization by poly-ADP-ribose formation. *Cell. Mol. Life Sci.* **67**, 433–443.
- Dumitriu, I. E., Baruah, P., Valentinis, B., Voll, R. E., Herrmann, M., Nawroth, P. P., Arnold, B., Bianchi, M. E., Manfredi, A. A. and Rovere-Querini, P.** (2005). Release of high mobility group box 1 by dendritic cells controls T cell activation via the receptor for advanced glycation end products. *J. Immunol.* **174**, 7506–7515.
- Eichwald, V., Daeffler, L., Klein, M., Rommelaere, J. and Salomé, N.** (2002). The NS2 proteins of parvovirus minute virus of mice are required for efficient nuclear egress of progeny virions in mouse cells. *J. Virol.* **76**, 10307–10319.
- El-Andaloussi, N., Bonifati, S., Kaufmann, J. K., Maily, L., Daeffler, L., Deryckère, F., Nettelbeck, D. M., Rommelaere, J. and Marchini, A.** (2012). Generation of an adenovirus-parvovirus chimera with enhanced oncolytic potential. *J. Virol.* **86**, 10418–10431.
- Ewart, G. D., Sutherland, T., Gage, P. W. and Cox, G. B.** (1996). The Vpu protein of human immunodeficiency virus type 1 forms cation-selective ion channels. *J. Virol.* **70**, 7108–7115.
- Fischer, W. B.** (2003). Vpu from HIV-1 on an atomic scale: experiments and computer simulations. *FEBS Lett.* **552**, 39–46.
- Geletneky, K., Hajda, J., Angelova, A. L., Leuchs, B., Capper, D., Bartsch, A. J., Neumann, J.-O., Schöning, T., Hüsing, J., Beelte, B., et al.** (2017). Oncolytic H-1 Parvovirus Shows Safety and Signs of Immunogenic Activity in a First Phase I/IIa Glioblastoma Trial. *Mol. Ther.* **25**, 2620–2634.

- Georgieva, E. R., Borbat, P. P., Norman, H. D. and Freed, J. H.** (2015). Mechanism of influenza A M2 transmembrane domain assembly in lipid membranes. *Sci. Rep.* **5**, 11757.
- Giese, N. A., Raykov, Z., DeMartino, L., Vecchi, A., Sozzani, S., Dinsart, C., Cornelis, J. J. and Rommelaere, J.** (2002). Suppression of metastatic hemangiosarcoma by a parvovirus MVMP vector transducing the IP-10 chemokine into immunocompetent mice. *Cancer Gene Ther.* **9**, 432–442.
- Gordon J.C., Angrick E.J.** (1986). Canine parvovirus: environmental effects on infectivity. *Am J Vet Res.* 1986 Jul;47(7):1464-7.
- Grekova, S., Zawatzky, R., Hörlein, R., Cziepluch, C., Mincberg, M., Davis, C., Rommelaere, J. and Daeffler, L.** (2010a). Activation of an antiviral response in normal but not transformed mouse cells: a new determinant of minute virus of mice oncotropism. *J. Virol.* **84**, 516–531.
- Grekova, S., Aprahamian, M., Giese, N., Schmitt, S., Giese, T., Falk, C. S., Daeffler, L., Cziepluch, C., Rommelaere, J. and Raykov, Z.** (2010b). Immune cells participate in the oncosuppressive activity of parvovirus H-1PV and are activated as a result of their abortive infection with this agent. *Cancer Biol. Ther.* **10**, 1280–1289.
- Grekova, S. P., Aprahamian, M., Daeffler, L., Leuchs, B., Angelova, A., Giese, T., Galabov, A., Heller, A., Giese, N. A., Rommelaere, J., et al.** (2011). Interferon γ improves the vaccination potential of oncolytic parvovirus H-1PV for the treatment of peritoneal carcinomatosis in pancreatic cancer. *Cancer Biol. Ther.* **12**, 888–895.
- Grekova, S. P., Raykov, Z., Zawatzky, R., Rommelaere, J. and Koch, U.** (2012). Activation of a glioma-specific immune response by oncolytic parvovirus Minute Virus of Mice infection. *Cancer Gene Ther.* **19**, 468–475.
- Griffin, S. D. C., Beales, L. P., Clarke, D. S., Worsfold, O., Evans, S. D., Jaeger, J., Harris, M. P. G. and Rowlands, D. J.** (2003). The p7 protein of hepatitis C virus forms an ion channel that is blocked by the antiviral drug, Amantadine. *FEBS Lett.* **535**, 34–38.
- Halder, S., Nam, H.-J., Govindasamy, L., Vogel, M., Dinsart, C., Salomé, N., McKenna, R. and Agbandje-McKenna, M.** (2013). Structural characterization of H-1 parvovirus: comparison of infectious virions to empty capsids. *J. Virol.* **87**, 5128–5140.
- Hay, A. J., Wolstenholme, A. J., Skehel, J. J. and Smith, M. H.** (1985). The molecular basis of the specific anti-influenza action of amantadine. *EMBO J.* **4**, 3021–3024.
- Hay, A. J., Zambon, M. C., Wolstenholme, A. J., Skehel, J. J. and Smith, M. H.** (1986). Molecular basis of resistance of influenza A viruses to amantadine. *J. Antimicrob. Chemother.* **18 Suppl B**, 19–29.
- He, B., Gross, M. and Roizman, B.** (1997). The gamma(1)34.5 protein of herpes simplex virus 1 complexes with protein phosphatase 1 α to dephosphorylate the α subunit of the eukaryotic translation initiation factor 2 and preclude the shutoff of protein synthesis by double-stranded RNA-activated protein kinase. *Proc Natl Acad Sci*

- USA* **94**, 843–848.
- Hong, Y., Nie, H., Wu, D., Wei, X., Ding, X. and Ying, W.** (2014). NAD(+) treatment prevents rotenone-induced apoptosis and necrosis of differentiated PC12 cells. *Neurosci. Lett.* **560**, 46–50.
- Hoppe, G., Talcott, K. E., Bhattacharya, S. K., Crabb, J. W. and Sears, J. E.** (2006). Molecular basis for the redox control of nuclear transport of the structural chromatin protein Hmgb1. *Exp. Cell Res.* **312**, 3526–3538.
- Hristov, G., Krämer, M., Li, J., El-Andaloussi, N., Mora, R., Daeffler, L., Zentgraf, H., Rommelaere, J. and Marchini, A.** (2010). Through its nonstructural protein NS1, parvovirus H-1 induces apoptosis via accumulation of reactive oxygen species. *J. Virol.* **84**, 5909–5922.
- Hussain, A., Das, S. R., Tanwar, C. and Jameel, S.** (2007). Oligomerization of the human immunodeficiency virus type 1 (HIV-1) Vpu protein—a genetic, biochemical and biophysical analysis. *Virol. J.* **4**, 81.
- Janko, C., Filipović, M., Munoz, L. E., Schorn, C., Schett, G., Ivanović-Burmazović, I. and Herrmann, M.** (2014). Redox modulation of HMGB1-related signaling. *Antioxid. Redox Signal.* **20**, 1075–1085.
- Jhawar, S. R., Thandoni, A., Bommareddy, P. K., Hassan, S., Kohlhapp, F. J., Goyal, S., Schenkel, J. M., Silk, A. W. and Zloza, A.** (2017). Oncolytic Viruses-Natural and Genetically Engineered Cancer Immunotherapies. *Front. Oncol.* **7**, 202.
- de Jong, D.H., Singh, G., Bennett, W.F., Arnarez, C., Wassenaar, T.A., Schäfer, L.V., Periole, X., Tieleman, D.P., Marrink, S.J.** (2013) Improved Parameters for the Martini Coarse-Grained Protein Force Field. *J Chem Theory Comput.* 2013 Jan 8;9(1):687-97.
- F. Brent Johnson and Enkhmart Dudleenamjil** (2012). Clathrin-Associated Endocytosis as a Route of Entry into Cells for Parvoviruses, Molecular Regulation of Endocytosis Brian Ceresa, IntechOpen, DOI: 10.5772/48510. Available from: <https://www.intechopen.com/books/molecular-regulation-of-endocytosis/clathrin-associated-endocytosis-as-a-route-of-entry-into-cells-for-parvoviruses>
- Jongeneel, C. V., Sahli, R., McMaster, G. K. and Hirt, B.** (1986). A precise map of splice junctions in the mRNAs of minute virus of mice, an autonomous parvovirus. *J. Virol.* **59**, 564–573.
- Josuweit, R., Bender, S., Kern, S., Leuchs, B., Hielscher, T., Herold-Mende, C., Schlehofer, J. R., Dinsart, C., Witt, O., Rommelaere, J., et al.** (2016). Pediatric and Adult High-Grade Glioma Stem Cell Culture Models Are Permissive to Lytic Infection with Parvovirus H-1. *Viruses* **8**,
- Kambara, H., Okano, H., Chiocca, E. A. and Saeki, Y.** (2005). An oncolytic HSV-1 mutant expressing ICP34.5 under control of a nestin promoter increases survival of animals even when symptomatic from a brain tumor. *Cancer Res.* **65**, 2832–2839.
- Kazama, H., Ricci, J.-E., Herndon, J. M., Hoppe, G., Green, D. R. and Ferguson, T.**

- A.** (2008). Induction of immunological tolerance by apoptotic cells requires caspase-dependent oxidation of high-mobility group box-1 protein. *Immunity* **29**, 21–32.
- Kelley, L. A. and Sternberg, M. J. E.** (2009). Protein structure prediction on the Web: a case study using the Phyre server. *Nat. Protoc.* **4**, 363–371.
- Kerr, J.R., Cotmore, S.F., Bloom, M.E., Linden, R.M., Parrish, C.R.** (2006). Parvoviruses. Great Britain: Hodder Arnold.
- Kestler, J., Neeb, B., Struyf, S., Van Damme, J., Cotmore, S. F., D'Abramo, A., Tattersall, P., Rommelaere, J., Dinsart, C. and Cornelis, J. J.** (1999). cis requirements for the efficient production of recombinant DNA vectors based on autonomous parvoviruses. *Hum. Gene Ther.* **10**, 1619–1632.
- Kozak, M.** (1995). Adherence to the first-AUG rule when a second AUG codon follows closely upon the first. *Proc Natl Acad Sci USA* **92**, 7134.
- Kozak, M.** (2002). Pushing the limits of the scanning mechanism for initiation of translation. *Gene* **299**, 1–34.
- Krady, J. K. and Ward, D. C.** (1995). Transcriptional activation by the parvoviral nonstructural protein NS-1 is mediated via a direct interaction with Sp1. *Mol. Cell. Biol.* **15**, 524–533.
- Kuruppu, D. and Tanabe, K. K.** (2005). Viral oncolysis by herpes simplex virus and other viruses. *Cancer Biol. Ther.* **4**, 524–531.
- Lawler, S. E., Speranza, M.-C., Cho, C.-F. and Chiocca, E. A.** (2017). Oncolytic viruses in cancer treatment: A review. *JAMA Oncol.* **3**, 841–849.
- Legendre, D. and Rommelaere, J.** (1994). Targeting of promoters for trans activation by a carboxy-terminal domain of the NS-1 protein of the parvovirus minute virus of mice. *J. Virol.* **68**, 7974–7985.
- Li, X. and Rhode, S. L.** (1990). Mutation of lysine 405 to serine in the parvovirus H-1 NS1 abolishes its functions for viral DNA replication, late promoter trans activation, and cytotoxicity. *J. Virol.* **64**, 4654–4660.
- Li, X. and Rhode, S. L.** (1991). Nonstructural protein NS2 of parvovirus H-1 is required for efficient viral protein synthesis and virus production in rat cells in vivo and in vitro. *Virology* **184**, 117–130.
- Li, J., Bonifati, S., Hristov, G., Marttila, T., Valmary-Degano, S., Stanzel, S., Schnölzer, M., Mougin, C., Arahamian, M., Grekova, S. P., et al.** (2013). Synergistic combination of valproic acid and oncolytic parvovirus H-1PV as a potential therapy against cervical and pancreatic carcinomas. *EMBO Mol. Med.* **5**, 1537–1555.
- Linser, P., Bruning, H. and Armentrout, R. W.** (1979). Uptake of minute virus of mice into cultured rodent cells. *J. Virol.* **31**, 537–545.
- Llamas-Saiz, A. L., Agbandje-McKenna, M., Wikoff, W. R., Bratton, J., Tattersall, P. and Rossmann, M. G.** (1997). Structure determination of minute virus of mice. *Acta Crystallogr. D Biol. Crystallogr.* **53**, 93–102.

- Lodish H, Berk A, Zipursky SL, et al.** (2000). *Molecular Cell Biology*. 4th edition. New York: W. H. Freeman; 2000. Section 15.4, Intracellular Ion Environment and Membrane Electric Potential. Available from: <https://www.ncbi.nlm.nih.gov/books/NBK21627/>
- Lombardo, E., Ramírez, J. C., Agbandje-McKenna, M. and Almendral, J. M.** (2000). A beta-stranded motif drives capsid protein oligomers of the parvovirus minute virus of mice into the nucleus for viral assembly. *J. Virol.* **74**, 3804–3814.
- Lombardo, E., Ramírez, J. C., Garcia, J. and Almendral, J. M.** (2002). Complementary roles of multiple nuclear targeting signals in the capsid proteins of the parvovirus minute virus of mice during assembly and onset of infection. *J. Virol.* **76**, 7049–7059.
- López-Bueno, A., Rubio, M.-P., Bryant, N., McKenna, R., Agbandje-McKenna, M. and Almendral, J. M.** (2006). Host-selected amino acid changes at the sialic acid binding pocket of the parvovirus capsid modulate cell binding affinity and determine virulence. *J. Virol.* **80**, 1563–1573.
- Lorson, C., Pearson, J., Burger, L. and Pintel, D. J.** (1998). An Sp1-binding site and TATA element are sufficient to support full transactivation by proximally bound NS1 protein of minute virus of mice. *Virology* **240**, 326–337.
- Madan, V. and Bartenschlager, R.** (2015). Structural and functional properties of the hepatitis C virus p7 viroporin. *Viruses* **7**, 4461–4481.
- Madan, V., Sánchez-Martínez, S., Vedovato, N., Rispoli, G., Carrasco, L. and Nieva, J. L.** (2007). Plasma membrane-porating domain in poliovirus 2B protein. A short peptide mimics viroporin activity. *J. Mol. Biol.* **374**, 951–964.
- Magadán, J. G., Pérez-Victoria, F. J., Sougrat, R., Ye, Y., Strebel, K. and Bonifacino, J. S.** (2010). Multilayered mechanism of CD4 downregulation by HIV-1 Vpu involving distinct ER retention and ERAD targeting steps. *PLoS Pathog.* **6**, e1000869.
- Mani, B., Baltzer, C., Valle, N., Almendral, J. M., Kempf, C. and Ros, C.** (2006). Low pH-dependent endosomal processing of the incoming parvovirus minute virus of mice virion leads to externalization of the VP1 N-terminal sequence (N-VP1), N-VP2 cleavage, and uncoating of the full-length genome. *J. Virol.* **80**, 1015–1024.
- Marchini, A., Bonifati, S., Scott, E. M., Angelova, A. L. and Rommelaere, J.** (2015). Oncolytic parvoviruses: from basic virology to clinical applications. *Virol. J.* **12**, 6.
- Maroto, B., Valle, N., Saffrich, R. and Almendral, J. M.** (2004). Nuclear export of the nonenveloped parvovirus virion is directed by an unordered protein signal exposed on the capsid surface. *J. Virol.* **78**, 10685–10694.
- McNatt, M. W., Zang, T. and Bieniasz, P. D.** (2013). Vpu binds directly to tetherin and displaces it from nascent virions. *PLoS Pathog.* **9**, e1003299.
- Medigeshi, G. R., Lancaster, A. M., Hirsch, A. J., Briese, T., Lipkin, W. I., Defilippis, V., Früh, K., Mason, P. W., Nikolich-Zugich, J. and Nelson, J. A.** (2007). West Nile virus infection activates the unfolded protein response, leading to CHOP induction and apoptosis. *J. Virol.* **81**, 10849–10860.

- Mészáros, I., Tóth, R., Olasz, F., Tijssen, P. and Zádori, Z.** (2017). The SAT Protein of Porcine Parvovirus Accelerates Viral Spreading through Induction of Irreversible Endoplasmic Reticulum Stress. *J. Virol.* **91**,
- Moehler, M., Blechacz, B., Weiskopf, N., Zeidler, M., Stremmel, W., Rommelaere, J., Galle, P. R. and Cornelis, J. J.** (2001). Effective infection, apoptotic cell killing and gene transfer of human hepatoma cells but not primary hepatocytes by parvovirus H1 and derived vectors. *Cancer Gene Ther.* **8**, 158–167.
- Moehler, M. H., Zeidler, M., Wilsberg, V., Cornelis, J. J., Woelfel, T., Rommelaere, J., Galle, P. R. and Heike, M.** (2005). Parvovirus H-1-induced tumor cell death enhances human immune response in vitro via increased phagocytosis, maturation, and cross-presentation by dendritic cells. *Hum. Gene Ther.* **16**, 996–1005.
- Morgan, W. R. and Ward, D. C.** (1986). Three splicing patterns are used to excise the small intron common to all minute virus of mice RNAs. *J. Virol.* **60**, 1170–1174.
- Mousset, S., Ouadrhiri, Y., Caillet-Fauquet, P. and Rommelaere, J.** (1994). The cytotoxicity of the autonomous parvovirus minute virus of mice nonstructural proteins in FR3T3 rat cells depends on oncogene expression. *J. Virol.* **68**, 6446–6453.
- Mueller, P., Rudin, D. O., Tien, H. T. and Wescott, W. C.** (1962). Reconstitution of cell membrane structure in vitro and its transformation into an excitable system. *Nature* **194**, 979–980.
- Mustafa, G., Nandekar, PP., Yu, X., Wade, R.C.** (2015). On the application of the MARTINI coarse-grained model to immersion of a protein in a phospholipid bilayer. *J Chem Phys.* 2015 Dec 28;143(24):243139
- Naeger, L. K., Cater, J. and Pintel, D. J.** (1990). The small nonstructural protein (NS2) of the parvovirus minute virus of mice is required for efficient DNA replication and infectious virus production in a cell-type-specific manner. *J. Virol.* **64**, 6166–6175.
- Neil, S. J. D., Zang, T. and Bieniasz, P. D.** (2008). Tetherin inhibits retrovirus release and is antagonized by HIV-1 Vpu. *Nature* **451**, 425–430.
- Nieva, J. L., Madan, V. and Carrasco, L.** (2012). Viroporins: structure and biological functions. *Nat. Rev. Microbiol.* **10**, 563–574.
- Nüesch, J. P. F. and Rommelaere, J.** (2007). A viral adaptor protein modulating casein kinase II activity induces cytopathic effects in permissive cells. *Proc Natl Acad Sci USA* **104**, 12482–12487.
- Nüesch, J. P. F. and Rommelaere, J.** (2014). Tumor suppressing properties of rodent parvovirus NS1 proteins and their derivatives. *Adv. Exp. Med. Biol.* **818**, 99–124.
- Nüesch, J. P. and Tattersall, P.** (1993). Nuclear targeting of the parvoviral replicator molecule NS1: evidence for self-association prior to nuclear transport. *Virology* **196**, 637–651.
- Nüesch, J. P., Cotmore, S. F. and Tattersall, P.** (1995). Sequence motifs in the replicator protein of parvovirus MVM essential for nicking and covalent attachment to the viral origin: identification of the linking tyrosine. *Virology* **209**, 122–135.

- Nüesch, J. P. F., Lachmann, S., Corbau, R. and Rommelaere, J.** (2003). Regulation of minute virus of mice NS1 replicative functions by atypical PKC λ in vivo. *J. Virol.* **77**, 433–442.
- Nüesch, J. P. F., Lachmann, S. and Rommelaere, J.** (2005). Selective alterations of the host cell architecture upon infection with parvovirus minute virus of mice. *Virology* **331**, 159–174.
- Nüesch, J. P. F., Lacroix, J., Marchini, A. and Rommelaere, J.** (2012). Molecular pathways: rodent parvoviruses—mechanisms of oncolysis and prospects for clinical cancer treatment. *Clin. Cancer Res.* **18**, 3516–3523.
- Nykky, J., Tuusa, J. E., Kirjavainen, S., Vuento, M. and Gilbert, L.** (2010). Mechanisms of cell death in canine parvovirus-infected cells provide intuitive insights to developing nanotools for medicine. *Int. J. Nanomedicine* **5**, 417–428.
- Ohshima, T., Nakajima, T., Oishi, T., Imamoto, N., Yoneda, Y., Fukamizu, A. and Yagami, K. i** (1999). CRM1 mediates nuclear export of nonstructural protein 2 from parvovirus minute virus of mice. *Biochem. Biophys. Res. Commun.* **264**, 144–150.
- Op De Beeck, A. and Caillet-Fauquet, P.** (1997). The NS1 protein of the autonomous parvovirus minute virus of mice blocks cellular DNA replication: a consequence of lesions to the chromatin? *J. Virol.* **71**, 5323–5329.
- Op De Beeck, A., Anouja, F., Mousset, S., Rommelaere, J. and Caillet-Fauquet, P.** (1995). The nonstructural proteins of the autonomous parvovirus minute virus of mice interfere with the cell cycle, inducing accumulation in G2. *Cell Growth Differ.* **6**, 781–787.
- Paglino, J. C., Andres, W. and van den Pol, A. N.** (2014). Autonomous parvoviruses neither stimulate nor are inhibited by the type I interferon response in human normal or cancer cells. *J. Virol.* **88**, 4932–4942.
- Pang, X., Moussa, S. H., Targy, N. M., Bose, J. L., George, N. M., Gries, C., Lopez, H., Zhang, L., Bayles, K. W., Young, R., et al.** (2011). Active Bax and Bak are functional holins. *Genes Dev.* **25**, 2278–2290.
- Parker, J. S. and Parrish, C. R.** (2000). Cellular uptake and infection by canine parvovirus involves rapid dynamin-regulated clathrin-mediated endocytosis, followed by slower intracellular trafficking. *J. Virol.* **74**, 1919–1930.
- Parker, J. S., Murphy, W. J., Wang, D., O'Brien, S. J. and Parrish, C. R.** (2001). Canine and feline parvoviruses can use human or feline transferrin receptors to bind, enter, and infect cells. *J. Virol.* **75**, 3896–3902.
- Pear, W. S., Nolan, G. P., Scott, M. L. and Baltimore, D.** (1993). Production of high-titer helper-free retroviruses by transient transfection. *Proc Natl Acad Sci USA* **90**, 8392–8396.
- Pinto, L. H., Holsinger, L. J. and Lamb, R. A.** (1992). Influenza virus M2 protein has ion channel activity. *Cell* **69**, 517–528.
- Plevka, P., Hafenstein, S., Li, L., D'Abbramo, A., Cotmore, S. F., Rossmann, M. G. and Tattersall, P.** (2011). Structure of a packaging-defective mutant of minute virus of

- mice indicates that the genome is packaged via a pore at a 5-fold axis. *J. Virol.* **85**, 4822–4827.
- Porwal, M., Cohen, S., Snoussi, K., Popa-Wagner, R., Anderson, F., Dugot-Senant, N., Wodrich, H., Dinsart, C., Kleinschmidt, J. A., Panté, N., et al.** (2013). Parvoviruses cause nuclear envelope breakdown by activating key enzymes of mitosis. *PLoS Pathog.* **9**, e1003671.
- Pujol, A., Deleu, L., Nüesch, J. P., Cziepluch, C., Jauniaux, J. C. and Rommelaere, J.** (1997). Inhibition of parvovirus minute virus of mice replication by a peptide involved in the oligomerization of nonstructural protein NS1. *J. Virol.* **71**, 7393–7403.
- Ran, Z., Rayet, B., Rommelaere, J. and Faisst, S.** (1999). Parvovirus H-1-induced cell death: influence of intracellular NAD consumption on the regulation of necrosis and apoptosis. *Virus Res.* **65**, 161–174.
- Rayet, B., Lopez-Guerrero, J. A., Rommelaere, J. and Dinsart, C.** (1998). Induction of programmed cell death by parvovirus H-1 in U937 cells: connection with the tumor necrosis factor alpha signalling pathway. *J. Virol.* **72**, 8893–8903.
- Rhode, S. L.** (1985). trans-Activation of parvovirus P38 promoter by the 76K noncapsid protein. *J. Virol.* **55**, 886–889.
- Rhode, S. L. and Richard, S. M.** (1987). Characterization of the trans-activation-responsive element of the parvovirus H-1 P38 promoter. *J. Virol.* **61**, 2807–2815.
- Römer, W., Lam, Y. H., Fischer, D., Watts, A., Fischer, W. B., Göring, P., Wehrspohn, R. B., Gösele, U. and Steinem, C.** (2004). Channel activity of a viral transmembrane peptide in micro-BLMs: Vpu(1-32) from HIV-1. *J. Am. Chem. Soc.* **126**, 16267–16274.
- Rossman, J. S., Jing, X., Leser, G. P. and Lamb, R. A.** (2010). Influenza virus M2 protein mediates ESCRT-independent membrane scission. *Cell* **142**, 902–913.
- Rovere-Querini, P., Capobianco, A., Scaffidi, P., Valentinis, B., Catalanotti, F., Giazoni, M., Dumitriu, I. E., Müller, S., Iannaccone, M., Traversari, C., et al.** (2004). HMGB1 is an endogenous immune adjuvant released by necrotic cells. *EMBO Rep.* **5**, 825–830.
- Saier, M. H. and Reddy, B. L.** (2015). Holins in bacteria, eukaryotes, and archaea: multifunctional xenologues with potential biotechnological and biomedical applications. *J. Bacteriol.* **197**, 7–17.
- Scaffidi, P., Misteli, T. and Bianchi, M. E.** (2002). Release of chromatin protein HMGB1 by necrotic cells triggers inflammation. *Nature* **418**, 191–195.
- Sen, A., Sen, N. and Mackow, E. R.** (2007). The formation of viroplasm-like structures by the rotavirus NSP5 protein is calcium regulated and directed by a C-terminal helical domain. *J. Virol.* **81**, 11758–11767.
- Shukla, A., Dey, D., Banerjee, K., Nain, A. and Banerjee, M.** (2015). The C-terminal region of the non-structural protein 2B from Hepatitis A Virus demonstrates lipid-specific viroporin-like activity. *Sci. Rep.* **5**, 15884.

- Siegl G.** (1984) Biology and Pathogenicity of Autonomous Parvoviruses. In: Berns K.I. (eds) *The Parvoviruses. The Viruses*. Springer, Boston, MA
- Soranzo, T., Cortès, S., Gilde, F., Kreir, M., Picart, C. and Lenormand, J.-L.** (2016). Functional characterization of p7 viroporin from hepatitis C virus produced in a cell-free expression system. *Protein Expr. Purif.* **118**, 83–91.
- Spalholz, B. A. and Tattersall, P.** (1983). Interaction of minute virus of mice with differentiated cells: strain-dependent target cell specificity is mediated by intracellular factors. *J. Virol.* **46**, 937–943.
- Steinmann, E., Penin, F., Kallis, S., Patel, A. H., Bartenschlager, R. and Pietschmann, T.** (2007). Hepatitis C virus p7 protein is crucial for assembly and release of infectious virions. *PLoS Pathog.* **3**, e103.
- Suikkanen, S., Aaltonen, T., Nevalainen, M., Vålilehto, O., Lindholm, L., Vuento, M. and Vihinen-Ranta, M.** (2003a). Exploitation of microtubule cytoskeleton and dynein during parvoviral traffic toward the nucleus. *J. Virol.* **77**, 10270–10279.
- Suikkanen, S., Antila, M., Jaatinen, A., Vihinen-Ranta, M. and Vuento, M.** (2003b). Release of canine parvovirus from endocytic vesicles. *Virology* **316**, 267–280.
- Suzuki, T., Orba, Y., Okada, Y., Sunden, Y., Kimura, T., Tanaka, S., Nagashima, K., Hall, W. W. and Sawa, H.** (2010). The human polyoma JC virus agnoprotein acts as a viroporin. *PLoS Pathog.* **6**, e1000801.
- Tattersall, P.** 1978. Susceptibility to minute virus of mice as a function of host-cell differentiation, p. 131-149. In D. C. Ward and P. Tattersall (ed.), *Replication of mammalian parvoviruses*. Cold Spring Harbor Laboratory, Cold Spring Harbor, N.Y.
- Tattersall, P. and Bratton, J.** (1983). Reciprocal productive and restrictive virus-cell interactions of immunosuppressive and prototype strains of minute virus of mice. *J. Virol.* **46**, 944–955.
- Tattersall, P., Cawte, P. J., Shatkin, A. J. and Ward, D. C.** (1976). Three structural polypeptides coded for by minute virus of mice, a parvovirus. *J. Virol.* **20**, 273–289.
- Tattersall, P., Shatkin, A. J. and Ward, D. C.** (1977). Sequence homology between the structural polypeptides of minute virus of mice. *J. Mol. Biol.* **111**, 375–394.
- Titz, S., Hans, M., Kelsch, W., Lewen, A., Swandulla, D. and Misgeld, U.** (2003). Hyperpolarizing inhibition develops without trophic support by GABA in cultured rat midbrain neurons. *J Physiol (Lond)* **550**, 719–730.
- Trowbridge, I. S. and Omary, M. B.** (1981). Human cell surface glycoprotein related to cell proliferation is the receptor for transferrin. *Proc Natl Acad Sci USA* **78**, 3039–3043.
- Tsao, J., Chapman, M. S., Agbandje, M., Keller, W., Smith, K., Wu, H., Luo, M., Smith, T. J., Rossmann, M. G. and Compans, R. W.** (1991). The three-dimensional structure of canine parvovirus and its functional implications. *Science* **251**, 1456–1464.
- Urano, F., Wang, X., Bertolotti, A., Zhang, Y., Chung, P., Harding, H. P. and Ron, D.** (2000). Coupling of stress in the ER to activation of JNK protein kinases by transmembrane protein kinase IRE1. *Science* **287**, 664–666.

- Väisänen, E., Fu, Y., Hedman, K. and Söderlund-Venermo, M. (2017). Human Protoparvoviruses. *Viruses* **9**,
- Venereau, E., Casalgrandi, M., Schiraldi, M., Antoine, D. J., Cattaneo, A., De Marchis, F., Liu, J., Antonelli, A., Preti, A., Raeli, L., et al. (2012). Mutually exclusive redox forms of HMGB1 promote cell recruitment or proinflammatory cytokine release. *J. Exp. Med.* **209**, 1519–1528.
- Vihinen-Ranta, M., Kakkola, L., Kalela, A., Vilja, P. and Vuento, M. (1997). Characterization of a nuclear localization signal of canine parvovirus capsid proteins. *Eur. J. Biochem.* **250**, 389–394.
- Vihinen-Ranta, M., Kalela, A., Mäkinen, P., Kakkola, L., Marjomäki, V. and Vuento, M. (1998). Intracellular route of canine parvovirus entry. *J. Virol.* **72**, 802–806.
- Vihinen-Ranta, M., Yuan, W. and Parrish, C. R. (2000). Cytoplasmic trafficking of the canine parvovirus capsid and its role in infection and nuclear transport. *J. Virol.* **74**, 4853–4859.
- Watanabe, T., Watanabe, S., Ito, H., Kida, H. and Kawaoka, Y. (2001). Influenza A virus can undergo multiple cycles of replication without M2 ion channel activity. *J. Virol.* **75**, 5656–5662.
- White, R., Chiba, S., Pang, T., Dewey, J. S., Savva, C. G., Holzenburg, A., Pogliano, K. and Young, R. (2011). Holin triggering in real time. *Proc Natl Acad Sci USA* **108**, 798–803.
- Willwand, K., Moroianu, A., Hörlein, R., Stremmel, W. and Rommelaere, J. (2002). Specific interaction of the nonstructural protein NS1 of minute virus of mice (MVM) with [ACCA]₂ motifs in the centre of the right-end MVM DNA palindrome induces hairpin-primed viral DNA replication. *J. Gen. Virol.* **83**, 1659–1664.
- Wilson, G. M., Jindal, H. K., Yeung, D. E., Chen, W. and Astell, C. R. (1991). Expression of minute virus of mice major nonstructural protein in insect cells: purification and identification of ATPase and helicase activities. *Virology* **185**, 90–98.
- Wozniak, A. L., Griffin, S., Rowlands, D., Harris, M., Yi, M., Lemon, S. M. and Weinman, S. A. (2010). Intracellular proton conductance of the hepatitis C virus p7 protein and its contribution to infectious virus production. *PLoS Pathog.* **6**, e1001087.
- Xie, Q. and Chapman, M. S. (1996). Canine parvovirus capsid structure, analyzed at 2.9 Å resolution. *J. Mol. Biol.* **264**, 497–520.
- Yachdav, G., Kloppmann, E., Kajan, L., Hecht, M., Goldberg, T., Hamp, T., Hönigschmid, P., Schafferhans, A., Roos, M., Bernhofer, M., Richter, L., Ashkenazy, H., Punta, M., Schlessinger, A., Bromberg, Y., Schneider, R., Vriend, G., Sander, C., Ben-Tal, N., Rost, B. (2014). PredictProtein—an open resource for online prediction of protein structural and functional features. *Nucleic Acids Res.* 2014 Jul;42(Web Server issue):W337-43.
- Yang, H., Lundbäck, P., Ottosson, L., Erlandsson-Harris, H., Venereau, E., Bianchi, M. E., Al-Abed, Y., Andersson, U., Tracey, K. J. and Antoine, D. J.

- (2012). Redox modification of cysteine residues regulates the cytokine activity of high mobility group box-1 (HMGB1). *Mol. Med.* **18**, 250–259.
- Zádori, Z., Szelei, J., Lacoste, M. C., Li, Y., Gariépy, S., Raymond, P., Allaire, M., Nabi, I. R. and Tijssen, P.** (2001). A viral phospholipase A2 is required for parvovirus infectivity. *Dev. Cell* **1**, 291–302.
- Zádori, Z., Szelei, J. and Tijssen, P.** (2005). SAT: a late NS protein of porcine parvovirus. *J. Virol.* **79**, 13129–13138.
- Zebedee, S. L. and Lamb, R. A.** (1988). Influenza A virus M2 protein: monoclonal antibody restriction of virus growth and detection of M2 in virions. *J. Virol.* **62**, 2762–2772.
- Zhang, L. and Wang, A.** (2012). Virus-induced ER stress and the unfolded protein response. *Front. Plant Sci.* **3**, 293.
- Zheng, T., Xu, S. Y., Zhou, S. Q., Lai, L. Y. and Li, L.** (2013). Nicotinamide adenine dinucleotide (NAD⁺) repletion attenuates bupivacaine-induced neurotoxicity. *Neurochem. Res.* **38**, 1880–1894.

Online resources:

https://talk.ictvonline.org/ictv-reports/ictv_9th_report/ssdna-viruses-2011/w/ssdna_viruses/152/parvoviridae-figures

https://www.sigmaaldrich.com/content/dam/sigma-aldrich/docs/Sigma-Aldrich/General_Information/1/duolink-short-protocol.pdf

<https://www.addgene.org/tools/protocols/plko/>

https://en.wikipedia.org/wiki/Model_lipid_bilayer